Synthesis and Characterization of Novel Nonlinear Optical Polyimide

Ren Li

School of Materials Science and Engineering

A thesis submitted to the Nanyang Technological University
in fulfilment of the requirement for the degree of
Doctor of Philosophy in Materials Engineering

2006

SYNTHESIS AND CHARACTERIZATION OF NOVEL NONLINEAR OPTICAL POLYIMIDE

REN LI

SCHOOL OF MATERIALS SCIENCE & ENGINEERING
NANYANG TECHNOLOGICAL UNIVERSITY

2006

SYNTHESIS AND CHARACTERIZATION OF NOVEL NONLINEAR OPTICAL POLYIMIDE

Submitted by

REN LI

School of Materials Science & Engineering

A thesis submitted to Nanyang Technological University
in fulfillment of the requirement for the degree of
Doctor of Philosophy in Materials Engineering

2006

TABLE OF CONTENTS

LIST OF TABLES

LIST OF FIGURES

Deleted: 7

ABBREVIATION

A	Electron Acceptor
AM1	Austin Model 1
BTDA	3,3',4,4'-Benzophenonetetracarboxylic Dianhydride
D	Electron Donor
DABP	4,4'-Diaminobenzenephenone
DANS	Dimethylaminonitrostilbene
DBTDL	Dibutyltin Dilaurate
DCM	Dichloromethane
DDS	4,4'-Diaminodiphenyl Sulfone
DMAc	N,N-dimethylacetamide
DMF	N,N-dimethylformamide
DMSO	Dimethyl Sulfoxide
D_2O	Deuterium-oxide
DR1	Disperse Red 1
DSC	Differential Scanning Calorimetry Analysis
EO	Electro-optic
EFISH	Electric Field-induced Second-harmonic Generation
ESI-MS	Electrospray Ionization Mass Spectra
2-F-5-NA	2-Fluoro-5-nitroaniline
4-F-3-NA	4-Fluoro-3-nitroaniline
6FDA	4,4'-(Hexafluoroisopropylidene) Diphthalic Anhydride
FTIR	Fourier Transform Infrared Spectroscopy
GaAs	Gallium Arsenide
HOMO	the Highest Occupied Molecular Orbital
HRS	Hyper-Rayleigh Scattering
ICTES	3-Isocyanatopropyl Triethoxysilane
IPA	Isopropanol

IPN	Interpenetrating Polymer Network
ITO	Indium Tin Oxide
KTP	Potassium Titanyl phosphate
LCAO	Linear Combination of Atomic Orbital
$LiNbO_3$	Lithium Niobate
LUMO	the Lowest Unoccupied Molecular Orbital
M_n	Number-average Molecular Weight
M_w	Weight-average Molecular Weight
M_w/M_n	Polydispersity
MNDO	Modified Neglect of Differential Overlap
3-NA	3-Nitroaniline
4-NA	4-Nitroaniline
NLO	Nonlinear Optical
NMP	1-Methyl-2-pyrrolidone
NMR	Nuclear Magnetic Resonance Spectroscopy
ODA	4,4'-Oxydianiline
ODPA	Oxydiphthalic Dianhydride
PA	Poly(amic acid)
PDA	1,4-Phenylene Diamine
PI	Polyimide
PMDA	Pyromellitic Dianhydride
PMMA	Poly (methylmethacrylate)
PMT	Photomultiplier Tube
2R-2F-5N-DIAMINE	2,4-Diamino-2'-fluoro-5'-nitroazobenzene
2R-4F-3N-DIAMINE	2,4-Diamino-4'-fluoro-3'-nitroazobenzene
2R-3N-DIAMINE	2,4-Diamino-3'-nitroazobenzene
2R-4N-DIAMINE	2,4-Diamino-4'-nitroazobenzene
SCF	Self-consistent Field
SGDR1	NLO-active Triethoxysilane
SHG	Second Harmonic Generation
T_d	Decomposition Temperature
T_g	Glass translation Temperature

TEOS	Tetraethoxysilane
TGA	Thermogravimetric Analysis
THF	Tetrahydrofuran
TMU	Tetramethylurea
UV-Vis Spectra	Ultraviolet-visible Spectra
VLSI	Very Large Scale Integration
c	Velocity of Light
d_{33}	Second Harmonic Coefficient
ε	Dielectric Constant
$\varepsilon(\nu)$	the Molar Extinction Coefficient ($mol^{-1}l \cdot cm^{-1}$)
h	Planck's Constant
ρ	Density
β	Molecular Hyperpolarizability
n	Refractive Index
μ	Molecular Dipole Moment
λ_{max}	Maximum Absorption Wavelength
γ_{33}	Electro-optical Coefficient
ν_{eg}	the Transition Frequency(cm^{-1})
γ_{eg}	Transition Dipole Moment
$\Delta\mu_{eg}$	the Difference between the Excited State (μ_e) and the Ground State (μ_g) Molecular Dipole Moment
ν_L	the Frequency of the Incident Radiation, to which the β value is referred
N_A	Avogadro's Number

Abstract

Nonlinear optical (NLO) polymers have attracted extensive attention because of their potential applications in integrated optical devices such as optical switching, frequency conversion and high-speed electro-optic (EO) devices. However, the stability and optical loss of currently used polymers limit their applications. It is very important to develop NLO polymers with better transparency and higher stability without sacrificing other properties. This study focused on the development of new side-chain NLO polyimides based on the novel fluoronitroaryl diaminoazobenzene chromophores and polyimide/silicon composites. The effects of the fluorine and the fluorine position in the chromophores on the structures and properties of the chromophores and polyimides were studied. The influences of the silicon network on the properties of the composite films were also investigated.

Two novel fluorinated diaminoazobenzene chromophore monomers and their non-fluorinated analogues, which can be used for synthesis of side-chain NLO polyimide, were successfully synthesized. The new fluorinated diaminoazobenzene chromophore monomers have very good thermal stability and large hyperpolarizability. It was found that the incorporation of fluorine into the chromophore can lead to higher thermal stability. The fluorine position can lead to the different maximum absorption wavelength λ_{max} and thermal stability.

Three series of novel NLO polyimides based on the fluorinated diaminoazobenzene chromophores and their analogue were successfully synthesized. All NLO polyimides possess high thermal stability, excellent transparency (λ_{max}: 298.5~355 nm) and large

second harmonic coefficient d_{33} value. At 100 °C in air, 88%~94% of the original d_{33} remained over 720 hrs, which confirms that the synthesized polyimides exhibit excellent stability of d_{33} value. The effects of fluorine and fluorine position in the chromophore side chain on the structures and properties of polyimide were studied in detail. The optimized polyimide unit conformation structure was modeled to understand the mechanism. It was found that the incorporation of fluorine can significantly increase the thermal stability and hydrophobic properties of the polyimide. Results revealed that the fluorine in ortho position in chromophore side chain can lead to larger torsion of the chromophore side chain and the fluorine in para position can lead to smaller torsion. The larger torsion can significantly increase the non-planarity and the steric hinder effect of chromophore side chain, which can lead to an increase in thermal stability, transparency, and d_{33} values.

A series of new NLO polyimide/silicon composite films were prepared through a NLO-active silane chromophore, which can be used for sol-gel process. It is found that the composites can be prepared under lower imidization temperature than that of the corresponding polyimides. However, all NLO composite films have higher thermal stability, larger d_{33} value, higher stability of d_{33} at 100 °C and better hydrophobic properties than that of the corresponding NLO polyimides. Investigation revealed that the crosslink silicon network can significantly increase thermal stability and hydrophobic properties and hinder the relaxation of the chromophore side chain more efficiently. The effects of fluorine and fluorine position in the chromophore side chain of polyimide on the properties of composite were the same with that of the corresponding polyimides.

Acknowledgments

The author wishes to extend his sincerest gratitude and appreciation to the following persons, who have made invaluable contribution towards the completion of this research project:

First of all, I would like to express my heartfelt gratitude to my supervisor, Dr. Li Guoyuan, for his invaluable supervision and encouragement throughout the course of my Ph.D. research. He has shown me the way of critical and scientific thinking. He has been patient with my inexperience and provided insightful advice when I sometimes blindly pursue new but unpractical ideas. Through him, I have also learned to exercise independence in everything I do. I really appreciate his effort and patience in guiding me to become a good research student in the unique research environment he has created. His commitment to hard work and discipline has inspired me through the course of this study.

Next, I would also like to express my gratitude to Dr. Hu Xiao, for his great help and useful advice in this research. With his great help, my experiments could be carried out promptly.

I would like to thank Ms Xie Hong from Singapore Institute of Manufacturing Technology for her kind assistance in my sample characterization and Ms Lin Tingting from Institute of Materials Research & Engineering for her cooperation in structure modeling.

I am thankful to See-Toh Swee Sing, Wu Shucheng, Tan Hui Nai Loreen, Fiona Sze, Mustura, Heryani, Sng Jing Li and Sandy Leong for their technical assistance that facilitated the completion of this investigative work.

I thank my friends at NTU: Dr. Hao Jiyuan, Dr. Xia Xulin, Dr. He Guosen, Dr. Lim Boon Kiat, Dr. Chen Binling, Dr. Zhang Jixuan, Dr. Qu Yi, Ms Lau Ping Ping, Mr. Song Lixin, Mr. Tay Yee Yan and Mr. Ma Siguang, for their friendship and inspiration. Special thanks go to all of my fellow colleagues in the Microelectronics Materials and Polymer Lab, School of Materials Engineering at NTU for their cherished friendship and precious time spent in discussions.

I also thank my sincerest friends Mr. Qin Xiaojie for his sincerest help in my life.

Finally, I would like to thank my family especially my wife Ms Huang Liyi, for their great love, understanding, care, concern, and encouragement. I have made many wonderful and helpful friends during my graduate years and I will have fond memories of this place.

Chapter 1 Introduction

1.1 Background and Motivation

As compared to traditional second-order NLO inorganic materials, there are many advantages for using NLO polymeric materials. NLO polymeric materials possess low dielectric constant, high nonlinearity, fast response time, and large laser damage threshold. Furthermore, great flexibility exists in the choice of molecular and polymeric constituents, allowing for systematic design and optimization of materials. Solvent-coated polymers lead themselves well to planar fabrication approaches so that waveguide and integrated optical devices can be easily fabricated at low cost. The second-order NLO polymer materials have tremendous potential applications in all-optical communication network such as waveguide modulators, electro-optical switches, data manipulation, and information processing. Recently, techniques have been developed for seamlessly integrating polymeric electro-optic circuitry with passive low loss optical circuitry (e.g. silica long-haul transmission fiber and medium-range fluoropolymer fiber) and with very large scale integration (VLSI) semiconductor electronics. These advances have created a considerable interest in the commercialization of polymeric electro-optic materials. It has already been demonstrated that high performance electro-optic prototype devices based on polymeric materials can be made.

Generally, to be used successfully in nonlinear optical applications, NLO polymers need to meet the most important requirements simultaneously: high stability (including thermal, chemical, photochemical and mechanical), high second order

nonlinearity and low optical loss, which are the challenging tasks for the materials scientists and researchers. Polyimides are known to exhibit excellent thermal, chemical, photochemical and mechanical properties. They have been widely used in VLSI circuit. Hence, researchers have concentrated on NLO polyimide especially side-chain NLO polyimide ever since chromophores were first incorporated into polyimide because they exhibit large second-order nonlinearity and excellent stability.

There are mainly two approaches for synthesizing the side-chain polyimides. One approach is the post-reaction method. In this approach, the soluble polyimides were first synthesized. Then, the chromophores were incorporated into the polyimides through the reaction between the functional group in the polyimide and chromophore, such as Mitsunobu reaction, post-azo reaction and coordination reaction. Although this approach can cause the chromophore to avoid the harsh imidization, it leads to a significant decrease in thermal stability and temporal stability of the chromophore orientation because the NLO chromophore was incorporated into polyimide only through a single bonding site which can reduce the orientational stability at high temperatures. These polyimides still exhibit low transparency and large resonance d_{33}.

In the second approach, the monomer containing chromophore such as diamine or dianhydride containing chromophore is synthesized first. Then, the side-chain polyimide is synthesized through the condensation polymerization of the monomers containing chromophore with other monomers. Synthesis of the monomers is a key step. Most of researches have concentrated on this approach because the second-order NLO polyimides prepared from this method are highly stable and have large second harmonic coefficient or EO coefficient. The highest stable NLO polyimides, which

can meet the actual application requirements, were synthesized through this approach. However, their transparency is low and the λ_{max} in the UV absorption is basically in the range of 400~600 nm which is not desirable for application. Furthermore, this approach involves a harsh imidization such as high imidization temperature. The two main drawbacks limit their applications in photonic and electro-optical devices. Therefore, improvement of the transparency and lowering the imidization temperature of the NLO polyimides are very important for application.

As mentioned above, the main disadvantage of NLO side-chain polyimide is low transparency. To date, the optical loss of the side-chain polyimides was rarely reported. It was explained that the high optical loss is mainly from intrinsic absorption by both chromophore and polyimide. Some research work [1-2] used a fluorinated dianhydride or diamine such as 4,4'-(hexafluoroisopropylidene) diphthalic anhydride (6FDA) in order to reduce the optical loss from polyimide backbone. It is believed that reduced intrinsic absorption of polyimide backbone at visible wavelengths is accomplished by the reduction of in-planing packing and polymer deformation. However, the optical losses from the chromophore still cannot be decreased. For the polyimides containing fluorine in the main chain, the loss is mainly form the chromophore absorption.

It is difficult for chromophore to meet all requirements at the same time because there are some trade-offs between these requirements. Among these trade-offs, the most difficult thing is to defeat the nonlinearity–transparency trade-off. Recently, it was found that fluorinated chromophores displayed higher transparency and keep the nonlinearity at the same order with their non-fluorinated analogue, and could defeat

the nonlinearity–transparency trade-off. However, until now, the developed fluorinated chromophores lack reactive functional groups, and so it is difficult to incorporate them into polymers through covalent bonds as side-chain. The effects of fluorine and fluorine position in the chromophore side chain on the properties of NLO polymer are very rarely studied. Therefore, the development of new fluorinated chromophores isomers that have reactive amino groups so that they can be easily incorporated into polyimide as side chain might be a solution, and this is a challenging task.

Furthermore, how to reduce the fabrication temperature without sacrificing thermal stability is still a challenge for NLO polyimide prepared from monomer containing chromophore. The high processing temperature can increase the possibility of the chromophore decomposition and decrease nonlinearity. At the same time, it can also increase the light scattering and shrinkage so that it can increase the optical loss from the cure. Hence, it is quite important to lower the imidization temperature of the polyimides.

1.2 Objectives of This Work

This research work aimed to develop new NLO polyimide and polyimide/silicon composites materials based on the fluorinated diaminoazobenzene chromophores and to study the effects of the fluorine and its position in chromophore on the properties of the fluorinated chromophore and polyimides. The research comprised the following parts:

- Design, synthesize and characterize the new fluorinated chromophore isomers that possess reactive amino group for the development of the side-chain NLO polyimide.

- Investigate the effects of fluorine and fluorine position on the properties of chromophores.
- Prepare and characterize the new NLO side-chain polyimide from the above developed fluorinated chromophores and their analogues.
- Study the effects of fluorine and the fluorine position in chromophore side chain on properties of the polyimides. And study the mechanism through the structure modeling.
- Prepare and characterize the second-order NLO polyimide/silicon composite through NLO alkoxysilane dye and investigate the influence of silicon network on properties of the composite films.

Deleted: t

1.3 Organization of This Thesis

This thesis is divided into 7 chapters:

A brief description on the motivation and scope of the research is summarized in chapter 1.

Chapter 2 reviews the research on second-order NLO polyimides. The preparation and properties of all kinds of the second-order NLO polymer are described. Then, the poling method and measurement technology for second-order NLO effect are introduced, and the synthesis and properties of the NLO polyimides were detailed. Finally, the major problems of the NLO polyimide are summarized.

Chapter 3 focuses on the synthesis and characterization of the novel fluorinated diaminoazobenzene chromphores and their analogues for NLO polyimides. The

effects of the fluorine and fluorine position on the thermal properties and UV absorption are reported.

Chapter 4 discusses the hyperpolarizability of chromophore. The methodology and programs for the determination of the hyperpolarizability are confirmed through well known chromophores of 4-nitroaniline and Disperse Red 1. The effects of the fluorine and fluorine position on the hyperpolarizability are reported.

Synthesis and characterization of novel side-chain NLO polyimides films from the fluorinated diaminoazobenzene chromphores and their analogues are presented in Chapter 5. The optimized conformation structures of the polyimide unit were modeled through AM1/VAMP/Materials Studio. In order to get the largest d_{33} value, imidization temperature and poling voltage were optimized. The effects of the fluorine and fluorine position in chromophore side chain on the properties were studied. The mechanisms of the effect of fluorine and fluorine position on the properties were proposed. Furthermore, the effects of the main chain structure of polyimide on the properties were also investigated.

Chapter 6 reports on the synthesis and characterization of an alkoxysilane chromophore, which can be used for sol-gel process. Novel NLO polyimide/silicon composites films were prepared and characterized. Effects of silicon network on the properties of composite films were studied. Effects of fluorine and the fluorine position in the chromophore moiety on the properties of composite films were also investigated.

Finally, Chapter 7 concludes this thesis and recommends direction for future studies.

Chapter 2 Literature Review

While most of the progress in information processing has involved microelectronics technology, we are currently reaching the physical limitation of conventional electronic signal processing and transmission. To achieve a data processing bandwidth greater than 50 GHz and transmission distance longer than 1 meter, photon is required to work with or replace electron as the functional medium. Under such a background, photonics, which is the analog of the electronics, describes the technology where photons are used to acquire, store, transmit and process information. It is generally regarded as the next generation media in data storage and manipulation, which is estimated to be worth US$90 billion today and will be approximately US$700 billion in 2025 [3].

Nonlinear optics involves the interactions of applied electromagnetic fields in various materials for the generation of new electromagnetic fields, altered in frequency, phase or other physical properties [3]. Nonlinear optics is the basis of all the fledgling photonics technologies [4]. Recent developments in the field of nonlinear optics hold promise for important applications in optical information processing, telecommunication and integrated optics. Thus, advancements in nonlinear optical (NLO) materials which can be used in a variety of optoelectronic and photonic devices will have a direct effect on the progress of photonic technology.

2.1 Second-order NLO Materials

Second-order NLO materials are mainly used in optical switching, frequency conversion and electro-optic (EO) applications, especially in EO modulators. All these applications depend on their second harmonic generation (SHG) or electro-optical effect originated from the molecular hyperpolarizability and the second-order susceptibility of bulk material. The second-order NLO materials can be classified into inorganic and organic materials. Table 2-1 summarizes the NLO properties of typical inorganic crystals, typical chromophore dimethylaminonitrostilbene (DANS) and E-O polymers [5-6]. The inorganic materials suffered from several drawbacks, such as high cost, high dielectric constant and difficulties in processing and large scale production limit the further expansion in NLO applications. Organic materials especially polymeric NLO materials are increasingly being recognized as the materials for the future alternatives because their molecular nature combined with the versatility of synthetic chemistry can be used to design, alter and optimize molecular structure to maximize nonlinear response and other properties [7]. Other advantages for use of polymeric NLO materials include low dielectric constant, high nonlinearity, fast response time, large laser damage threshold, good processability and compatibility with VLSI circuit.

Table 2-1 Comparison of the NLO properties of GaAs, $LiNbO_3$, DANS and E-O polymer

Physical properties	GaAs	$LiNbO_3$	DANS	E-O polymer
E-O coefficient r_{33} (at 1.3 μm) (pm/V)	1.5	31	-[a]	30-100
SHG coefficient (pm/V)	-	13[b]	27[c]	-
Dielectric constant, ε	10-12	28	-	2.5-4
Refractive index, n	3.5	2.2	1.2	1.6-1.7
Bandwidth-length product, ΔωL (GHZ-cm)	>100	10	-	>150
Figure of merit for EO (n^3r/ε)	6	10	40-100	-
Figure of merit for SHG (d/n^3)	-	16	420	-

[a]: No data, [b]: d_{31}, [c]: deff.

Since Meredith et al [8] reported second-order NLO polymer in 1982, the study of NLO polymer has enjoyed rapid and sustained growth. Generally, a second-order NLO polymer film is fabricated by solvent-coating and then subjected to an external electric field usually at an elevated temperature where segmental mobility in the polymer is significant and cooled to room temperature before the field is removed. Dipolar molecule in the film can reorient during this process provided viscous forces can be overcome and a net alignment is then retained in the film. As a result, polymeric materials promise to make optoelectronic and photonic technologies more practical and widespread. They could make major impacts on telecommunications, as polymer based modulators and switches begin to enter the market. Other applications are waiting in the wings.

2.2 Second-order NLO Polymer

2.2.1 Criteria for Second-order NLO Polymer

Although polymeric NLO materials offer great potentials in fiber optic communication and information processing, a series of stringent criteria has to be met simultaneously before these materials can be used for real commercial applications. To be successfully used in NLO application, second-order NLO polymers need to meet following requirements:

- High SHG or E-O coefficient
- No orientational relaxation at 80 °C over a few years
- No orientational relaxation at 200 °C over a short time
- No physical/chemical degradation up to 300 °C
- Low optical loss (<2dB/cm) and broadband transparency
- Compatibility with different substrates and good thin film processability
- Low fabrication cost

Among these requirements, the most important requirements are high stability (thermal, chemical, photochemical and mechanical), large E-O coefficient or second order nonlinearity and low optical loss. The stability of the NLO polymer is mostly affected by the stability of the polymer matrix and the chromophore, and the relationship between chromophore and polymer. To ensure the high stability, the high glass transition temperature polymers or crosslinked polymers are the better choice. IBM research center described a class of exceptionally stable NLO

polyimides (Figure 2-1), which can meet the actual application requirement of the stability [9]. However, their nonlinearity is very low (γ_{33}: 4~7 pm/V at 1305 nm).

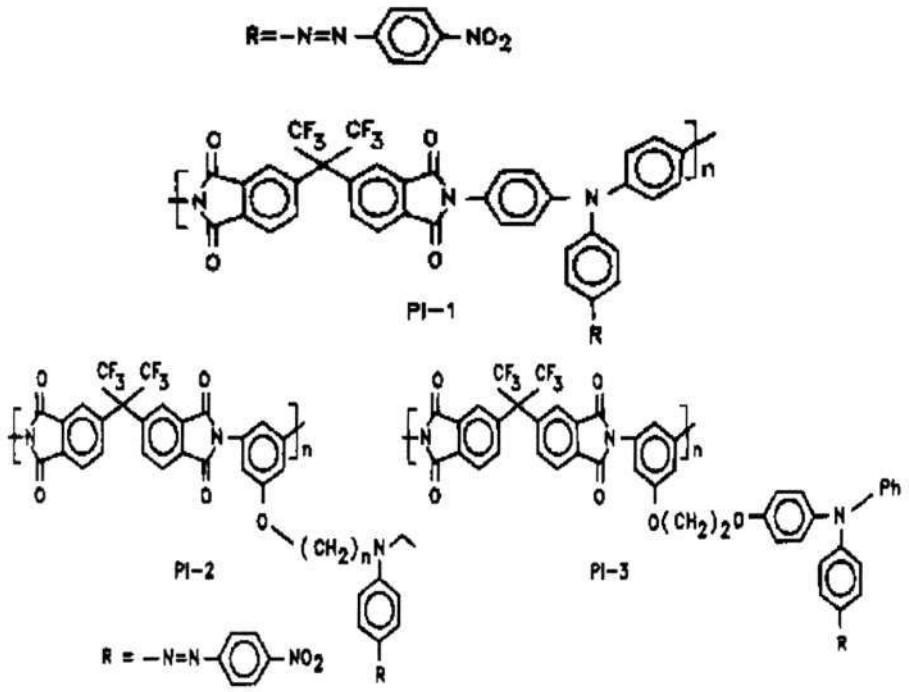

Figure 2-1 Chemical structure of high stability polyimide [9]

The large second-order nonlinearity is mainly affected by the number concentration of the chromophore, the molecular hyperpolarizability (β) of the chromophore and the intermolecular electrostatic interaction. Meticulous efforts have been taken to synthesize dipolar chromophores with several magnitudes of increase in hyperpolarizability. However, strong electrostatic interaction among dipolar chromophores has dragged the progress so far as to efficiently translate this molecular nonlinearity into macroscopic EO coefficients. Dalton reported that this interaction could be alleviated by modifying the geometry of chromophore [10]. Based on the results, the EO coefficient of the prepared polymeric electro optic modulator is about 60 pm/V, through modification of the shape of the chromophores to sterically inhibit the intermolecular electrostatic interaction. The

structure of the chromophore (CLD-1) is shown in Figure 2-2. However, the thermal properties of the guest-host system was limited because these chromophores were doped with poly (methylmethacrylate) (PMMA), other high thermal stability polymer or cross-linked systems.

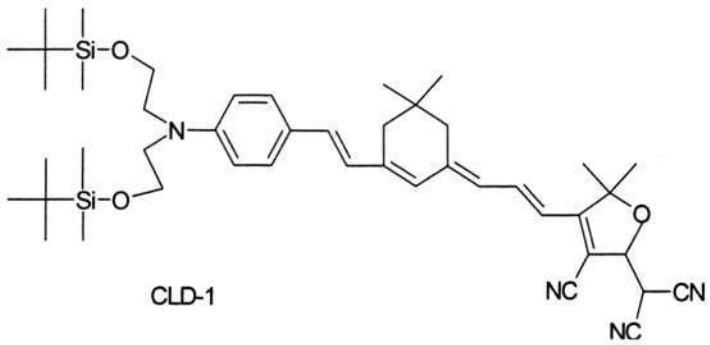

Figure 2-2 Chemical structure of CLD-1

It has been found that there are three major components of optical loss: the intrinsic absorption of chromophores and polymers; reflection of NLO polymer including rayleigh scattering, impurities and fabrication errors; coupling loss when coupling with optical fiber [4]. Basically, the absorption of the chromophore should distance the operating wavelengths to reduce the absorption loss in the materials. Chromophore domain aggregation and phase separation between chromophores and polymers could also drastically increase the scattering loss. It was found that these requirements could affect and restrict each other as shown in Figure 2-3. Therefore, it is a challenge to meet these requirements simultaneously.

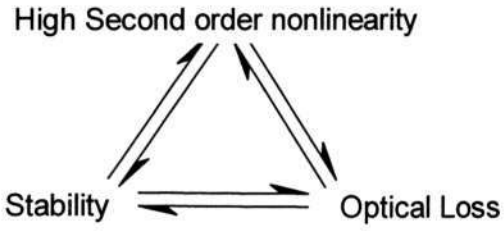

Figure 2-3 Relationship among the stability, second-order nonlinearity and optical loss

2.2.2 Chromophores for Second-order NLO Polymers

2.2.2.1 Traditional NLO Chromophores

Macroscopic NLO effect originates from microscopic nonlinearity. To enhance macroscopic NLO effect, molecular optical nonlinearity must be optimized. According to the theory [11], large macroscopic second-harmonic coefficient (d_{33} value) requires high number concentration of NLO chromophore (*N*), large molecular dipole moment (μ) and molecular hyperpolarizability (β), which is shown as follows:

$$d_{33} = \frac{1}{2}\chi_{333}{}^{2}(-2\omega;\omega,\omega) \cong \frac{Nf^{2}(\omega)f(2\omega)f(0)\mu E}{10kT}\beta(-2\omega;\omega,\omega) \qquad (2\text{-}1)$$

where $\chi_{333}{}^{2}(-2\omega,\omega,\omega)$ is the second-order susceptibility, f is the Lorenz-Lorenz local field factors at optical frequency (ω), $f(0)$ is the Onsager local field factor, k is the Boltzmann constant, and E and T are the applied field and the poling temperature, respectively.

A simple two-level model [11] can be used in the calculations of the molecular hyperpolarizability, which depends on the transition dipole moment $\mu_{g,e}$, the difference between the dipole moments of the ground and excited state $\mu_{ee} - \mu_{gg}$ and the optical gap (HOMO-LUMO) E_{ge},

$$\beta \propto \frac{(\mu_{ee} - \mu_{gg})\mu_{ge}{}^{2}}{E_{ge}{}^{2}} \qquad (2\text{-}2)$$

According to Equation (2-2), tremendous efforts have been made to design and synthesize NLO chromophore molecules with large hyperpolarizability during the past decades. Most attempts to design chromophores with large β have been focused

on "push-pull" type of dipole compounds, which are generally represented as D-π-A, where the electron donor (D) and the electron acceptor (A) are linked by a π-conjugation bridge. Associating the higher electron donating ability and the ease of preparation, amino type donor is considered to be the optimal choice. A large number of acceptor moieties including nitro, cyanovinyl groups have been studied [12-13]. These common acceptors are listed according to their strength of accepting electrons:

$$-NO > -NO_2 > -SO_2Me > -COCF_3 > -CHO > -CN$$

An efficient bridge should have small or no barrier at all to such a charge transfer. The efficiency of the conjugation moiety is assigned in the descending order as follows:

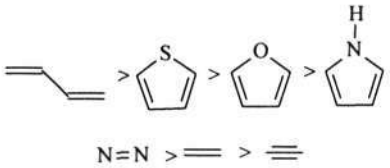

Equation (2-2) reveals that β could increase with the increasing strengths of donor and acceptor and with the increasing length of π-conjugation bridges. In the early nineties, Marder and co-workers reported that for a given conjugation bridge, there is an optimal combination of donor and acceptor strength to maximum ofμβ, and beyond this point, increased donor-acceptor strength will attenuate μβ [14-15]. And it was shown that bond length alternation, i.e. the average carbon-carbon single and double bonds in the molecule, is the relevant parameter in the optimization of the hyperpolarizability of molecule [16-18]. Furthermore, the chromophore should meet other requirements, high stability and transparency.

Tricyanovinyl groups lead to some of the largest observed electro-optic coefficients and also lead to the lower chemical stability [19]. Increase in thermal stability of

chromophores can, in principle, be achieved by replacing aliphatic structure by aromatic ones along the conjugation path of the molecules. However, as indicated above, additional aromaticity tends to decrease the hyperpolarizability. Moylan found that replacing aliphatic dialkylamino donor groups with diarylamino groups could result in a substantial increase in thermal stability of a wide range of chromophores without compromising the nonlinearity of the chromophore [20].

Another important issue for the development of chromophore is the nonlinearity-transparency trade-off. The absorption of the chromophore should be far away from the communication wavelengths to reduce the absorption loss in the materials. From a two-level model, it is clear that the hyperpolarizability is a strong increase function of the absorption maximum wavelength. For most of the chromophores with high β value, their maximum absorption peaks are higher than 650 nm, whose low energy tails can extend several hundreds of nanometers into the long wavelength region. Because even a small absorption at the operating wavelength of electro-optic devices (typically 1.3 or 1.5 μm) can be detrimental, it is important to make NLO chromophores as transparent as possible without compromising the molecule's nonlinearity.

Furthermore, for frequency doubling applications, materials that are simultaneously transparent at the fundamental and second-harmonic wavelength would be required. Less success has been achieved in the development of the chromophores for frequency doubling applications. In summary, chromophores with excellent comprehensive properties have yet to be found. How to produce chromophores with excellent comprehensive properties is the most important task for the development of the NLO polymers.

2.2.2.2 Fluorinated NLO Chromophores

Fluorinated materials are of great research interest since it has been demonstrated that the fluorinated materials exhibit a comprehensive combination of high thermal stability, chemical inertness, low dielectric constant and high optical transparency. Electronegative fluorine substituted systems are weak π donors and strong σ acceptors. In an early study on NLO chromophores, many chromophores containing fluorine substituted groups as acceptors, such as CF_3, $SO_2C_nF_{2n+1}$ and $COCF_3$, and their NLO parameters were listed (Table 2-2) [12-13, 21-25].

However, in the past, the study on chromophores has been concentrated on how to obtain large β value. Fluorinated chromophores were not hot spot although all these fluorinated chromophores exhibited excellent comprehensive properties. It should be noted that these fluorinated chromophores all exhibit better transparency and blue-shift of λ_{max} compared with their analogue. This result suggests that incorporation of fluorine into chromophore could be a new approach to overcome the trade-off between nonlinearity and transparency.

Some theoretical calculation results [3] strongly suggest that so-called inductive acceptors can be used to produce highly efficient chromophores. And the theoretical calculations of Liu *et al* [26] showed that fluorine in different positions in the fluoroazulene isomers could lead to different UV absorbance. Although Matsui [27] reported some chromophores containing C_nF_{2n+1} or $C_nF_{2n+1}S$ as acceptors display red-shift λ_{max} compared with their non-fluorinated analogues, the fluorinated chromophore is very promising for next generation NLO materials.

Table 2-2 Molecular parameters of nonlinear optical fluorinated chromophores and their analogues

Structure	R_1	R_2	R_3	$\beta_0 \times 10^{30}$ (esu)	μ (D)	λ_{max}	Ref
	$COCF_3$	OMe		3.6	3.5	292	[23]
	$SO_2C_3F_7$	OMe		3.3	5.4	290	[23]
	NO_2	OMe		5.1	4.6	302	[23]
	$SO_2C_{10}F_{21}$	NMe_2		9.0	7.3	314	[21]
	NO_2	NMe_2		12	6.4	376	[23]
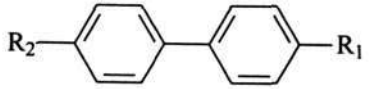	$SO_2C_4F_9$	OMe		8.2	6.3	310	[24]
	NO_2	OMe		9.2	4.5	332	[12]
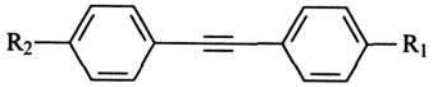	$SO_2C_6F_{13}$	OMe		10.7	6.8	334	[24]
	NO_2	OMe		14	4.4	356	[12]
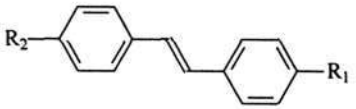	$SO_2C_6F_{13}$	OMe		14	7.8	347	[13]
	NO_2	OMe		28	4.5	364	[13]

Table 2-2 continued

Structure	R_1	R_2	R_3	$\beta_0 \times 10^{30}$ (esu)	μ (D)	λ_{max}	Ref
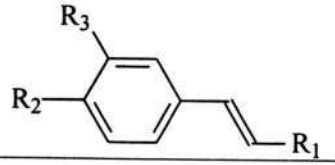	NO_2	NEt_2	F	58	6.8	274	[22]
	NO_2	NEt_2	H	60	8.0	282	[22]
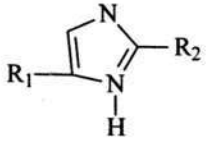	$SO_2C_4F_9$	MeOPh		1.8	6.0	282	[24]
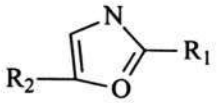	$SO_2C_4F_9$	MeOPh		7.1	5.1	312	[24]
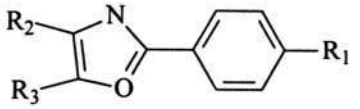	C_6F_{13}	MeOPh	MeOPh	7.2	5.7	344	[25]
	$SO_2C_4F_9$	MeOPh	MeOPh	13.4	7.9	378	[25]
	CF_3	MeOPh	MeOPh	4.2	5.3	338	[25]
	NO_2	MeOPh	MeOPh	18.9	6.3	390	[25]
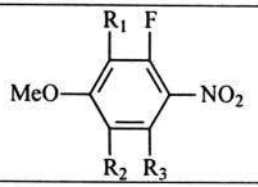	H	H	H	2.5	4.4	304	[23]
	H	F	H	2.5	4.9	304	[23]
	F	F	F	1.7	4.2	270	[23]

Table 2-2 continued

Structure	R_1	R_2	R_3	$\beta_0 \times 10^{30}$ (esu)	μ (D)	λ_{max}	Ref
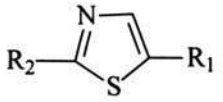	$SO_2C_4F_9$	MeOPh		8.0	6.0	338	[24]
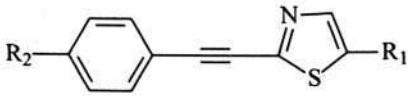	$SO_2C_4F_9$	OMe		13.1	7.4	358	[24]
	NO_2	OMe		14.2	5.9	382	[24]
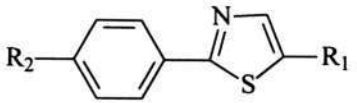	$SO_2C_4F_9$	OMe		8.0	6.0	338	[24]
	NO_2	OMe		17.8	5.4	378	[24]
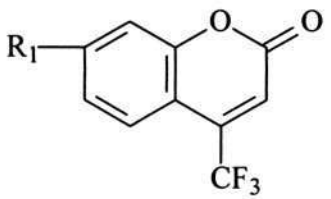	NH_2			9.0	4.59	358	[22]
	NMe_2			10.6	5.71	392	[22]
	NHEt			12.6	5.59	378	[22]
	NEt_2			15.7	6.07	400	[22]

Jen [28] reported that the incorporation of chromophore based on perfluoroaryldicyanovinyl electron acceptors into polyquinoline as a guest led to both high electro-optical property and low optical loss. Recently, Qin [29] synthesized a series of new aryhydrazone chromophore containing pentafluorophenyl as electronic acceptor (Figure 2-4). It was found that the new chromophores exhibited significantly blue-shifted absorption in comparison with the corresponding 4-nitrophenyl analogues: 87 nm for 2a; 92 nm for 2b; 91 nm for 2c and 32 nm for 2d, while keeping the hyperpolarizability in the same order. UV-Vis absorption phenomena of 2a-2d highlight the unusual structure and properties of pentafluorophenyl acceptor and indicate that the pentafluorophenyl group as the electron acceptor gives rise to better transparency. Jen [30] also synthesized a 3-D shape NLO chromophore encapsulated by highly-fluorinated dendrons as shown in Figure 2-5. It was found that, in comparison with its analog, it displayed a large (~30-40 nm) blue shifts of the λ_{max}, and 20 °C higher decomposition temperature (Td 265 °C). And blue-shifted λ_{max} and high content of C-F bond can also contribute to the material's lower optical loss at 1.3 and 1.55 μ m, the two-operation wavelengths of telecommunication. As the chromophore was doped into amorphous polycarbonate, the optical loss of the materials was only around 0.65 and 0.85 dB cm^{-1} 1.3 and 1.55 μ m and the EO coefficient at 1.3 μ m is about 30 pm/V. Although it exhibited good properties, the nonlinearity decayed fast due to orientational relaxation, which limits the application. From the structures of these fluorinated chromophores, it can be concluded that these fluorinated chromophores have fewer reactive functional groups and so it is difficult to incorporate them into polymer through covalent bond. Guest-host NLO polymer materials have some fatal disadvantages such as the fast decay of NLO activity due to orientational relaxation. This significantly limits their applications in optoelectronic

and photonic devices. Furthermore, the effects of fluorine and fluorine position on the structures and properties of the chromophores and NLO polymer are rarely investigated. Therefore, it is very necessary and important to study the effects of the fluorine and fluorine position in detail and understand the mechanism for the development of the NLO polymers.

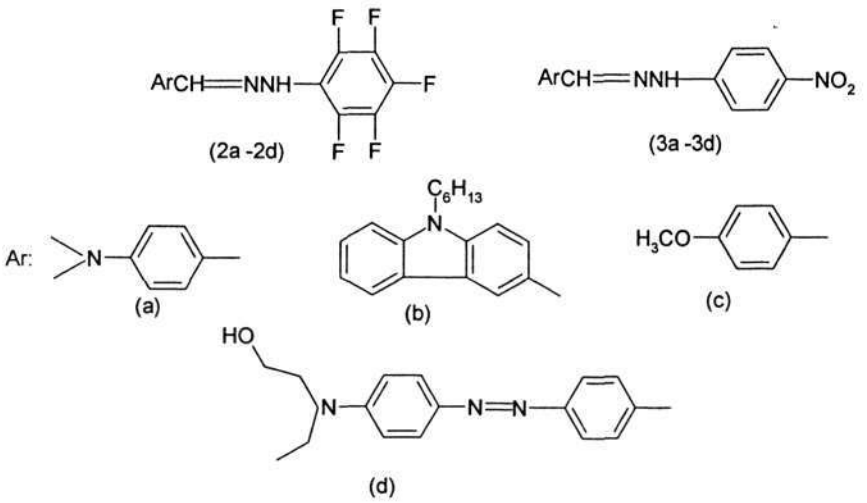

Figure 2-4 The chemical structure of 2a –2d and its 4-nitrophenyl analogues (3a-3d)

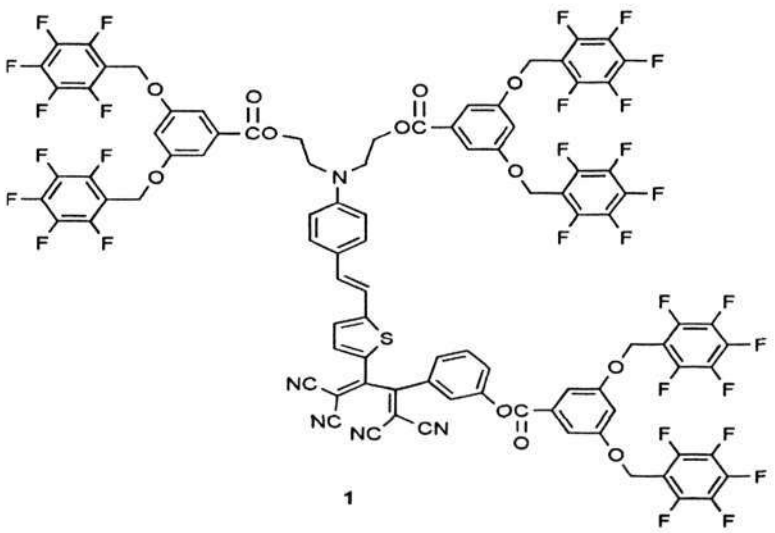

Figure 2-5 The chemical structure of fluorinated dendritic NLO chromophore [30]

2.2.3 Second-order NLO Polymers

Second-order NLO polymers can be classified into four types according to the approach for the incorporation of NLO molecules into polymers. The simplest one is the doping of the NLO molecules into a polymer matrix forming a guest-host system. Alternative methods are the covalent linking of the molecules to a polymer backbone in the form of a side-chain, main-chain or their cross-linking between two polymers. Figure 2-6 depicts schematically these four types of NLO polymers and Table 2-3 summarizes their advantages and disadvantages [31].

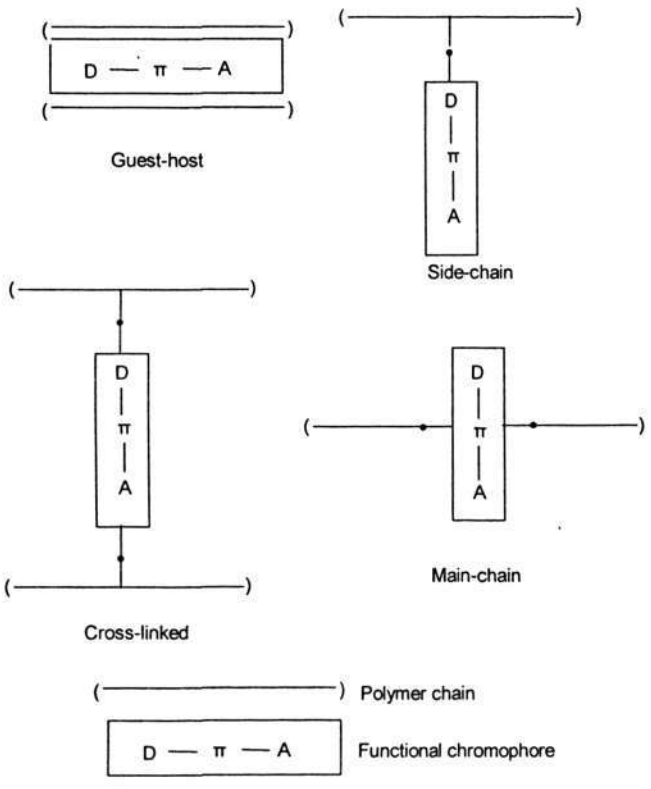

Figure 2-6 Types of NLO polymers

Table 2-3 Advantages and disadvantages of the different types of NLO polymers [31]

Polymer Type	Advantages	Disadvantages
Guest-host	Unlimited selection of desired NLO guests and polymer hosts Easy thin-film processing Inexpensive mass production	Decay of NLO activity due to orientational relaxation Low NLO activity due to limited solubility of NLO molecules in polymer matrix Scattering losses due to inhomogeneity Sublimation of NLO molecules at elevated temperature
Side-chain	High concentration of NLO molecules Tailoring of NLO properties via chemical modification Increased orientational stability Low scattering losses	
Main-chain	High concentration of NLO molecules Tailoring of NLO properties via chemical modification Increased orientational stability Low scattering losses	Molecules difficult to orient to externally applied field Poor solubility
Cross-linked	Tailoring of NLO properties via chemical modification High orientational stability	Increased scattering losses Poor solubility

2.2.3.1 Guest-host System

The earliest second-order NLO polymer system to be investigated was guest-host system. One of the most thoroughly studied guest-host system was PMMA doped with the chromophores [32]. The researchers then focused on the increasing both the susceptibility and the thermal stability of the poling order. A wide variety of chromophores have been investigated as guest in a number of polymer hosts, such as, thermally stable and high T_g polycarbonate, polyimides (PIQ-2200 10, Ultrdel 4212 7, U-100 9) and polyquinolines. However, their nonlinearities were limited because the

chromophore concentration could not reach a high level due to phase separation and the stability of the poling order was low because of the plasticization effect of small chromophore molecules in the polymer. These fatal disadvantages of guest-host systems limited their actual application.

2.2.3.2 Side-chain System

One of the first side-chain systems studied was a random copolymer of methyl methacrylate and a 4-(dicyanovinyl)-4'-(dialkylamino)azobenzene-substituted methacrylate [33], or DR1-substituted methacrylate [34]. Recently, a new poly[2-(trifluoromethyl) acrylate-methyl vinyl urethane] based on the thiophene-bridge chromophore displayed higher poling stabilities compared with other kind of NLO PMMA [35]. However, their orientational relaxation is still fast due to the low thermal stability of PMMA. High resonantly enhanced $\chi^{(2)}$ values were reported for a polyester polymer with Disperse Red 19 side group [36], where the dye concentration was 68%. Ye [37] synthesized a side-chain polymer having a strong hydrogen-bonded network by partially functionalizing poly (p-hydroxystyrene) with the tosylate of N-(4-nitrophenyl)-(l)-prolinol. The poling stabilities of these side-chain polymers were significantly improved by the hydrogen-bonded network. A highly functionalized side-chain and high T_g thermoplastic polymers were synthesized such as poly (2,6-dimethyl-1,4-diphenylen oxide) (PPO) [38], polyamides [39,40], polyurethanes [41-42], polysiloxanes and polyphophazenes [43-44]. The most common polymers for side-chain systems are polyimides, as they have thermal stabilities such as higher glass transition temperatures, which will be discussed in details in section 2.3. In most cases, these side-chain polymers have this advantage so that a high concentration of NLO

chromophore can be incorporated into the polymer system through covalent bond without crystallization, phase separation, or the formation of concentration gradients. In addition, the relaxation of poled order might be expected to substantially slower because motion of the chromophore is hindered by its attachment to the polymer. Due to many advantages of side-chain NLO polymer, the side-chain NLO polymer especially high T_g polymer, such as polyimide, has attracted much attention nowadays.

2.2.3.3 Main-chain System

Main chain polymers are comprised of chromophores or majority of the chromophore linked in the backbone through the end of the chromophore. The earliest studied main-chain polymers consisted of chromophores with their dipole moments oriented "head-to-tail" along the polymer chain [45-49]. Main-chain epoxy polymers in which the dipole moment of the NLO chromophore is perpendicular to the polymer chain were also synthesized [50-51]. After that, a series of main-chain NLO polyurethanes [52] and polyester containing azobenzene mesogens in the main chain [53] have been synthesized. The major drawbacks for main-chain polymer, the low poling efficiency and nonlinearity, seriously limit their application and these days researchers show little interest in it.

2.2.3.4 Cross-linked System

Epoxy resins are the most intensively investigated classes of thermosetting materials [54-57]. Epoxy resins for second-order NLO polymer application may be roughly classified: (1) the use of difunctional epoxides and NLO diamines [58], (2) materials formed from polyfunctional epoxides and NLO diamines [59]. Besides epoxy resins, other NLO-

containing thermosetting polymers such as polyurethanes [60] and polyacrylonitrile [61] have been described recently. Jen [62] developed a novel post-crosslinked polymer system through the Diels-Alder cycloaddition reaction. Cross-linking can also be accomplished by photochemical reaction other than thermally induced reaction [63-66]. Cross-linked system increases the stability because cross-linking can reduce the free volume and increase chain entanglement in the polymer matrix. However, it should be noted that there is often a price to be paid for restricting polymer mobility by cross-linking in terms of polymer insolubility, light scattering, shrinkage, adhesion problems and embrittlement, which could result in large optical loss and their applications were limited. Therefore, research work has concentrated on how to improve their cure process and properties. To date, less success has been reported.

2.2.3.5 Sol-gel System

The sol-gel methodology (Figure 2-7) has been widely used in the processing of optical materials and was incorporated into the preparation of NLO materials Because it allows low-temperature fabrication of networks facilitating the introduction of organic chromophores and the resulting hybrids possess low beam propagation loss, refractive index control of films and ease of device fabrication [67-69].

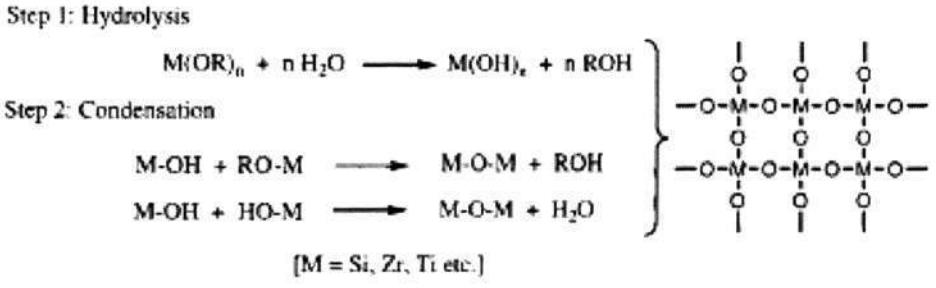

Figure 2-7 Traditional sol-gel methodologies

Sol-gel based NLO materials can be divided into two classes. Class 1 is the guest-host matrix, for example, methylnitroaniline trapped in an aluminum oxide matrix [70] and N-(4-nitrophenyl)-(s)-prolinol doped in a SiO_2-TiO_2 network [71], and DR1 doped into PMMA first and then mixed with tetraethoxysilane (TEOS) [72]. Similar with guest-host system, their applications were also limited.

Class 2 includes the side-chain tethered hybrid materials and main-chain embedded hybrid materials. A typical reaction sequence for the synthesis of such a hybrid is shown in Figure 2-8 [73]. NLO-active chromophores are designed to have one reactive end group and are covalently attached to a polymerizable silane to yield a precursor, which can be copolymerized with TEOS under sol-gel hydrolysis/condensation processing conditions to yield hybrid materials. A number of inorganic-organic hybrid materials were prepared using several chromophore-grafted silane precursors with moderate success in achieving high and stable nonlinear optical coefficient [73-79]. Choi [76-77] prepared sol-gel materials by linking 4'-[(2-hydroxyethyl)methylamino]-4-nitrostilbene or 4'-[(6-hydroxyhexyl)methylamino]-4-nitroazobenzene to 3-isocyanatopropyltriethoxysilane and condensation. They exhibited d_{33} of 20~44 pm/V at the 1064 nm and 20-24% decay of the second harmonic signal was observed over 1 month at ambient temperature. Jeng [79] mixed prepolymers of melamines and an alkoxysilane-functionalized dye in aid to enhance compatibility between the organic and inorganic phase and thus reduce phase separation. These films exhibited 10~54 pm/V and ~ 60% d_{33} value were retained after heating at 100 °C for 250 hours. Sung [80] and Kim [81] prepared NLO hybrid materials based on trifunctional chromophore, respectively. However, one of the major issues with side-chain-tethered sol-gel second-order NLO materials is the low temporal stability of the SHG signal because the chromophore was linked the hybrid through single bond.

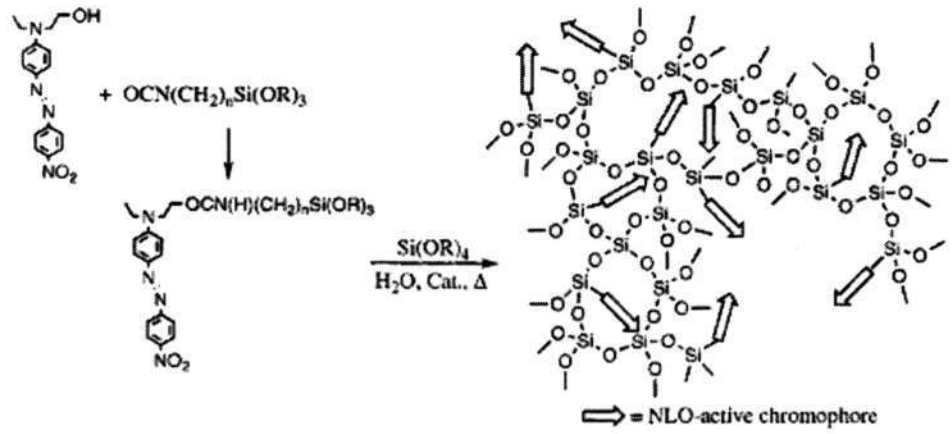

Figure 2-8 Chromophore-linked-side-chain-tethered-hybrid [73]

In the sol-gel process, the catalysts were often used, which led to inorganic and organic phase separation. Therefore, Jiang [82-83] developed a new approach for preparing hybrid materials using aminosilanes as network-forming reagents and NLO-active chromophores without catalysts. Although the property of covalent-tether sol-gel system was improved, the stability of sol-gel is still lower than the requirement of actual application and the brittlement of the film is large. These disadvantages limit their applications. However, it is worth noting that the fabrication of amorphous three-dimensional optical networks can be carried out at low temperature. Therefore, incorporation of the advantages into the mature organic polymer system could improve the good comprehensive properties of sol-gel systems.

2.2.4 Poling Methods

In order to obtain second-order NLO properties, polymer films need to be made with the required noncentrosymmetry, which is usually achieved by poling method. There are mainly three poling methods used at the present, thermally assisted poling [84], photoassisted poling [85] and all-optical poling [86].

Thermally assisted poling involves heating of the sample, applying a high electric field for a certain time and subsequently cooling of the sample back to room temperature and removing the field. This method has been widely studied. Several approaches of electrodes poling have been used to induce this polar order, such as interdigitated and coplanar electrodes [87-88] Interdigitated and coplanar electrodes methods are limited by charge injection processes at regions of high electric field near the sharp electrode edge [88-91].

Perhaps the most commonly used electric field poling method is corona poling [92-94]. A typical corona-poling setup is illustrated in Figure 2-9 [92]. A sharp needle, wire, or grid is charged to several kilovolts until electric breakdown of the surrounding atmosphere occurs. Depending on the polarity of the corona needle, either positive or negative ions can be deposited on the surface of the polymer film. Fields across the polymer film exceeding 4 MV/cm can be obtained in this way [94]. Such high fields are very difficult to achieve using electrode poling. It was found that the positive corona tends to more stable than the negative corona [93].

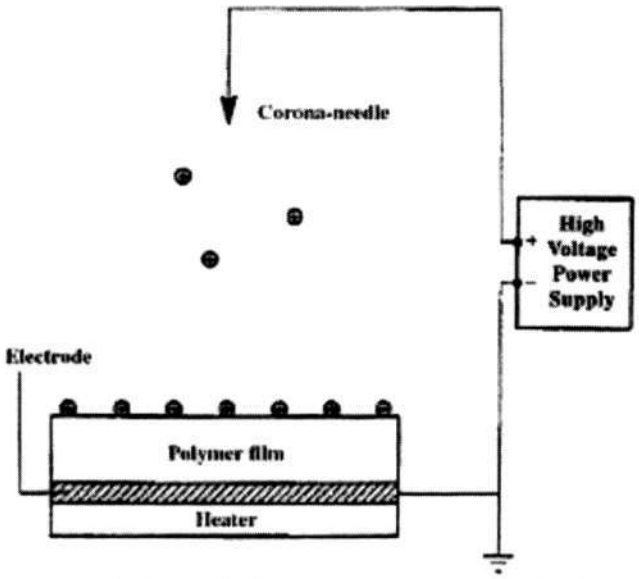

Figure 2-9 A typical setup for corona poling [92]

Alternatively, two optical methods have been developed for poling chromophores at room temperature or at temperatures much lower than T_g. For photoassisted poling, the noncentrosymmetry is achieved by applying a small dc electric field during irradiation. All-optical poling is a new method for producing second-order NLO effects in an initially isotropic material [95] and can only be used for the special chromophore, which can have trans↔cis isomerization easily. Therefore, corona poling will be adopted in our experiment due to high electric field strength, simple experimental setup and wide applications.

2.2.5 Measurement Techniques for Second-order NLO Effect

2.2.5.1 Measurement Techniques of Molecular Hyperpolarizability

Various techniques have been employed in the past for the measurement of molecular hyperpolarizabilities. The techniques that are commonly used are electric field-induced second-harmonic generation (EFISH) [96-98], solvatochromic method [99-104] and the hyper-Rayleigh scattering (HRS) [105]. To obtain β values from EFISH measurements, the molecular ground-state dipole moment must be known and the cubic hyperpolarizability γ must be negligible or otherwise determined. Moreover, only the component of the vectorial part of the tensor β along the dipole moment direction is obtained. This method still needs costly equipment, and a trained operator. Therefore, it is not widely used. The main drawback of HRS is the low signals due to the incoherent nature of the scattered light [106-107]. Moreover, the possible interference of fluorescent emission can lead to erroneous result. Therefore, it was only widely used for the octopolar molecules and ionic molecules.

Solvatochromic measurement was first applied with a certain success to a series of small dipole organic molecules by Paley [99] and later to more complex molecules by other authors [108-112]. It was based on the effect of a solvent on the position, shape, and intensity of absorption and emission bands of molecules with respect to their vapor-phase properties. The light absorption frequencies of dipolar molecules depend on the solvent polarity and the solvent dependent shift. The hyperpolarizability is calculated through the quantum-mechanical two-level model [11]. The experiments are relatively easy laboratory experiments and data can be quickly analyzed and readily fed back for the next research iteration. Moreover, the solvatochromic method provides also an interpretation of the magnitude of the quadratic hyperpolarizability, in terms of frequency, intensity and assignment of the electronic transitions, which are involved in the second-order NLO response. At present this is the most widely used method.

2.2.5.2 Techniques for Determination of Second-harmonic Generation

A variety of experimental techniques have been used to obtain both absolute and relative values of the second-order susceptibility. The absolute methods include phase-matched second-harmonic generation [113], parametric fluorescence [114-115], and Raman scattering [116]. The second-harmonic powder test, the wedge technique [117] and the maker-fringe method [118] are relative methods. For second-order NLO polymer systems, the maker fringe second-harmonic generation technique is the most widely used method. Jerphagon and Kurtz (JK) have described this method in detail [118]. This technique is illustrated in Figure 2-10 [118]. In this method, a plane-parallel slab of material is rotated about an axis perpendicular to the laser beam, giving rise to a fringe pattern. The fringes are caused by the angular dependence of the

phase mismatch between the forced and harmonic waves. In these experiments the SHG intensity from the second-order NLO polymer film is measured relative to the intensity of a reference material, often quartz. The most frequently used value of d_{11} for quartz is 1.2×10^{-9} esu (0.5 pm/V) measured at 1.064 μm [119].

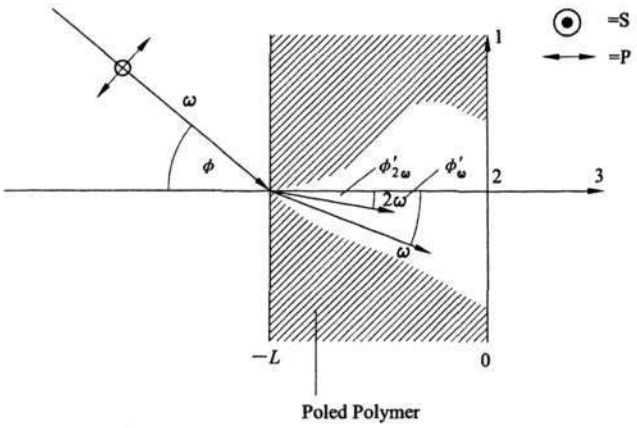

Figure 2-10 Maker fringe technique for poled polymers. The fundamental light beam at frequency ω is incident at an angle ϕ on the polymer film of thickness L (poled along axis 3). The angles of the fundamental and second-harmonic beams inside the polymer are given by ϕ'_{ω} and $\phi'_{2\omega}$ respectively [118]

2.2.6 Application in Photonic Devices

Inorganic crystals such as lithium niobate are expensive and difficult to fabricate into electronic devices. These polymeric materials are more adept at manipulating light than inorganic crystals because they are less expensive, easier to prepare, process and integrate with semiconductor electronics and fiber transmission lines. These advances have created a considerable interest in the commercialization of polymeric electro-optic materials. Polymeric electro-optic materials are now being evaluated for applications such as phase array radar, satellite and fiber telecommunication, cable television, optical gyroscope, electronic counter measure system, backplane interconnects for high-speed computers, ultrafast (100 Gbit/s) analog-to-digital (A/D)

converters, land mine detection, radio frequency (rf) photonics, and spatial light modulators. Polymeric materials will have a major impact on telecommunication, data storage, computing and optical signal processing.

Some prototype NLO devices based on polymeric materials have been developed in several companies and academic institutes. it was reported that an electro-optic polymeric phase modulator with an electrical bandwidth of 113GHz was fabricated at the University of California Los Angeles [120]. A typical polymeric channel waveguide structure for second-harmonic generation and polymeric Mach-Zehnder interferometric electro-optic modulator are shown in Figure 2-11 and Figure 2-12, respectively [31].

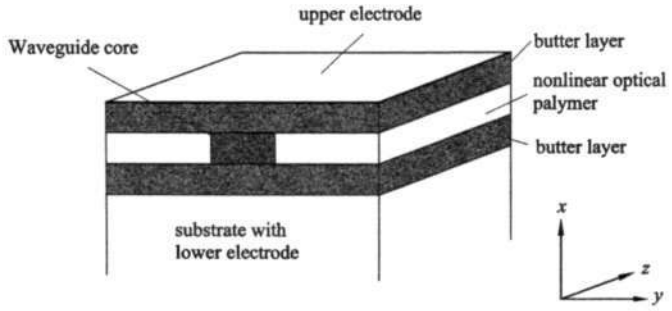

Figure 2-11 Polymeric channel waveguide geometry for second-harmonic generation [31]

The application of NLO polymers, which has turned out to be the most important one in the last few years, is their use as electro-optic waveguide modulator. The EO modulators are needed in telecommunication applications to transmit information through an optical fiber at very high bit rates. In order to reach bit rates of gigabits or terabits per second, it is necessary to develop modulators having a bandwidth of 100 GHz or more. It is not yet possible for inorganic materials, such as lithium niobate, to fulfill the task because of their high dielectric constants. The materials commercially

used for electro-optic modulators reach up to 20GHz. And it was demonstrated that electro-optic modulators from inorganic materials could reach the cost-effective limits of 75GHz by choosing special modulator electrode arrangement. However, from the material point of view, such high bandwidth is easily possible because of the subpicosecond response time of the electro-optic effect and low dielectric constant in organic materials. Most work in the field of EO modulators is performed using so called Mach-Zehnder interferometric structures. In summary, the second-order NLO polymeric materials with the best comprehensive properties is expected to be widely used and have large potential market value.

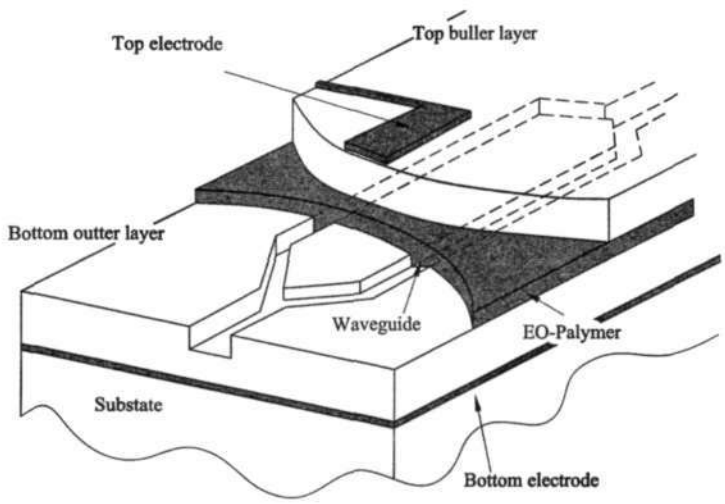

Figure2-12 A typical polymeric Mach-Zehnder interferometeric electro-optic modulator [31]

2.3 Second-order NLO Polyimide

2.3.1 Introduction of Polyimide

Aromatic polyimide, one of the most highly stable polymers, was first produced in

1908 by Marston Bogert through polycondensation of ethers or anhydride of 4-aminophthalic acid. In 1955, high molecular weight products were synthesized by two-stage polycondensation of pyromellitic dianhydride with diamine [121]. Since then, researcher interest in this class of polymers has been growing steadily because it possesses a number of valuable physic-mechanical, thermal, chemical and photochemical stability. Prolonged use of polyimides is possible at temperature of up to 200 °C, and short–term heating at temperatures up to 480 °C. Therefore, polyimides have been widely used in microelectronics processing of VLSI circuits.

Conventionally, polyimide synthesis is carried out by the polycondensation of a dianhydride and a primary diamine via a poly (amic acid) precursor. Subsequent thermal or chemical treatment converts the poly (amic acid) to polyimide (Figure 2-13) [122]. The chemical structures and abbreviations of some dianhydride and diamine monomers are presented in Table 2-4 [122]. Due to the rigid ladder structure systems, polyimides usually have glass translation temperature above 300 °C, which are much higher than that of the most other polymers. Table 2-5 lists the glass translation temperatures and decomposition temperatures of typical polyimides reported in literature [122].

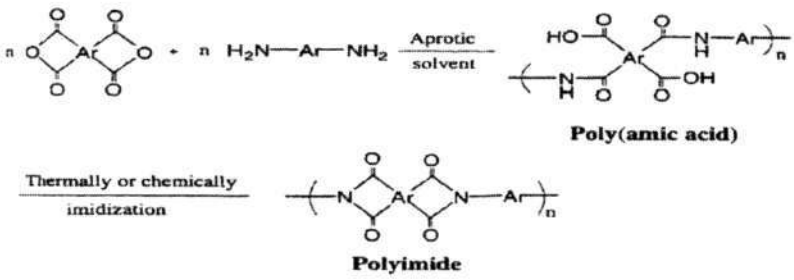

Figure 2-13 The scheme of two step synthesis of polyimide [122]

Table 2-4 Monomers commonly used in polyimide synthesis [122]

Dianhydride	Diamine
Pyromellitic dianhydride (PMDA) 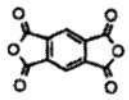	1,4-Phenylene diamine (PDA) 
Oxydiphthalic anhydride (ODPA) 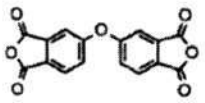	4,4'-Oxydianiline (ODA) 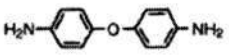
3,3',4,4'-Benzophenone-tetracarboxylic dianhydride (BTDA) 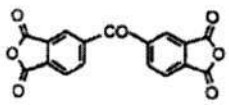	4,4'-Diaminobenzophenone (DABP) 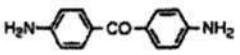
4,4'-(Hexafluoroisopropylidene)-diphthalic anhydride (6FDA) 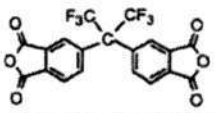	4,4'-Diaminodiphenyl sulfone (DDS) 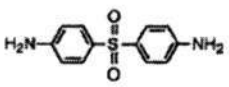

Table 2-5 Glass transition temperature (T_g) and decomposition temperature (T_d) of typical polyimide [123]

Polyimide	Dianhydride	Diamine	T_g (°C)	T_d (°C)
1	PMDA	PDA	---	529
2	PMDA	ODA	399	519
3	OPDA	PDA	342	529
4	PMDA	DABP	412	---
5	BTDA	PDA	333	---
6	6FDA	DDS	319	---
7	6FDA	PDA	338	500

Researchers have concentrated on polyimide ever since chromophores were first incorporated into polyimide [123], because a higher glass transition temperature in a NLO polymer system will result in improved temporal stability of optical nonlinearity.

2.3.2 Research Progress on Second-order NLO Polyimide

2.3.2.1 Guest-host Polyimide

Wu [123] first synthesized the guest-host second-order NLO polyimide through doping Eriochrome Black T (3-hydroxy-4-[(1-hydroxy-2-naphthalenyl)azo]-7-nitro-1-naphthalenesulfonic acid monosodium salt) into a kind of polyimide, Pyralin 2611D. Then, DR1 was doped into Poly(amic acid) LQ-2200（Hitachi） and obtained better results than other kinds of guest-host polymers [124]. Hence, more research work was concentrated on the guest-host polyimide[1, 125-126]. Singer [1] reported that the films exhibited 4.9 pm/V of d_{33} value, optical loss of 13.3 and 9.3 dB/cm in TE and TM model, respectively and keep 60% of d_{33} value after heating 300 hours at 80 °C. The optical loss was studied and the results indicated that the mechanism for the high loss seen in these polyimide waveguides was mainly from the absorption tails of both chromophore and the polyimide host. Ermer [127] reported the development of the first all-polyimide system (cladding/core/cladding) suitable for fabrication of electro-optic waveguide devices on silicon substrates. And dye-doped second-order NLO polyimide thin films were also prepared via real-time poling vapor co-deposition process [128]. Some chromophores doped in polyimide are shown in Figure 2-14. Second-order NLO $LiNbO_3$ and $BaTiO_3$ were doped into polyimide through in-situ polymerization of polyimide and gelation of $LiNbO_3$ and $BaTiO_3$ [129]. Compared

with other kinds of guest-host polymers, their thermal stability was higher. However, they could not change the intrinsic disadvantages of the guest-host kind polymer, such as fast decay of nonlinear optical activity due to orientational relaxation, low nonlinear optical activity due to limited solubility of nonlinear optical molecules in polymer matrix and larger scattering losses due to inhomogeneity. Thus, researchers have become less interested in the guest-host polyimide due to the fatal drawbacks of guest-host polyimide.

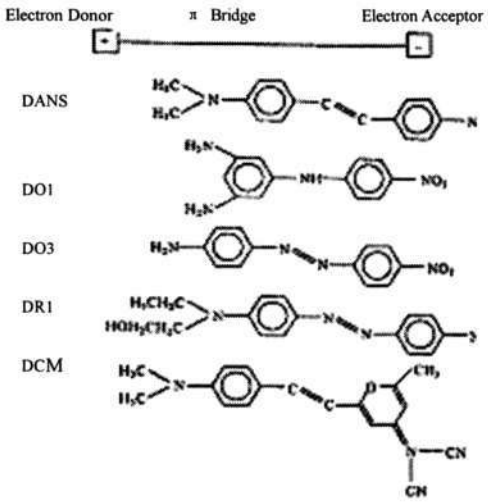

Figure 2-14 Some chromophores doped in polyimide

2.3.2.2 Side-chain Polyimide

In 1992, Lin [130] synthesized the side-chain polyimide, which attracted more research interest. There are mainly two kinds of methods for synthesizing the side-chain polyimides. In first method, the side-chain NLO polyimide was synthesized through the condensation polymerization of the monomer containing chromophore, such as diamine or dianhydride containing chromophore with other monomers. In this method, synthesis of the NLO monomers is the key step. The monomers containing

chromophore should have high thermal stability, high hyperpolarizability and low absorption at application wavelength. Sotoyama et al [131] synthesized NLO polyimide film through a dianhydride containing chromophore, which showed EO coefficient γ_{33} of 10.8 pm/V at λ = 1.3 μm, λ_{max} around 480 nm and 90% of the initial γ_{33} value retained after more than 200 hours at 120 °C. Jung et al [132] synthesized side-chain NLO polyimide Langmuir-Blodgett film through dianhydride containing chromophore, which showed to be thermally stable to 240 °C and λ_{max} of 650 nm. However, its NLO property was not reported. An alternate soluble NLO polyimide was also synthesized through a chromophore-containing dianhydride [133]. The d_{33} of the polyimide is 27-34 pm/V at 1064 nm and nonresonant d_{33} (∞) is 7-10 pm/V because of their λ_{max} around 435 nm near the double frequency 532 nm. Recently, some photocrosslinkable side-chain NLO poly(ester imide)s were synthesized through a dianhydride bearing azo chromophore and obtained γ_{33} of ~11.5 pm/V at 650 nm, λ_{max} of 468~475 nm and high thermal stability of the NLO chromophore alignment at 120 °C [134-135]. Because dianhydride containing chromophore has less stability than diamine containing chromophore and was more difficult to prepare, most research has concentrated on synthesis of the diamine containing chromophore.

Yu et al [136-140] synthesized a series of diamines containing chromophore whose structures are shown in Figure 2-15, and the properties of the NLO polyimide film are listed in Table 2-6. These polyimide films exhibited high thermal stability and temporal stability of d_{33} value and large resonant enhanced d_{33} value (46-169 pm/V). However, it should be noted that from the approximate two-level mode, the nonresonant value d_{33} (∞) were evaluated to be ~ 18 pm/V. This indicates that the major component in the d_{33} (532 nm) was from the resonant contribution, which is not a desired properties, due to their

λ_{max} (383-532 nm) near 532 nm. Burland et al [9,141] synthesized donor-embedded NLO side chain polyimides, which is of the highest stable NLO polyimide and can meet the stability of application requirement. However, they displayed γ_{33} of 4-7 pm/V at 1305 nm. A new type of soluble calix[4] arene-based polyimides was synthesized, which is highly transparent above 410 nm (λ_{max} = 292 nm), but exhibits small d_{33} value of 2.3~4.0 pm/V at 1064 nm [142]. Ueda et al [143] synthesized positive-working alkaline developable photosensitive NLO polyimide (λ_{max} = 500 nm). And Yin et al [144] synthesized novel NLO copolyimides possessing direct photolithographic features from chromophore-containing diamine. Jung [145] and Davey [146] developed new series donor-embedded side-chain polyimide, respectively. The donor-embedded side-chain polyimide containing no flexible connectors displayed higher thermal stability and negligible decay in response upon aging in air at 100 °C for over 1000 hours. Kaatz [147] studied the relaxation process in NLO side-chain polyimide and found the nonexponential relaxation can be modeled by the Kohlrausch-Williams-Watts function and the nonlinear relaxation can be modeled in terms of Tool-Narayanaswamy of glassy state. And Jung [148] investigated the orientational changes of NLO chromophore side chain in polyimide LB films. As reviewed as noted, second-order NLO polyimides prepared from this method are highly stable. However, they all exhibit larger λ_{max} and lower transparency. Although the d_{33} value was larger, non-resonant d_{33} value was not large and part of the d_{33} value was from resonance absorption because the λ_{max} was near 532 nm. Furthermore, the method involves a harsh imidization so that the monomer containing chromophore could be damaged. The higher imidization temperature could also increase the probability of chromophore decomposition. Therefore, how to improve the transparency and lower the imidization temperature without sacrificing stability is major challenge in the development of the side-chain polyimide.

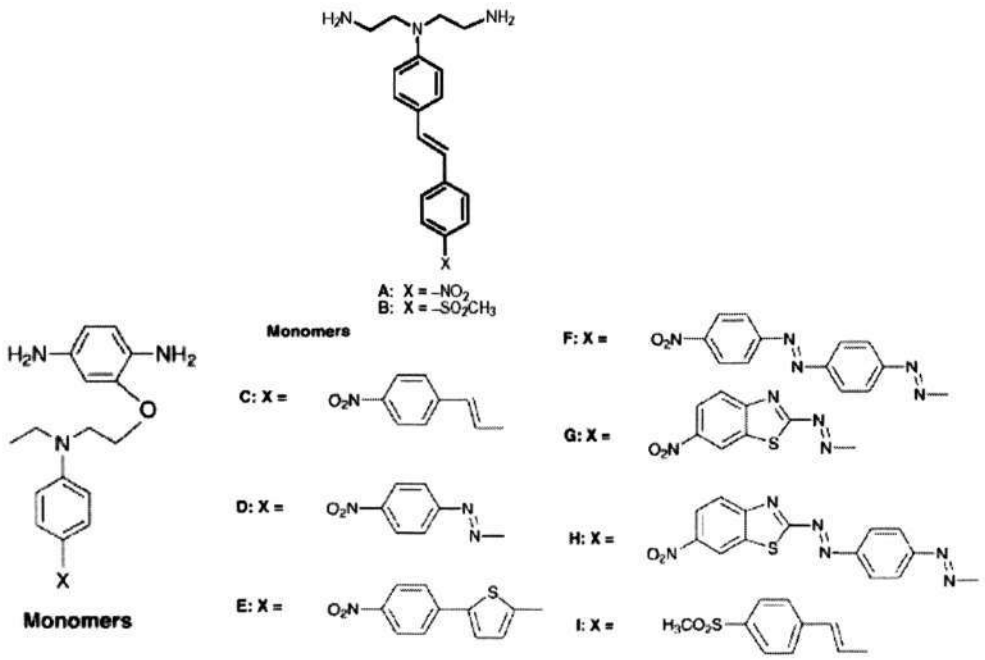

Figure 2-15 Diamine bearing chromophore synthesized by Yu [136-140]

Table 2-6 Compositions of Polyimides and their properties (a: At 1300nm) [136-140]

Polymer	Dianhydride	Diamine	T_g	T_d	$d_{33}^{(532nm)}$ pm V^{-1}	$\gamma_{33}^{(780nm)}$ pm V^{-1}	λ_{max}/nm
1	BTDA	B	209	420	61	4	385
2	BTDA	D	-	303	59	7	490
3	BTDA	I	230	327	46	4	383
4	PMDA	A	230	340	115	23	438
5	PMDA	B	250	437	61	5	372
6	PMDA	D	-	291	69	7	470
7	PMDA	I	240	367	51	5	383
8	6FDA	C	229	321	146	24[a]	440
9	6FDA	D	235	319	169	25[a]	477
10	6FDA	E	227	322	103	24	445
11	6FDA	F	218	300	-	35[a]	505
12	6FDA	G	200	289	-	30	532

The second method is the post-reaction method. First, the soluble polyimides were synthesized. Then, the chromophores were incorporated into the polyimide through reaction with the functional group in the polyimide such as Mitsunobu reaction or post-azo reaction. New side-chain soluble polyimide bearing DR1 groups was synthesized through Mitsunobu reaction between DR1 and the hydroxyl group in the polyimide backbone [149]. They displayed d_{33} of 60 pm/V at 1064 nm, λ_{max} of 510 nm and 15% of d_{33} loss after 10 hour at 100 °C. Rousseau et al [150] also incorporated DR1 into different structure polyimide using the same method. The polyimide films had d_{33} of ~30 pm/V at 1320 nm, λ_{max} around 510 nm and keep moderate thermal and temporal stabilities of the NLO properties. The typical synthesis schemes are shown in Figure 2-16. Samyn [151] and Do [152] incorporated a series of NLO chromophores containing hydroxyl group into polyimide through Mitsunobu reaction. They showed λ_{max} around 400~500 nm, moderate d_{33} or γ_{33} and their thermal and temporal stabilities. Recently, a side-chain dendronized NLO chromophore was incorporated into polyimide structure via Mitsunobu reaction [153]. They displayed λ_{max} of 711 nm, large E-O coefficient 71 pm/V at 1.3 μm and more than 90% of this value can be retained at 85 °C for more than 650 hours. Shen et al [154] reported that two series of poly(amic acid) were synthesized with different NLO chromophores using the post-azo coupling reaction in dimethyl formamide, which displayed d_{33} of 19.5~50.4 pm/V at 1064 nm, λ_{max} of 471~630 nm and retained 50% of the original d_{33} value after 1000 hours at 100 °C. The post-azo reaction scheme is shown in Figure 2-17. A processable NLO polyimide was prepared through the aldehyde group in the polyimide reacted with methanesulfonylacetonitrile [155]. Lee [156] incorporated the tricyanovinyl group into the polyimide through thiophene group in the polyimide

reacted with tetracyanoethylene. And the NLO polyimide copolymers were synthesized through the 2,2'-bipyridine coordinated with nickel malenonitriledithiolate inorganic chromophores [157]. Some NLO octopolar chromophore and muti-octopolar tri(bipyridine) ruthenium complex were also incorporated into polyimide through coordination with bipyridyl in the backbone of PI [158-159]. They displayed λ_{max} 440~520 nm, ~ 1300 × 10^{-30} of β_{zzz} esu at 1.91 μm and high thermal stability. In summary, the NLO polyimides through the post-reaction have a large second harmonic coefficient because this approach allows some flexibility in the selection of the polymer backbone and the chromophore. Although the NLO polyimides through the post-reaction avoid harsh imidization conditions, the stability such as thermal stability or solvent resistance decreased because the NLO chromophore was incorporated into polyimide only through a single bonding site which can reduce the orientational stability at high temperatures. And the drawback of transparency was still not removed.

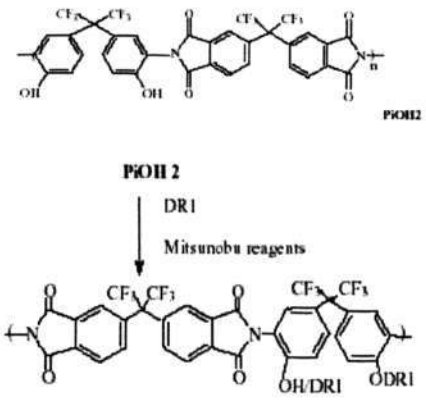

Figure 2-16 Reaction schemes for the synthesis of the NLO polyimide through Mitsunobu reaction [150]

Formatted: Not Expanded by / Condensed by

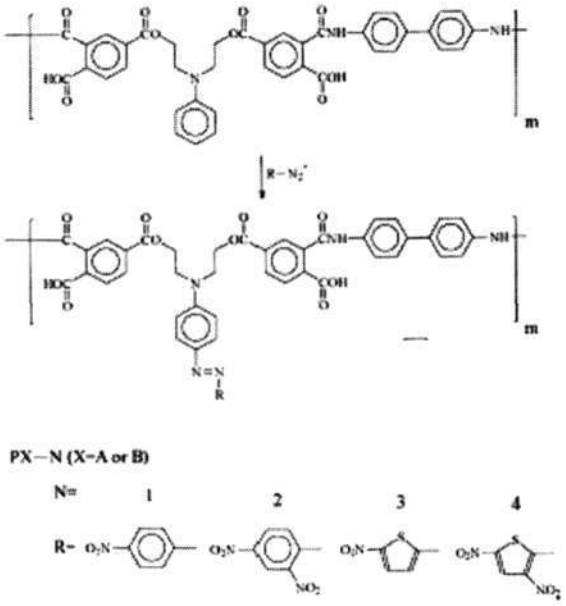

Figure 2-17 Post-azo reaction schemes for the synthesis of the NLO polyimide [154].

Formatted: Not Expanded by / Condensed by

In addition, one-step polymerization between a NLO chromophore-containing diol and a diimide compound via Mitsunobu reaction was reported [160-161]. They gave resonant-enhanced nonlinearities and smaller nonresonant nonlinearities due to their λ_{max} around 427-489 nm near 532 nm. The Stille coupling reaction was also explored to synthesize side-chain NLO polyimide, which exhibited γ_{33} of 35 pm/V at 1300 nm, λ_{max} of 540 nm and retained ~82% of SHG signal at 80 °C [162]. And some NLO homo- or co-poly (urethane-imide) s were prepared through isocyanate containing DR19 [163-164]. There is no need to synthesize NLO-diamine or dianhydride monomers through one-step method. However, this method can only be used for some special monomer. And the polyimides have small molecular weight due to the limitation of reaction conditions.

2.3.2.3 Cross-linked Polyimide

Cross-link bond can increase the stability of the polyimide. There are two methods for

preparation of cross-linked polyimide system, thermally cross-linked and photochemical cross-linked method. Tripathy [165] synthesized a thermally cross-linked NLO polyimide through the reaction between polyimide containing reactive end group and a kind of functionalized silicon dye (ASD) as a cross-linking agent. The polyimide exhibited 17.8 pm/V of d_{33} value at 1064 nm, λ_{max} of 450 nm and higher thermal stability due to the Si-O crosslinked network. Both Ye [166-168] and Samyn [169] synthesized homo- or co-poly (maleimide). They also gave moderate d_{33} value at 1064 nm, λ_{max} of 400~500 nm and kept high thermal and temporal stability of NLO signal. Recently, two kinds of maleimide containing chromophores with good thermal stability were incorporated into the bismaleimide polymer matrices to form interpolymer networks [170]. And a full interpenetrating polymer network (IPN) was formed through simultaneous addition reaction of the bismaleimide and crosslinked alkoxysilane dyes. They obtained d_{33} value of 6.9~57.0 pm/V, λ_{max} around 550 nm and high temporal stability. Singer et al [2] prepared a kind of photochemically crosslinkable polyimide containing fluorine in the main chain electro-optic materials. They found that the absorption due to long tails of aromatic charge transfer states including the main chain and the chromophore is the primary source of optical loss in this class of polyimide through photothermal deflection spectroscopy, and incorporation of the fluorine into the main chain of polyimide could decrease the optical loss and index of refraction. Singer et al indicated that the long absorption tails of the chromophores lead to large optical losses even at long wavelength for polyimide containing fluorine in the main chain. The main disadvantages of these crosslinked polyimide are shrinkage and embrittlement.

2.4 Summary

In summary, most of NLO polyimide materials especially side-chain polyimides have good thermal stability and large second harmonic or EO coefficient. However, it

should be noted that the λ_{max} in the UV absorption is basically in the range of 400 ~ 600 nm and their transparency is low. Furthermore, a part of some large d_{33} values at 1064 nm is from the resonant d_{33} because λ_{max} is near to 532 nm, which is not the desired property. The low transparency will limit the applications of NLO polyimides in photonics industry. The results investigated by Singer et al show that the high loss is mainly from absorption by both chromophore and polyimide host because there are many aromatic conjugated structures. For polyimide containing fluorine in the backbone, which reduces intrinsic absorption from polyimide backbone through the reduction of in-plane packing and polymer deformation, the loss is mainly from the chromophore absorption. Therefore, how to reduce the absorption from chromophore is a major problem. The design and synthesis of chromophore with high stability, high nonlinearity and good transparency is important for the development of the polyimide. As is well known, it is difficult to meet all requirements at the same time. And the most difficult thing is to balance the nonlinearity-transparency trade-off. Until now, little progress has been made in synthesizing the molecule with good transparency and high nonlinearity simultaneously. The fluorinated NLO chromophores reported displayed good comprehensive properties especially in transparency. However, the fluorinated chromophore reported cannot be incorporated into the polyimide as side-chain because these fluorinated chromophores lack reactive functionalized groups. The effects of fluorine and fluorine position on the structures and properties of chromophore and NLO polyimide are rarely reported. Hence, the design and synthesis of fluorinated NLO chromophores, which can be incorporated into polyimide as a side chain, maybe new and effective approach to get better comprehensive properties.

Furthermore, the NLO polyimide from monomer containing chromophore involves the hash imidization, which could increase the probability of the chromophore

decomposition and limit their applications. How to decrease the imidization temperature without sacrificing the stability is also very important for the development of polyimide for photonic devices. This literature review shows that the organic-inorganic sol-gel materials have received significant attention because they have excellent optical quality, higher thermal stability and ease of device fabrication. It is noteworthy that although the amorphous three-dimension second-order optical networks are fabricated at low temperature, they exhibited higher stability. It has been reported that polyimide films containing Si-O network achieved by sol-gel process, exhibit higher thermal stability, higher modulus and strength even at a high temperatures and a lower thermal expansion coefficient than PI system. The formation of the silicon network in the polyimide enhanced the T_g of the composite materials. And the most important advantage is that the fabrication of amorphous three-dimension optical network was carried out at low temperature. The low processing temperature can decrease the possibility of the chromophore decomposition and increase nonlinearity at the same time; it can also decrease the light scattering and shrinkage so that it can decrease the optical loss from the cure. Furthermore, it has also been reported that the internal production of water due to the curing of poly (amic acid) aids the hydrolysis of the alkoxysilane and the carboxylic acid group of the poly (amic acid), being a Bronsted acid, might have a catalytic effect on hydrolysis and condensation of the alkoxysilane, which will lead to no addition of catalyst and water and decrease phase separation between the inorganic and organic phase. Therefore, incorporation of silicon-dye into polyimide through sol-gel process could be a new approach to solve the problem.

Chapter 3 Synthesis and Characterization of Diaminoazobenzene Chromophores for Development of NLO Polyimide

As suggested in Chapter 2, side-chain NLO polyimide can meet the application requirement of high thermal stability much better than other kinds of polymers. However, the low transparency caused by chromophore is a big problem that it encountered. Therefore, the challenging task in this project is to design and synthesize suitable chromophores.

Fluorinated NLO chromophores display good comprehensive properties such as good transparency. However, these fluorinated chromophore reported cannot be incorporated into the polyimide as side chain because of the lack of the reactive functional groups in their structures. The effect of fluorine and fluorine position on the structures and properties of chromophore and NLO polyimide are rarely reported. In this research, we have designed a series of novel fluorinated diaminoazobenzene chromophores that can be incorporated into polyimide through covalent bond as side chain. Based on these designs, two new fluorinated chromophores diamines have been synthesized and characterized. To study the effects of fluorine on the structures and properties of chromophores, their non-fluorinated analogues have also been synthesized and characterized. In addition, the effects of fluorine position on their structures and properties have been investigated.

3.1 Molecule Design of Fluorinated diaminoazobenzene Monomers

Second-order NLO chromophores need to meet the following requirements:

- Large hyperpolarizability
- High thermal stability
- High transparency
- High yield and cost-effective synthetic route

In order to synthesize the NLO polyimide with high molecular weight, the NLO chromophores also need to have enough reactivity so that a sufficient amount of NLO chromophores can be incorporated into the polyimide.

The chromophore monomers must be designed to meet these requirements. From the two-state charge-transfer equation (2-2), it is clear that the strength of the donor and acceptor moieties will directly affect the hyperpolarizability. The nitro group is known to be one of the strongest acceptors and the amino group is one of the strongest donors. It has been found that replacing the aliphatic structures by aromatic ones can lead to higher thermal stability. High transparency is another important requirement for NLO chromophores. It is clear that the hyperpolarizability is a strong increase function of the maximum absorption wavelength and the large maximum absorption wavelength will lead to large optical loss because of the low energy tails of the absorption. How to defeat this trade-off is a key problem for the design of the NLO chromophores. The

electronegativity of fluorine is the largest among all elements and its ionization potential is also the largest with the exception of helium and neon. The C-F bond length is the shortest next to a C-H bond but bond energy is much larger. The carbon of a C-F bond slightly polarized in sharp contrast to the carbon of a C-H bond. Fluorine group is a hydrophobic group. Accordingly, organofluorine compounds demonstrate a variety of unique properties, such as, high thermal stability, low dielectric constant, low moisture absorption, excellent weatherability, low flammability, low surface energy and outstanding resistance to most chemicals [171]. Based on the above analysis, incorporation of fluorine into the chromophore structure may be an answer for this key problem. The structures of the designed fluorinated diaminoazobenzene chromophore monomer, 2,4-diamino-2'-fluoro-5'-nitroazobenzene (2R-2F-5N-DIAMINE) and 2,4-diamino-4'-fluoro-3'-nitroazobenzene (2R-4F-3N-DIAMINE) are shown in Figure 3-1.

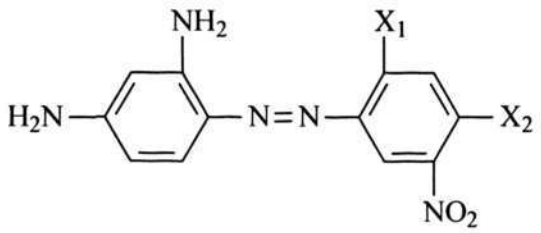

2R-4F-3N-DIAMINE: X_1: H, X_2: F
2R-2F-5N-DIAMINE: X_1: F, X_2: H

Figure 3-1 Structures of the fluorinated diaminoazobenzene chromophores monomers

In order to improve the reactivity of the chromophore monomers, the nitro group is designed to be located at meta position as the nitro group in meta position cannot form the conjugated system with the benzene ring. The fluorinated diaminoazobenzene chromophores monomer can be synthesized through

diazonium salt coupling reaction. As the diazonium salt coupling reaction conditions can be easily met, the synthesis approach will be simple and the yield is relative high. For comparison, two non-fluorinated analogues, 2,4-diamino-4'-nitroazobenzene (2R-4N-DIAMINE) and 2,4-diamino-3'-nitroazobenzene (2R-3N-DIAMINE) were synthesized through the similar synthesis route. Their structures are shown in Figure 3-2.

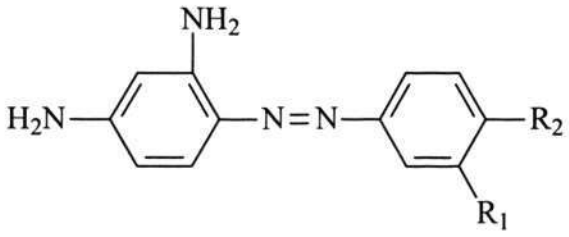

2R-4N-DIAMINE:R_1: H, R_2: NO_2
2R-3N-DIAMINE: R_1: NO_2, R_2: H

Formatted: Condensed by 0.4 pt

Figure 3-2 Structures of the non-fluorinated diaminoazobenzene chromophores monomers

3.2 Synthesis of Diaminoazobenzene Chromophores

3.2.1 Materials

The chemicals used in the experiment are listed in Table 3-1.

Table 3-1 Chemicals used in the synthesis of chromophores

Name	Molecular Formula	Supplier
4-Nitroaniline 97%		Merk
3-Nitroaniline 98%	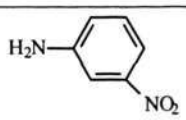	Aldrich
1,3-Phenylenediamine 98%	$NH_2C_6H_4NH_2$	Clariant
Sodium nitrite 98%	$NaNO_2$	Aldrich
Hydrochloric acid 37%	HCl	Merk
Sodium acetate 99%	CH_3COONa	Aldrich
2-Fluoro-5-nitroaniline 97%	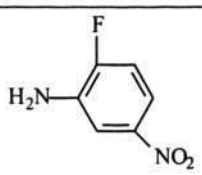	Clariant
4-Fluoro-3-nitroaniline 98%	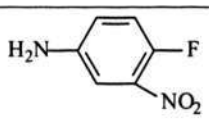	Clariant
Sulfuric acid 98%	H_2SO_4	Merk
Dimethyl sulfoxide (HPLC grade)	$(CH_3)_2SO$	Merk
Ethanol (HPLC grade)	CH_3CH_2OH	Aldrich
Tetrahydrofuran (HPLC grade)	CH_2CH_2CHCHO	Merk

3.2.2 Synthesis of 2R-4N-DIAMINE

2R-4N-DIAMINE was synthesized via the one-step diazonium coupling reaction of 4-

nitrobenzene diazonium chloride with 1,3-phenylenediamine as shown in Figure 3-3. A solution of sodium nitrite (1.41 g, 0.0205 mol) in 3 mL of water was added dropwise with stirring to a cooled solution of 4-nitroaniline (2.88 g, 0.0208 mol) dissolved in 5.25 mL of 35% hydrochloric acid and 20.0 mL of water at a temperature between 0 and 5 °C for 15 min. The diazonium salt obtained was coupled with 1,3-phenylenediamine (2.18 g, 0.0202 mol) dissolved in 1.80 mL of 35% hydrochloric acid and 15.0 mL of water at a temperature between 0 and 5 °C over 30 min. Then sodium acetate (2.30g, 0.028 mol) was added, and the solution was left in an ice bath for 1 hr. After that, additional sodium acetate (2.30 g, 0.028 mol) was added, and the reaction mixture was left for 0.5 hr. Once the temperature was raised to room temperature, a 20% sodium hydroxide solution was added until the pH value of the solution reached 7 and the mixture was stirred at room temperature for 1 hr. The precipitate was washed with deionized water and recrystallized from ethanol. Black red 2R-4N-DIAMINE crystals were obtained in 50% yield.

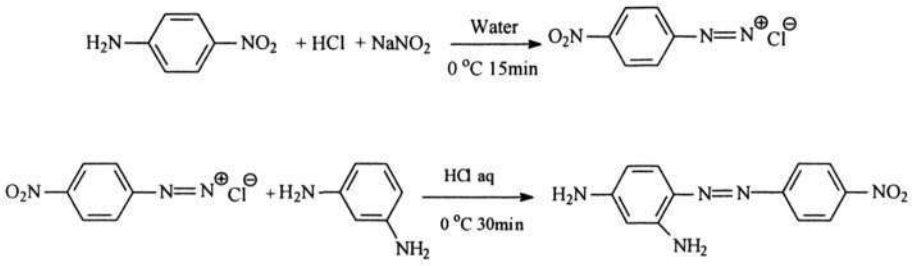

Figure 3-3 Synthetic route of 2R-4N-DIAMINE

3.2.3 Synthesis of 2R-3N-DIAMINE

2R-3N-DIAMINE was synthesized via the one-step diazonium coupling reaction of 3-nitrobenzene diazonium chloride with 1,3-phenylenediamine as shown in Figure 3-4. The synthesis procedure of 2R-3N-DIAMINE is similar with that of 2R-4N-

DIAMINE. The precipitate was recrystallized from ethanol as well. Orange red crystals were obtained in 80% yield.

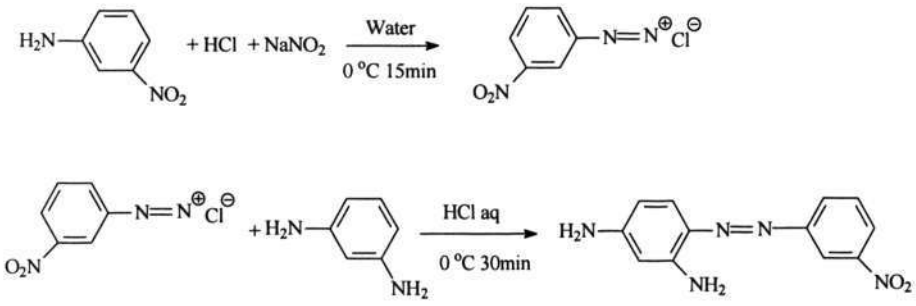

Figure 3-4 Synthetic route of 2R-3N-DIAMINE

3.2.4 Synthesis of 2R-2F-5N-DIAMINE

The synthesis procedure, especially the diazotization reaction of new compound, 2R-2F-5N-DIAMINE, is different because of the fluorinated nitroaniline. For weak basic amines, the concentrated acid method which the arylamine is dissolved in concentrated acid (sulphuric acid) and diazotized by addition of nitrosylsulphuric acid is used [172]. In our synthesis, 4-nitroaniline and 3-nitroaniline were diazotized through the direct method because they are common basic amines. However, 2-fluoro-5-nitroaniline and 4-fluoro-3-nitroaniline can only be diazotized through the concentrated acid method because of their weak basicity compared with the non-fluorinated nitroanilines. 2R-2F-5N-DIAMINE was synthesized via the one-step diazonium coupling reaction of 2-fluoro-5-nitrobenzene diazonium salt with 1,3-phenylenediamine as shown in Figure 3-5. Sodium nitrite (1.41 g, 0.0205 mol) was slowly added to 30 ml of 80% sulfuric acid at a temperature below 10 °C and stirred for 10 minutes, then the solution was heated in a water bath to 65 °C for 30 minutes until the solution was clear. 2-Fluoro-5-nitroaniline (3.20g, 0.0205mol) was added to

the solution at the temperature between 0 and 5 °C, and stirred for 2 hours. Then, the solution was added to 15g of ice. After the ice melts, the solution was filtered. The arenediazonium salt obtained was coupled with 1,3-phenylenediamine (2.18 g, 0.0202 mol) dissolved in 200.0 ml of water at a temperature between 0 and 5 °C for 30 min. Then sodium acetate (2.30g, 0.028 mol) was added, and the solution was left in an ice bath for 1 hr. After that, additional sodium acetate (2.30 g, 0.028 mol) was added, and the reaction mixture was left for 0.5 hr. Once the temperature was raised to room temperature, a 20% sodium hydroxide solution was added until the pH value of the solution reached 7 and the mixture was stirred at room temperature for 1 hr. Finally, product precipitate was recrystallized and the orange powder was obtained in 70% yield.

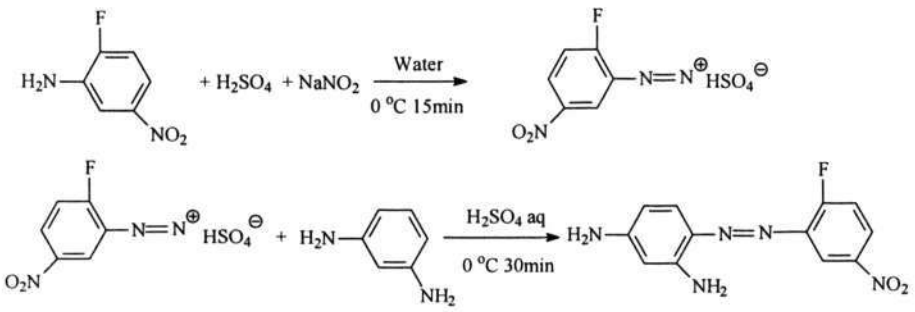

Figure 3-5 Synthetic route of 2R-2F-5N-DIAMINE

3.2.5 Synthesis of 2R-4F-3N-DIAMINE

2R-4F-3N-DIAMINE was synthesized via the one-step diazonium coupling reaction of 4-fluoro-3-nitrobenzene diazonium salt with 1,3-phenylenediamine (Figure 3-6). The synthesis procedure of 2R-4F-3N-DIAMINE is similar with that of 2R-2F-5N-DIAMINE. The final product of brown powder was obtained in 65% yield.

Figure 3-6 Synthetic route of 2R-4F-3N-DIAMINE

3.3 Characterization

3.3.1 Nuclear Magnetic Resonance Spectroscopy (NMR)

The NMR studies in this research were carried out by a Bruker 400MHz instrument, operating at 400MHz (^{1}H) at 20 °C. Dimethyl sulfoxide-d_6 (DMSO-d_6) was used as solvent, tetramethylsilane (TMS) as internal zero reference.

3.3.2 Fourier Transform Infrared Spectroscopy (FTIR)

FTIR spectroscopy was carried out with Perkin Elmer System 2000 FTIR. A background spectrum was run with pure KBr pellet. IR spectra were recorded in the region of 400-4000 cm^{-1} and scanned many times for each sample to decrease the noise.

3.3.3 Elemental Analysis

The elemental analysis was carried out with a EURO EA elemental analyzer through high temperature burning method. The samples were dried at 50 °C in vacuum oven

for 48 hours in order to get rid of solvent and moisture. The percentages of the C, H, O and N were analyzed, respectively.

3.3.4 Electrospray Ionization Mass Spectra (ESI-MS)

Positive or negative ion ESI-MS analyses with direct loop injection were carried out in the Finnigan TSQ 7000 mass spectrometer. ESI-MS was performed under the operating conditions of 5 kV of spray voltage, sheath gas setting at 50 psi, 15 units of auxiliary gas and a heated capillary temperature at 250 °C. Full scan mass spectra were obtained in a positive or negative ion mode.

3.3.5 Thermogravimetric Analysis (TGA)

In this work, TGA was performed with a Hi-Res TGA 2950 thermogravimetric analyzer at a heating rate of 10 °C /min in nitrogen atmosphere (50 cc /min). Test samples (10~20mg) was heated from room temperature to 400 °C. The onset decomposition temperature was taken as the decomposition temperature.

3.3.6 Differential Scanning Calorimetry Analysis (DSC)

DSC analysis was performed at 5 °C /min on a TA Instruments 2010 in nitrogen atmosphere (50 cc /min).

3.3.7 Ultraviolet-visible Spectra (UV-Vis Spectra)

In our study, UV-Vis spectra of the samples from 200~800 nm were measured with a

Shimadzu model UV-2501PC spectrophotometer.

3.4 Structures of Diaminoazobenzene Chromophores

The structures of the diaminoazobenzene chromophores were determined by ^{1}H NMR, FTIR, ESI-MS and elemental analysis. Based on the following data and analysis, the structures of synthesized chromophores were confirmed to be as expected.

3.4.1 2R-4N-DIAMINE

Figure 3-8 shows the ^{1}H NMR spectrum of 2R-4N-DIAMINE. The peaks at 3.35 ppm and 2.50 ppm are actually attributed to the water and the solvent of DMSO-d_6, respectively. According to the reference [173,174], six peaks located at 8.25 ppm, 7.83 ppm, 7.40 ppm, 6.09 ppm, 5.86 ppm and 6.44 ppm were attributed to the H atom of the 2R-4N-DIAMINE at the position of a, b, c, d, e and f, respectively.

C+ ESI-MS spectrum, FTIR spectra and elemental analysis results are shown in Figure 3-9, 3-10 and Table 3-2, respectively. The above data clearly support the proposed structure of 2R-4N-DIAMINE.

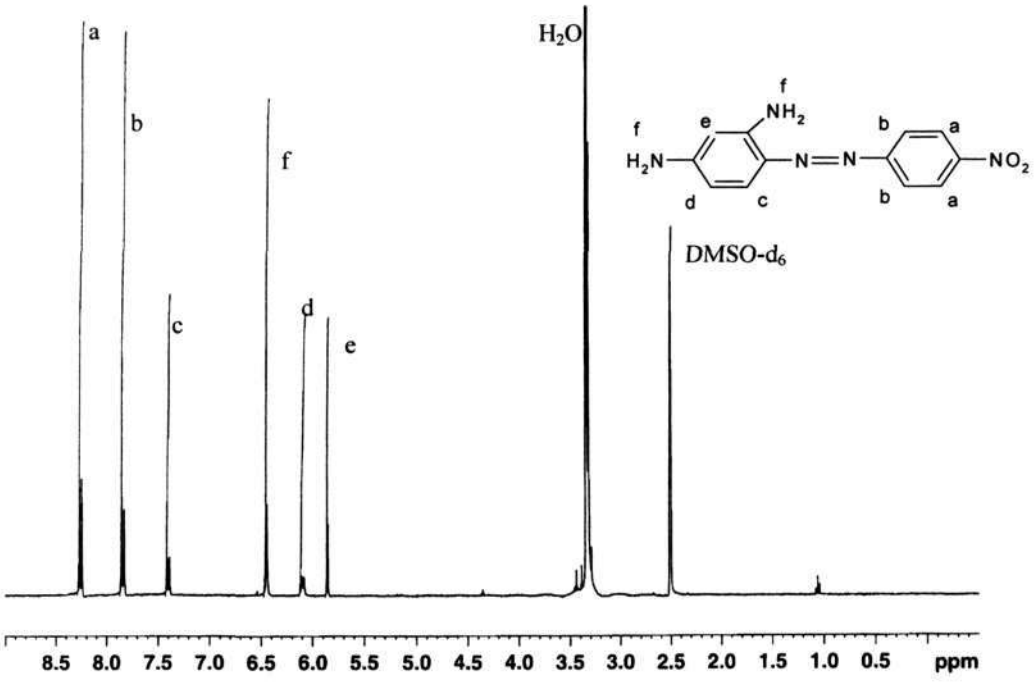

Figure 3-7 ^{1}H NMR spectrum of 2R-4N-DIAMINE in DMSO-d_6

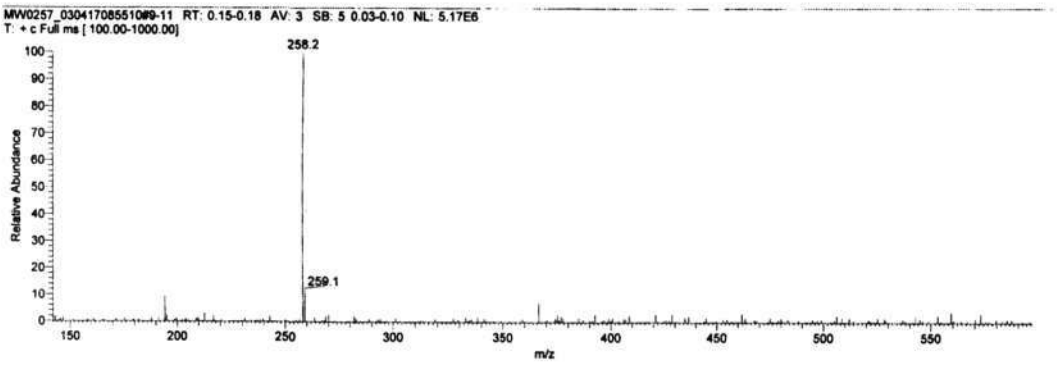

Figure 3-8 ESI-MS spectrum of 2R-4N-DIAMINE

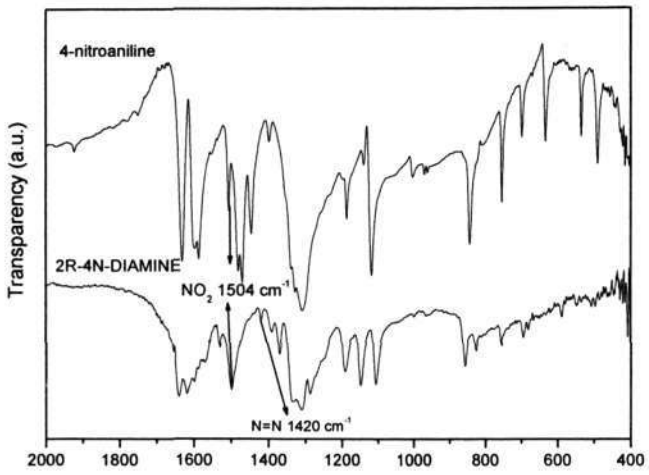

Figure 3-9 FTIR spectra of 4-nitroaniline and 2R-4N-DIAMINE

Table 3-2 Elemental analysis results of 2R-4N-DIAMINE

	C (%)	H (%)	O (%)	N (%)
Calculated	56.03	4.31	27.22	12.44
Experimental	55.89	4.31	26.89	12.91

3.4.2 2R-3N-DIAMINE

Figure 3-11 shows the ^{1}H NMR spectrum and spectral peak assignments of the 2R-3N-DIAMINE. The peak e and i were overlapped. However, if these peaks were enlarged, it was found that they were made up of one single peak (7.40 ppm) and one double peak (7.41 ppm). The integration of these peaks shows that it is attributed to 3 H atoms. The hydrogen atom in amino group is active and its position and peak area integration are often affected by temperature, concentration and solvent. The active hydrogen atom can be exchanged by deuterium in deuterium- oxide (D_2O) and the peak

of the active atom will disappear [175]. In order to confirm that the peak at 7.40 ppm is attributed to the H atom i in the amino group, the D_2O method was used and it was found that the peak at 7.40 ppm and 6.21 ppm disappeared. Therefore, these two peaks are attributed to the H atom h and i in the amino group, respectively.

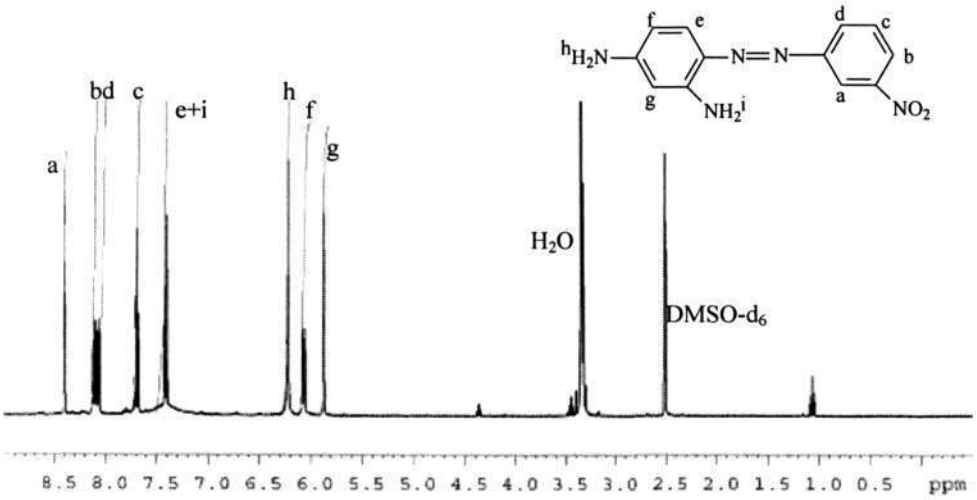

Figure 3-10 ^{1}H NMR spectrum of 2R-3N-DIAMINE in DMSO-d_6

C+ ESI-MS spectrum, FTIR spectra and elemental analysis results are shown in Figure 3-12, 3-13 and Table 3-3, respectively. The above data clearly support the proposed structure of 2R-3N-DIAMINE.

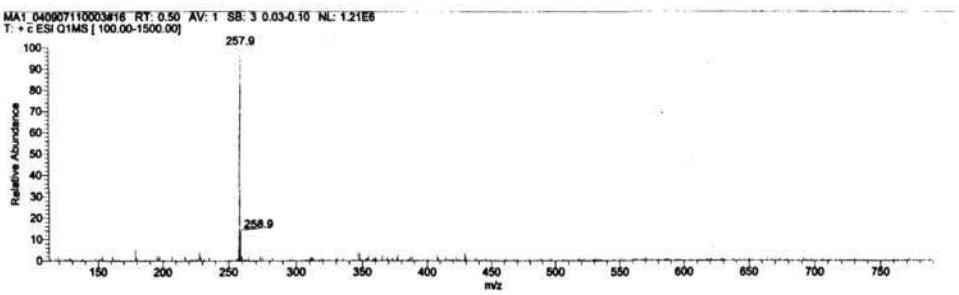

Figure 3-11 ESI-MS spectrum of 2R-3N-DIAMINE

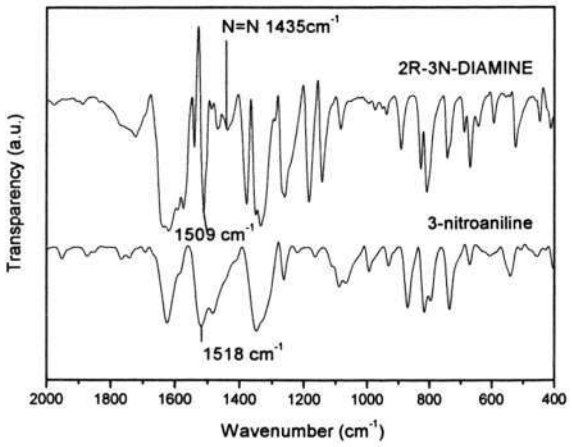

Figure 3-12 FTIR spectra of 3-nitroaniline and 2R-3N-DIAMINE

Table 3-3 Elemental analysis results of 2R-3N-DIAMINE

	C (%)	H (%)	O (%)	N (%)
Calculated	56.03	4.31	27.22	12.44
Experimental	55.94	4.31	26.97	12.78

3.4.3 2R-2F-5N-DIAMINE

The ^{1}H NMR spectrum and the spectrum peak assignments of 2R-2F-5N-DIAMINE are shown in Figure 3-14. Compared the ^{1}H NMR spectrum of 2R-3N-DIAMINE with that of 2R-2F-5N-DIAMINE, the chemical shifts of H atoms in 2R-2F-5N-DIAMINE were found to be different from that in 2R-3N-DIAMINE at the same position. The fluorine atom is a strong electronegative group in inductive effect and weak electrondonating group in resonance effect. Therefore, it can affect the electronic distribution so that their chemical shifts were changed.

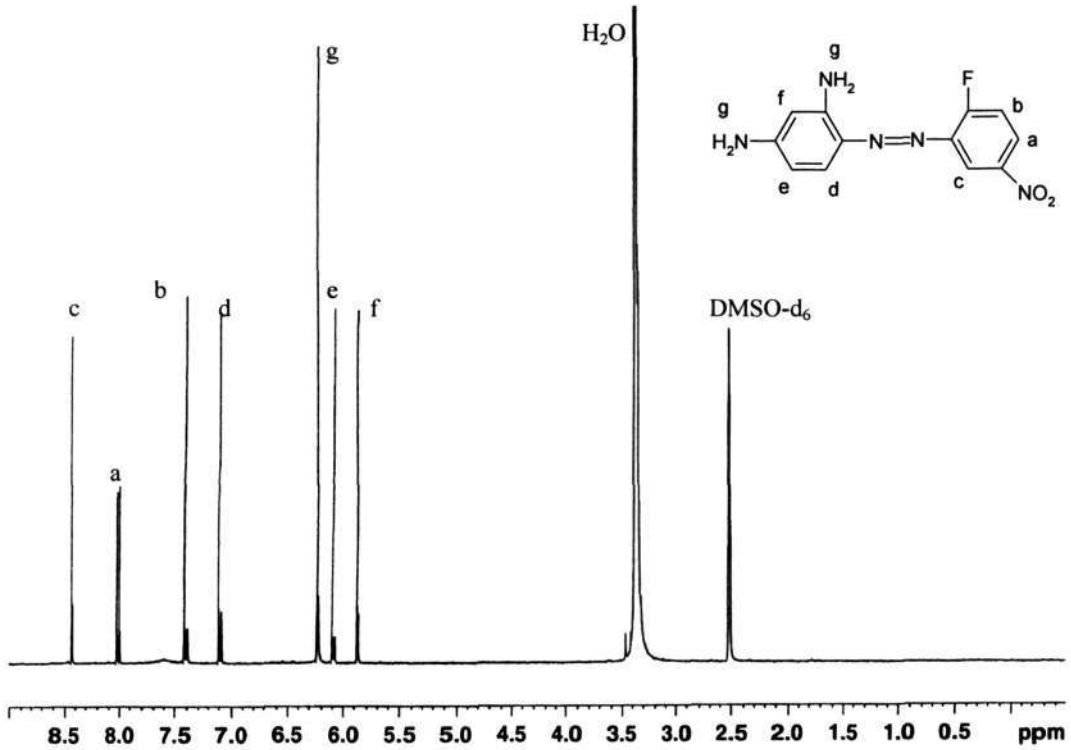

Figure 3-13 ^{1}H NMR spectrum of 2R-2F-5N-DIAMINE in DMSO-d_6

The ESI-MS spectrum is shown in Figure 3-15. It can be seen that the base peak is 276.2 (m/z) in C+ ESI-MS spectrum. This confirms that the molecular weight of the synthesized product is 275.2 and coincides with the molecular weight of 2R-2F-5N-DIAMINE.

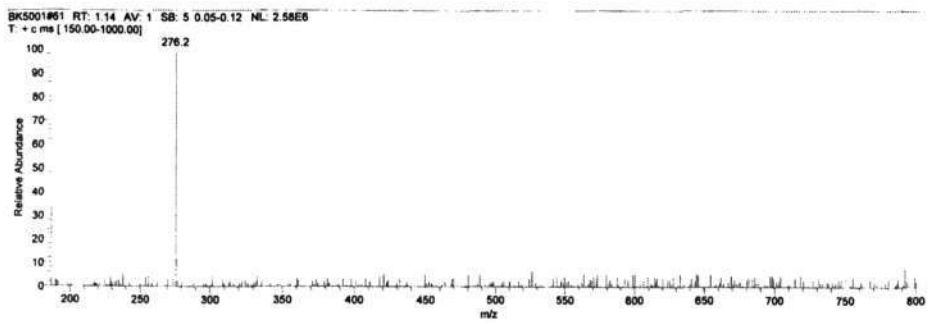

Figure 3-14 ESI-MS spectrum of 2R-2F-5N-DIAMINE

2R-2F-5N-DIAMINE and 2-fluoro-5-nitroaniline were then characterized using FTIR and the spectra are shown in Figure 3-16. The strong absorption peak at 1508 cm^{-1} is attributed to the asymmetric stretching vibration of the group of NO_2. Comparing the two spectra, it was found that the weak absorption peak at 1424 cm^{-1} only appeared in the spectrum of 2R-2F-5N-DIAMINE. The peak at 1424 cm^{-1} is attributed to the stretching vibration of the N=N group [176].

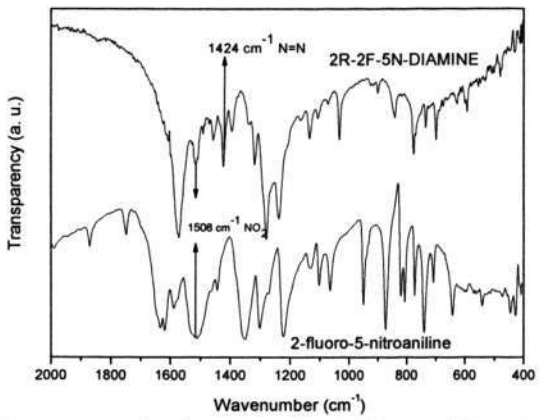

Figure 3-15 FTIR spectra of 2-fluoro-5-nitroaniline and 2R-2F-5N-DIAMINE

Table 3-4 Elemental analysis results of 2R-2F-5N-DIAMINE

	C (%)	H (%)	O (%)	N (%)
Calculated	52.36	3.64	25.45	11.64
Experimental	52.31	3.62	25.37	11.71

To further confirm the structure of the 2R-2F-5N-DIAMINE, the element analysis of 2R-2F-5N-DIAMINE was performed. The results listed in Table 3-4 show that the experimental element constitution of 2R-2F-5N-DIAMINE is basically the same with calculated results. Based on the above data and analysis, it was concluded that 2R-2F-

5N-DIAMINE was successfully synthesized.

3.4.4 2R-4F-3N-DIAMINE

Figure 3-17 shows the ^{1}H NMR spectrum and spectral peaks assignments of the 2R-4F-3N-DIAMINE. Compared ^{1}H NMR spectrum of 2R-3N-DIAMINE with that of 2R-4F-3N-DIAMINE, the fluorine group in 2R-4F-3N-DIAMINE were also to affect the chemical shift of H atom at the same position. In comparison ^{1}H NMR spectrum of 2R-4F-3N-DIAMINE with that of 2R-2F-5N-DIAMINE, it can be elucidated that the fluorine in different position will lead to different electron distribution and chemical shifts.

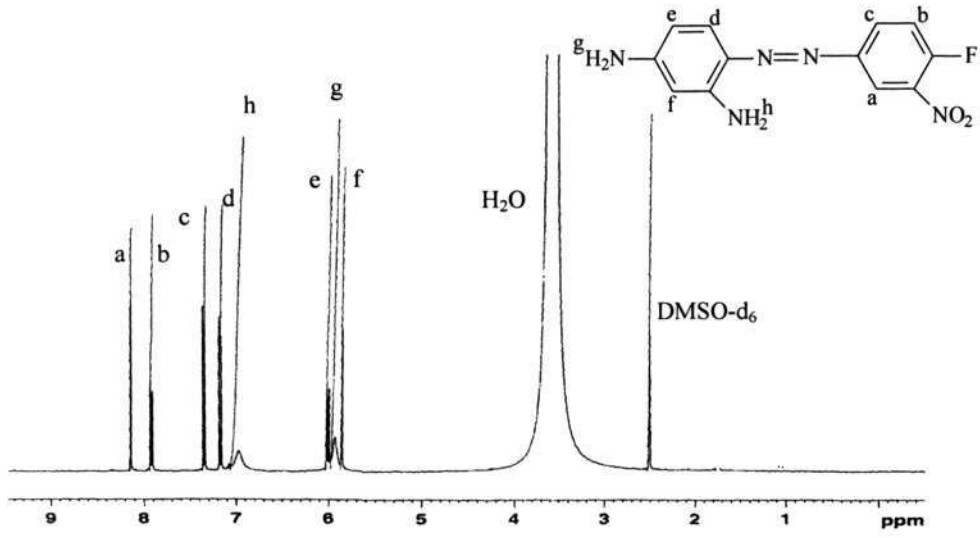

Figure 3-16 ^{1}H NMR of 2R-4F-3N-DIAMINE in DMSO-d_6

C- ESI-MS spectrum, FTIR spectrum and elemental analysis data were shown in Figure 3-18, 3-19, and Table 3-5, respectively. The above data confirmed that 2R-4F-

3N-DIAMINE was successfully synthesized.

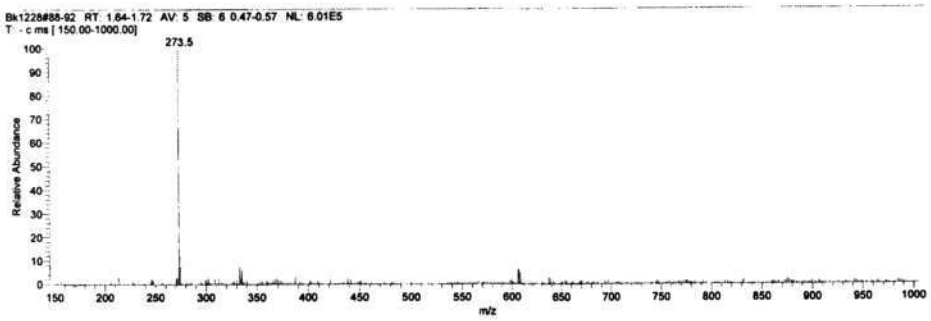

Figure 3-17 ESI-MS spectrum of 2R-4F-3N-DIAMINE

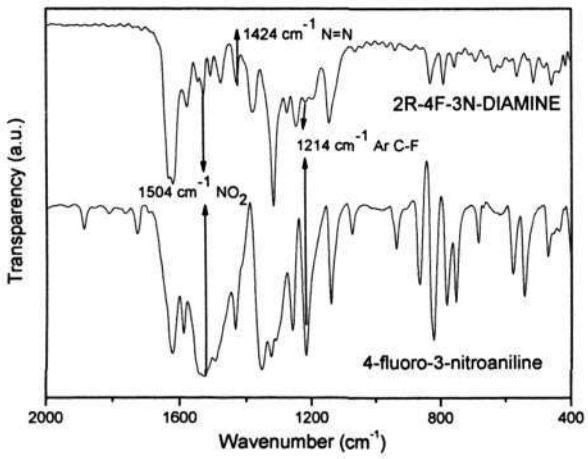

Figure 3-18 FTIR spectra of 2R-4F-3N-DIAMINE and 4-fluoro-3-nitronaniline

Table 3-5 Elemental analysis results of 2R-4F-3N-DIAMINE

	C (%)	H (%)	O (%)	N (%)
Calculated	52.36	3.64	25.45	11.64
Experimental	52.29	3.65	25.43	11.69

3.5 Thermal Properties and UV-Vis Absorption

3.5.1 Thermal Properties

Thermal stability is one of the most important properties of chromophore, especially for the chromophore used in NLO polyimide because it is required that the chromophore doesn't decompose during the higher temperature (>200 °C) imidization process. Thermal properties of the synthesized diaminoazobenzene chromophores were characterized using DSC and TGA. The DSC results shown in Figure 3-19 reveal that the melting points of 2R-4N-DIAMINE, 2R-3N-DIAMINE and 2R-2F-5N-DIAMINE are about 229, 175 and 194 °C, respectively. For 2R-4N-DIAMINE and 2R-3N-DIAMINE, needle crystals were obtained through the recrystallization. However, for 2R-2F-5N-DIAMINE and 2R-4F-3N-DIAMINE, powders with lower crystallinity or smaller size were obtained through the recrystallization. Hence, the melting point of 2R-4F-3N-DIAMINE cannot be observed and the melting peak of 2R-2F-5N-DIAMINE is not as perfect as that of 2R-4N-DIAMINE and 2R-3N-DIAMINE.

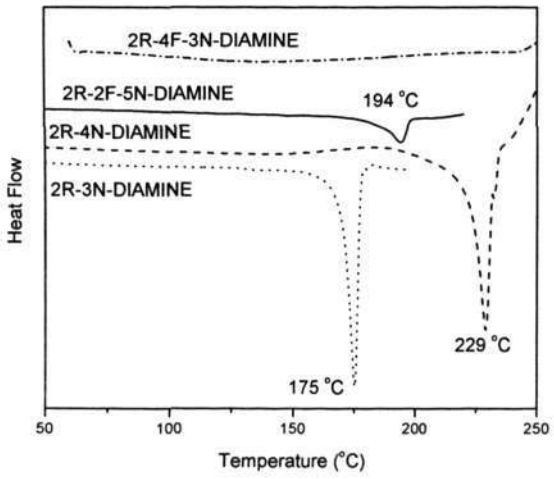

Figure 3-19 DSC of 2R-4N-DIAMINE, 2R-3N-DIAMINE, 2R-2F-5N-DIAMINE and 2R-4F-3N-DIAMINE

Thermal stabilities of the four diaminoazobenzene chromophore monomers were characterized using TGA and the results are shown in Figure 3-20. Figure 3-20 reveals that the onset decomposition temperatures of 2R-4N-DIAMINE, 2R-3N-DIAMINE, 2R-2F-5N-DIAMINE and 2R-4F-3N-DIAMINE are 242, 243, 270 and 245 °C, respectively. The thermal stability of 2R-3N-DIAMINE is slightly higher than that of 2R-4N-DIAMINE because the nitro group is located at a different position. 2R-2F-5N-DIAMINE and 2R-4F-3N-DIAMINE have higher thermal stability than 2R-3N-DIAMINE, possible due to the presence of the fluorine atom. As the fluorine group is incorporated into new compounds and the bond energy of C-F bonds (456-486 kJ/mol) is higher than that of C-H bond (356-435 kJ/mol); hence, the stronger C-F bonds might contribute to the higher thermal stabilities of organofluorine compounds. Our observation concurs with these reported by others [171]. In addition, it can be found that the thermal stability of 2R-2F-5N-DIAMINE is higher than that of 2R-4F-3N-DIAMINE, possibly because the fluorine group was at different position.

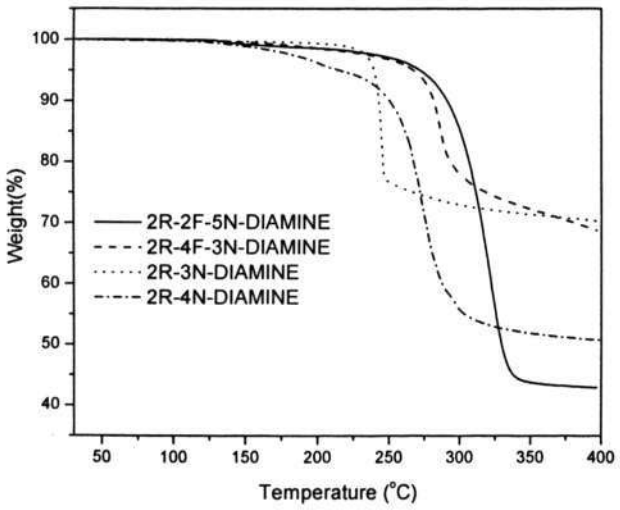

Figure 3-20 TGA of 2R-4N-DIAMINE, 2R-3N-DIAMINE, 2R-2F-5N-DIAMINE and 2R-4F-3N-DIAMINE

3.5.2 UV-Vis Absorption

Another important property of the chromophores is transparency. As noted in the literature review, the low energy tails of the electronic absorption bands of the chromophores can extend several hundred nanometers into the long wavelength region [170]. Because even a small absorption at the operating wavelength of the devices (typically 0.8, 1.3 and 1.5 μm) can be detrimental, it is important to make NLO chromophores as transparent as possible. Generally, the UV-Vis absorption can be used to assess the transparency. Figure 3-21 shows the UV-Vis absorption spectra of 2R-4N-DIAMINE, 2R-3N-DIAMINE, 2R-2F-5N-DIAMINE and 2R-4F-3N-DIAMINE in 1,4-dioxane. As well known, the UV-Vis absorption range from 300 to 700 nm is mainly due to the π-π^* and n-π^* electronic transitions of the azobenzene chromophore. The results show that the maximum absorption wavelengths (λ_{max}) of 2R-2F-5N-DIAMINE, 2R-4F-3N-DIAMINE, 2R-3N-DIAMINE and 2R-4N-DIAMINE are 467, 434.5, 447.5 and 482.5 nm, respectively. It indicates that the transparency of 2R-4N-DIAMINE is the lowest and that of 2R-4F-3N-DIAMINE is the highest. It can be concluded that 2R-3N-DIAMINE displays a blue-shift of λ_{max} compared with 2R-4N-DIAMINE. This suggests that the NO_2 group at the meta position may lead to the better transparency of 2R-3N-DIAMINE. Actually, the NO_2 group at meta position cannot form the conjugated system with the benzene ring. It might be the NO_2 group at meta position that increase the energy gap between the highest occupied molecular orbital (HOMO) and the lowest unoccupied molecular orbital (LUMO), leading to a decrease of the λ_{max}. The results reveal that 2R-4F-3N-DIAMINE displays a significant blue-shift of λ_{max} compared with 2R-3N-DIAMINE. However, 2R-2F-5N-DIAMINE displays a bathochromic shift of λ_{max}. The theoretical

calculation of Liu *et al* [31] shows that fluorine in different positions in the fluoroazulene isomers could lead to different UV absorbance. Our results confirm that the fluorine position in the structures can significantly influence the UV absorbance. The possible mechanism is that the position of fluorine group affects the energy gap between HOMO and LUMO of the chromophores. Generally, the fluorine group is a strong electron-withdrawing group in inductive effect and also a weak electron-donating group in resonance effect. The nitro group is a strong electron withdrawing group in inductive effect and resonance effect. Because the fluorine group is next to the nitro group in 2R-4F-3N-DIAMINE, there will be a repulsive effect between the fluorine group and nitro group. The repulsive effect will lead to the increase in the energy gap so that 2R-4F-3N-DIAMINE display blue-shift λ_{max} compared with 2R-3N-DIAMINE. However, in 2R-2F-5N-DIAMINE, there is no such repulsive effect because the fluorine group is not next to the nitro group. As the *p*- orbit in the fluorine atom will conjugate with the π^* orbit of benzene ring, which leads to the decrease in the energy gap, therefore, 2R-2F-5N-DIAMINE displays a red-shift in comparison with 2R-3N-DIAMINE.

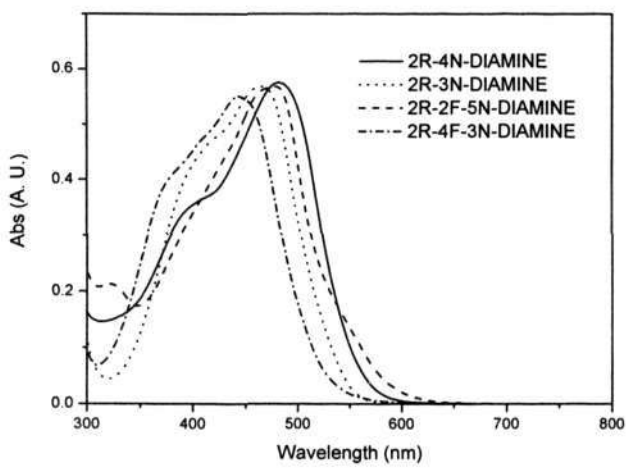

Figure 3-21 UV-Vis absorption spectra of 2R-4N-DIAMINE, 2R-3N-DIAMINE, 2R-2F-5N-DIAMINE and 2R-4F-3N-DIAMINE

3. 6 Summary

^{1}H NMR, ESI-MS, element analysis and FTIR results confirmed that two novel fluorinated diaminoazobenzene chromophore monomers and their non-fluorinated analogues, which can be used for the development of NLO polyimide, were successfully synthesized.

DSC and TGA results show that the melting points of 2R-4N-DIAMINE, 2R-3N-DIAMINE and 2R-2F-5N-DIAMINE are about 229, 175 and 194 °C respectively. The onset decomposition temperatures of 2R-4N-DIAMINE, 2R-3N-DIAMINE, 2R-2F-5N-DIAMINE and 2R-4F-3N-DIAMINE are 242, 243, 270 and 245 °C, respectively. The results reveal that these diaminoazobenzene chromophore monomers have a good thermal stability to endure the imidization temperature during the imidization. The results indicate that the incorporation of fluorine can increase thermal stability and the fluorine position also affects the thermal stability.

UV-Vis absorption results show that the λ_{max} of 2R-2F-5N-DIAMINE, 2R-4F-3N-DIAMINE, 2R-3N-DIAMINE and 2R-4N-DIAMINE in 1,4-dioxane are 467, 434.5, 447.5 and 482.5 nm, respectively. The results show that the transparency of 2R-4N-DIAMINE is lowest and that of 2R-4F-3N-DIAMINE is highest. Our results confirmed that the fluorine position can significantly influence the UV absorbance. The possible mechanism was proposed as well.

Chapter 4 Hyperpolarizability of the Chromophore

4.1 Introduction

Macroscopic nonlinearity of NLO polymers originated from microscopic nonlinearity of chromophores. Hence, it is very important to characterize the hyperpolarizability of chromophore. Various techniques such as electric field-induced second-harmonic generation (EFISH), solvatochromism method and the hyper-Rayleigh scattering (HRS) have been employed for the measurement of the molecular hyperpolarizability.

Solvatochromic method was chosen for the characterization of the hyperpolarizability of the chromophore in this research because the experiments are relatively easy and the data can be quickly analyzed and readily fed back for the next research iteration. Solvatochromic method is based on the effects of a solvent on the position, shape and intensity of the absorption and emission bands of molecules with respect to their vapor-phase properties. There are numerous models for the quantitative description of these solvatochromic shifts [177-180]. The hyperpolarizability can be simply calculated through the quantum-mechanical two-level model [11]. In order to calculate the hyperpolarizabilities of these synthesized chromophores, the programs have to be compiled and the correctness needs to be confirmed through the calibration of the well-known chromophore, 4-nitroaniline and DR1.

4.2 Theory

When light transfers in a dense-transparent matter, the electric field of the light induces a slight separation between the positive and negative charges on each molecule in the material. The polarization of charge induced by light, creates a small electric field that has a direction opposing the direction of the incident field and oscillates asynchronously with light. The small electric field changes the direction and the magnitude of the field of the light so that the speed of light in the materials decreases. The interaction between the light and the material gives rise to some familiar effects, such as refraction, reflection and diffraction in which the magnitudes of the effect changes are linearly related to the intensity of the light. However, since laser appeared in 1960, entirely different properties, such as second harmonic generation between the laser and the materials had been found. It was found that the high intensity of a laser beam can produce an electric field that rivals and disrupts the internal electric field of atoms in the material so that the input and output beams through the material cannot be related by a simple proportionality.

For an isolated molecule, the dipole moment p_i consists of its ground state dipole moment $\mu_{g,i}$ and the induced contribution. It can be expressed as,

$$p_i = \mu_{g,i} + \varepsilon_0 \alpha_{ij} E_j + \varepsilon_0 \beta_{ijk} E_j E_k + \varepsilon_0 \gamma_{ijkl} E_j E_k E_l + \cdots \qquad (4\text{-}1)$$

where α_{ij} is the linear polarizability, β_{ijk} is hyperpolarizability, γ_{ijkl} is the second-order hyperpolarizability, E is the electric field strength, i, j, k, l are the coordinates of the molecule, and ε_0 is the permittivity of free space.

The generic element β_{ijk} of the hyperpolarizability tensor can be expressed in the sum-

over-states approach derived from the perturbation theory as a sum of so-called two-level and three-level terms. The former one is involved in the ground electronic state and an excited state of the molecule, and the latter is involved in the ground and two excited states. The simplest and most useful model to take into account the contribution of charge-transfer resonances within a molecule to the hyperpolarizability was the two-level method [11]. This model assumes that the electronic properties of the molecule are determined by a ground state and low-lying charge-transfer excited state. For most organic molecules used for second-harmonic generation, the two-level model is a good approximation because the energy difference between the ground and first excited state is considerably less than that between the ground and higher excited states. Furthermore, both the fundamental and double laser frequencies are usually well below the frequencies of transition to the higher excited states. Typical chromophores have an electron-donor group and an acceptor group linked through a π–electron system. As a result, the first excited state is often a low-lying charge-transfer state, usually in the visible or near-UV region of the spectrum. Polarization results primarily from the admixing of the charge-transfer resonance state with the ground state through the action of the electric field $E(\omega)$. In the two-level model, the β_{zzz} component of the β tensor can be expressed by means of the simple Oudar formula [97]:

$$\beta_{zzz} = \frac{3}{2h^2c^2} \frac{\nu_{eg}^{\ 2}\gamma_{eg}^{\ 2}\Delta\mu_{eg}}{\left(\nu_{eg}^{\ 2} - \nu_L^{\ 2}\right)\left(\nu_{eg}^{\ 2} - 4\nu_L^{\ 2}\right)} \qquad (4\text{-}2)$$

where z is the direction of the charge-transfer; ν_{eg} and γ_{eg} are, respectively, the transition frequency (cm^{-1}) and transition dipole moment; $\Delta\mu_{eg}$ is the difference between the excited state (μ_e) and the ground state (μ_g) molecular dipole moment; ν_L is the frequency of the incident radiation, to which the β value is referred; h and c are

Planck's constant and velocity of light, respectively. The value of β_0 is often indicated as the hyperpolarizability when ν_L=0.

In order to calculate β, $\Delta\mu_{eg}$, ν_{eg} and γ_{eg} must be obtained. The solvatochromic method allows determining $\Delta\mu_{eg}$ and other quantities such as ν_{eg} and γ_{eg} could be obtained from spectrophotometric measurements, which are discussed below.

4.2.1 Determination of $\Delta\mu_{eg}$

Various theoretical treatments of solvatochromic shifts in absorption frequency of a molecule have been developed. Most of them are based on a continuum dielectric model in which the solute dipole polarizes surrounding solvent molecules, in turn creating an electric field that perturbs the energy levels of the solute. This perturbing electric field is known as the reaction field and was first described by Onsager. The McRae equation [177] was the most useful expression to interpret the shift of the absorption maximum for a molecular electronic transition on passing from the gaseous state to a solution. If μ_e and μ_g are assumed to be parallel to each other and if changes of the solvent polarizability and reorientation of the solvent dipoles upon excitation are neglected, the solvatochromic shift is given:

$$(\nu_{eg})_{s,a} = (\nu_{eg})_g{}^0 + \delta_a - \frac{\mu_e{}^2 - \mu_g{}^2}{2hca^3}\frac{n^2-1}{n^2+2} - \frac{2\mu_g(\mu_e-\mu_g)}{hca^3}\left(\frac{\varepsilon-1}{\varepsilon+2} - \frac{n^2-1}{n^2+2}\right) \quad (4\text{-}3)$$

where $(\nu_{eg})_{s,a}$ and $(\nu_{eg})_g{}^0$ are, respectively, the frequency (cm^{-1}) of the absorption maximum in a given solvent s and of the 0→0 transition in the gaseous phase; δ_a is the difference between the vibrational energies of the molecule in the excited and in the ground state; a is the radius (cm) of the cavity (supposed spherical) occupied by

the solute molecule in the solvent; ε and n are the solvent dielectric constant and refractive index, respectively [179].

If Eq. (4-3) is evaluated for two different solvents s and s', subtracting the two expressions from one another, we have

$$\left(\nu_{eg}\right)_{s,a}-\left(\nu_{eg}\right)_{s',a}=-\frac{\mu_e^{\,2}-\mu_g^{\,2}}{2hca^3}\left(\frac{n^2-1}{n^2+2}-\frac{n'^2-1}{n'^2+2}\right)-\frac{2\mu_g\left(\mu_e-\mu_g\right)}{2hca^3}\left(\frac{\varepsilon-1}{\varepsilon+2}-\frac{\varepsilon'-1}{\varepsilon'+2}+\frac{n'^2-1}{n'^2+2}-\frac{n^2-1}{n^2+2}\right) \quad (4\text{-}4)$$

To simplify the above expression, we define

$$\phi(\varepsilon)=\frac{\varepsilon-1}{\varepsilon+2} \quad (4\text{-}5)$$

$$\varphi(n)=\frac{n^2-1}{n^2+2} \quad (4\text{-}6)$$

The Eq. (4-4) becomes,

$$\left(\nu_{eg}\right)_{s,a}-\left(\nu_{eg}\right)_{s'a}=-\frac{\mu_e^{\,2}-\mu_g^{\,2}}{2hca^3}\left(\varphi(n)-\varphi(n')\right)-\frac{2\mu_g\left(\mu_e-\mu_g\right)}{hca^3}\left(\phi(\varepsilon)-\phi(\varepsilon')+\varphi(n')-\varphi(n)\right) \quad (4\text{-}7)$$

Rearranging Eq. (4-7) results in a linear equation:

$$y=Ax+B \quad (4\text{-}8)$$

where

$$y=\frac{\left(\nu_{eg}\right)_{s,a}-\left(\nu_{eg}\right)_{s'a}}{\phi(\varepsilon)-\phi(\varepsilon')+\varphi(n')-\varphi(n)} \quad (4\text{-}9)$$

$$x=\frac{\varphi(n)-\varphi(n')}{\phi(\varepsilon)-\phi(\varepsilon')+\varphi(n')-\varphi(n)} \quad (4\text{-}10)$$

So, the slope A and the intercept B is given by the Eq. (4-8):

$$A=-\frac{\mu_e^{\,2}-\mu_g^{\,2}}{2hca^3} \qquad B=-\frac{2\mu_g(\mu_e-\mu_g)}{hca^3} \quad (4\text{-}11)$$

The ground-state dipole moment can be determined by measuring the dielectric constant for several concentrations and using the Debye-Guggenheim equation [181]:

$$\mu_g^{\,2} = \frac{\varepsilon_0 3kT}{N_A} \frac{9}{(\varepsilon_v + 2)(n_v^{\,2} + 2)} \frac{M_u}{\rho_v} \left(\frac{\partial \varepsilon}{\partial w}\right)_0 \qquad (4\text{-}12)$$

where M_u is the molar mass of the dissolved substance; w is the weight fraction; ε_v, n_v and ρ_v denote the dielectric constant, the refractive index, and the density of the pure solvent, respectively; N_A is the Avogadro's constant; and ε_0 is the vacuum permittivity.

By measuring the absorption frequencies in different solvents and taking into account all the possible pairs, a series of x and y values, as defined in Eq. (4-9) and Eq. (4-10), are obtained and linearly correlated, thus allowing the determination of B. Finally, $\Delta\mu_{eg}$ can be derived from Eq. (4-11) and Eq. (4-12) if a is known. The most critical point in determining $\Delta\mu_{eg}$ is the cavity radius a which enters Eq. (4-7) as the third power. The uncertainty of a and the numerous assumptions made in the derivation of Eq. (4-7) is the main sources of error in the evaluation of β. The cavity radius a can be estimated by various means [104,180,182]. It was reported that a equals 0.7 times the length of the molecule [180]. However, this assumption will lead to lower β especially for very long molecule [182]. Emission solvatochromism was also used to evaluate a of the chromophores, which can exhibit fluorescent emission [104]. Some are based on the estimation of the solute radius a from the molecular weight and the density in the hypothesis of a spherical molecule. If accounting for the Van der Waals radius of the solvent molecules, a reasonable approximation for a is:

$$a = r_u + 0.5 r_v \qquad (4\text{-}13)$$

where r_u and r_v are the spherical radii of the solute u and solvent v molecules respectively. It is useful for $0.5r_u < r_v < 2r_u$, where in the hypothesis of a spherical molecule [179].

$$r_u = \left(\frac{3M_u}{4\pi N_A \rho_u} \right)^{1/3} \tag{4-14}$$

$$r_v = \left(\frac{3M_v}{4\pi N_A \rho_v} \right)^{1/3} \tag{4-15}$$

where M_u and M_v are the molecular weights of solute and solvent, respectively; ρ_u and ρ_v are the densities of solute and solvent respectively; N_A is Avogadro's number.

4.2.2 Determination of γ_{eg}

The oscillator strength f is related to the transition dipole moment γ_{eg}:

$$\gamma_{eg}^{\ 2} = \frac{3e^2 h}{8\pi^2 mc} \frac{f}{\nu_{eg}} = 2.13 \times 10^{-30} \frac{f}{\nu_{eg}} \tag{4-16}$$

where all constants are in (c.g.s) units and therefore γ_{eg} is in esu cm [183].

The oscillator strength f can be determined from the absorption spectrum by the following relation [183]:

$$f = 4.32 \times 10^{-9} \int \varepsilon(\nu) d\nu \tag{4-17}$$

where $\varepsilon(\nu)$ is the molar extinction coefficient ($mol^{-1}l \cdot cm^{-1}$), and the integration is carried out over the absorption band.

According to the Lambert-Beer law:

$$\varepsilon(\nu) = \frac{A(\nu)}{Ml} \tag{4-18}$$

where $A(\nu)$ is the measured absorbance, M is the concentration ($mol \cdot l^{-1}$) of the solution and l is the optical path length (cm).

So,

$$\int_{band} A(\nu)d\nu = Ml\int_{band} \varepsilon(\nu)d\nu \qquad (4\text{-}19)$$

4.3 Experimental

All chemicals were purchased from Merck, Aldrich and Clariant. 4-Nitroaniline (4-NA), 3-nitroaniline (3-NA), Disperse red1 (DR1), 4-fluoro-3-nitroaniline (4-F-3-NA) and 2-fluoro-5-nitroaniline (2-F-5-NA) were recrystallized before use. The parameters of the solvents (HPLC grade) were listed in Table 4-1 and used without purification. 2R-4N-DIAMINE, 2R-3N-DIAMINE, 2R-4F-3N-DIAMINE and 2R-2F-5N-DIAMINE were synthesized and described in Chapter 3.

The densities of the test samples were measured using pycnometric method by determining the weight of a volume-calibrated pycnometer filled with a liquid of known density in which a certain quantity of the sample is immersed. The method, however, requires that the solvent is less dense and inert to the sample and a series of experiments must be carried out to select the liquid reference. Finally, hexane was chosen as the liquid reference of known density ($\rho_{l(20^{\circ}C)}$) for all samples. A 10 ml pycnometer was used to measure the densities of the samples. The procedure for determining the density of the sample is as follows:

a. Weigh the pycnometer W_0

b. Fill the pycnometer with only hexane and put it in 20 °C water bath for 10 minutes, absorb the water outside the pycnometer and weigh it (W_1)

c. Empty and dry the pycnometer and put some sample into it and weigh it (W_2)

d. Add the hexane to the pycnometer containing the sample, and put it in the vacuum

desiccator for 10 minutes under vacuum in order to get rid of the air absorbed in the sample surface.

e. Fill it with the hexane, then put it in 20 °C water bath for 10 minutes, absorb the water outside the pycnometer and weigh it (W_3)

The density of the sample $\rho_{s(20°C)}$ can be determined by:

$$\rho_{s(20°C)} = \frac{W_2 - W_0}{(W_1 - W_0) - (W_3 - W_2)} \rho_{l(20°C)} \qquad (4\text{-}20)$$

The dielectric constants of the solutions were measured using a PGM-II digital capacitance measurement meter and a liquid dielectric test fixture (Nanjing Sang Li Electronic Equipments Factory, China). The refractive indices were measured through Abbe Refractometer (ATAGO, Japan). Both apparatus were calibrated by use of hexane, 1,4-dioxane and chloroform. Ultraviolet-visible spectra of the samples were measured with a Shimadzu model UV-2501PC spectrophotometer in different solvents, which should cover a wide polarity range. In this work, the following solvents were used: ethanol, acetone, methanol, N,N-dimethylacetamide (DMAc), dimethyl sulfoxide (DMSO), tetrahydrofuran (THF), 1,4-dioxane, 1-methyl-2-pyrrolidone (NMP) and chloroform. The molar concentrations of all samples are between 1.2×10^{-5} and 7.8×10^{-5} mol·l^{-1}. A quartz cuvette of 10 mm thick was used. The λ_{max} and the peak area were determined by software in UV-2501PC spectrophotometer. Two programs were compiled for calculation of y and x (in Eq. 4-8) and hyperpolarizability.

4.4 Hyperpolarizabilities of Chromophores

4.4.1 Calibration of the Experimental Procedure and the Programs

In order to confirm the correctness of the experimental procedure and the program, two well known reference chromophores, 4-nitroaniline and DR1 were selected. The dielectric constants, dipole moments, refractive indexes and densities of the used solvents are listed in Table 4-1 [184]. From the dielectric constants and dipole moments, it can be seen that these solvents show a wide polarity range so that the dipole moments of the chromophores can be affected differently. In general, the higher the dielectric constant and dipole moment, the higher the polarity of the solvent. Their polarities basically increase in the following order:

DMSO > DMAc > Methanol, Ethanol > Acetone, THF > Chloroform, 1,4-dioxane

Table 4-1 Dielectric constant, dipole moment, refractive index and density of various solvents [184]

	Ethanol	Acetone	Methanol	DMAc	DMSO	THF	1,4-dixoane	$CHCl_3$
n	1.3614	1.3590	0.7913	1.4384	1.4773	1.4073	1.4203	1.4467
μ_g ($\times 10^{-30}$ C·m)	5.60	8.97	5.55	12.41	13.34	5.70	1.5	3.84
ε	25.7	20.7	31.2	37.78	48.9	7.58	2.21	4.9
ρ(g/cm^3)	0.7893	0.7906	0.7913	0.9080	1.0958	0.8892	1.0356	1.4890

The UV-vis spectra of 4-NA and DR1 in different solvents are shown in Figure 4-1.

The wavelengths of the maximum absorption λ_{max} in different solvents are summarized in Table 4-2. Compared with the λ_{max} in different solvents, the λ_{max} of the two chromophores all exhibited a positive solvatochromism, i.e. red shift with increase in solvent polarity, which shows that an excited state is more polar than a ground state. Hence, the polar solvent can decrease the energy gap between the $\pi \rightarrow \pi^*$ excitation. Results also showed that the λ_{max} of DR1 is larger than that of 4-NA, which reveals that the energy gap of DR1 is smaller than that of 4-NA because its conjugated length is longer.

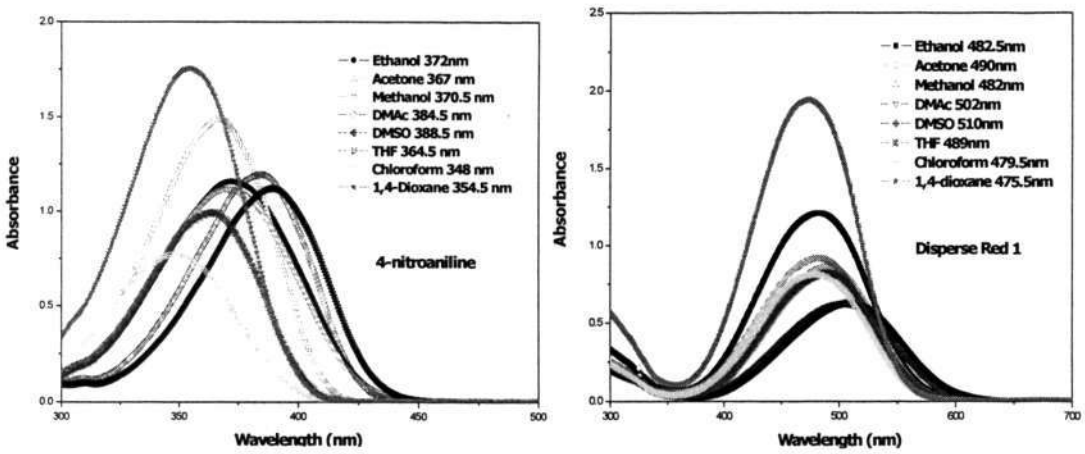

Figure 4-1 UV-vis spectra of 4-NA and DR1 in different solvents

Table 4-2 λ_{max} （nm） of 4-NA and DR1 in various solvents

	Ethanol	Acetone	Methanol	DMAc	DMSO	THF	1,4-dixoane	$CHCl_3$
4-NA	372	367	370.5	384.5	388.5	364.5	354.5	348
DR1	482.5	490	482	502	510	489	475.5	479.5

In order to determine the hyperpolarizability β, $\Delta\mu_{eg}$, ν_{eg} and γ_{eg}, must be calculated. $\Delta\mu_{eg}$ can be obtained through Eq. (4-11) and (4-12). In choosing the pairs of solvent

for Eq. (4-8), the experimental error must be considered. To check whether a combination of solutions gave reasonable results was made by calculating the transition frequency in vapor $(\nu_{eg})_g^0$ and $(\mu_e^2-\mu_g^2)$. If the values of $(\nu_{eg})_g^0$ obtained were within 5 nm and $(\mu_e^2-\mu_g^2)$ was positive, this pair of the solvents was employed. The plots of Eq. (4-8) for 4-NA and DR1 are shown in Figure 4-2. The linear correlation coefficients (r) of 0.93 and 0.95 for 4-NA and DR1 shows that linear correlations are satisfied. The intercepts of these plots B are shown in Table 4-3. The ground–state dipole moment μ_g can be determined by measuring the dielectric constant for several concentrations and using Debye-Guggenheim equation (Eq. 4-12). The concentration dependencies of the dielectric constants are shown in Figure 4-3. Their $(\partial\varepsilon/\partial w)_0$ and permanent ground state dipole moment are listed in Table 4-3. It can be concluded that the values μ_g of 4-NA and DR1 are 2.49×10^{-29} C·m and 2.98×10^{-29} C·m, respectively, which are quite close to the reported values 2.1×10^{-29} and 3×10^{-29} C·m [31]. The slope A can be also used to calculate $\Delta\mu_{eg}$. However, the values $\Delta\mu_{eg}$ obtained through slope A and intercept B is not accurate because the first term of Eq. 4-4, has almost no dependence on the solvent [182].

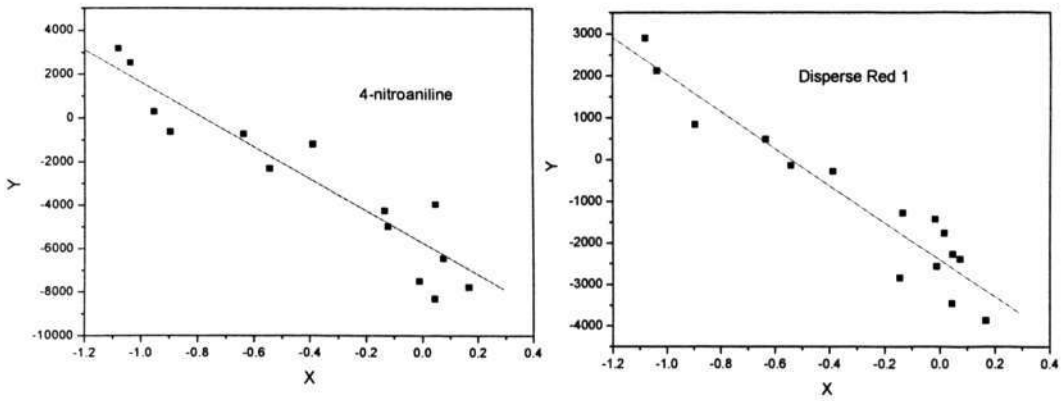

Figure 4-2 Plot of Eq. (4-8) for 4-NA (r = 0.93) and DR1 (r = 0.95)

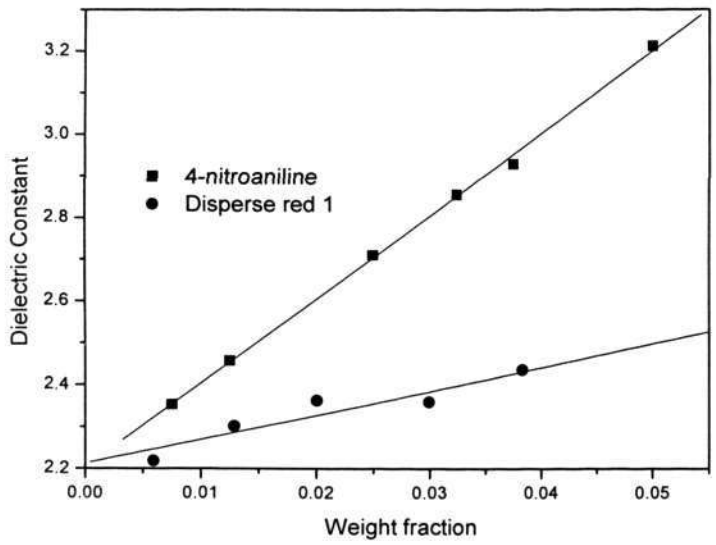

Figure 4-3 Concentration dependence of the dielectric constant of 4-NA and DR1 in 1,4-dioxane

In order to calculate $\Delta\mu_{eg}$, the radius a needs to be identified. To obtain the radius a, a half of the solvent radius is added to the radius of the solute in order to account for the Van der Waals radius of the solvent molecules. Actually, the radius of the solute or the solvent can be calculated through Eq. (4-14) or Eq. (4-15). The density of the solute can be obtained through pycnometric method. The radius of the solvent 1,4-dioxane was chosen because the peak area of the UV absorption in 1,4-dioxane was calculated. The values of B, ρ and a of 4-NA, and DR1 are listed in Table 4-3.

To obtain γ_{eg}^2, the area under the peak absorption was calculated through software in the UV-2501PC spectrophotometer. According to the Eq. (4-19), the area should be converted into the integration of ε_v over the absorption band. The area under the peak absorption in solvent of 1,4-dioxane was chosen to calculate the γ_{eg}^2, which are listed in Table 4-3 as well. The γ_{eg}^2 of the DR1 is found to be larger than that of 4-NA.

Table 4-3 Parameters derived from the solvatochromic methods and values of hyperpolarizabilities for 4-NA and DR1

	4-NA	DR1
$(\partial\varepsilon/\partial w)_0$*	48.01	30.37
$\mu_g(\times 10^{-29}$ C m)	2.49	2.98
B	-5718.3	-2406.1
ρ (g/cm^3)	1.44	1.33
a (Å)*	4.99	6.17
$\Delta\mu_{eg}$ ($\times 10^{-29}$C m)*	3.15	2.09
γ_{eg}^2 ($\times 10^{-35}$)*	2.83	6.43
β ($\times 10^{-38}$m^4/V)* (1907nm)	0.64	2.05
β_0 ($\times 10^{-38}$m^4/V)*	0.53	1.44

* Measured in 1,4-dioxane

When the values of the related parameters listed in Table 4-3 in Eq. (4-2) were substituted, the β values of 4-NA and DR1 in 1,4-dioxane referred to an incident wavelength of 1907 nm were determined to be 0.64×10^{-38} and 0.205×10^{-37} m^4/V, respectively, and the β_0 values of 4-NA and DR1 in 1,4-dioxane can be determined to be 0.53×10^{-38} and 0.144×10^{-37} m^4/V, respectively. The dispersions of the hyperpolarizability derived from Quantum-mechanical two-level model following Eq. (4-2) are shown in Figure 4-4, which makes it possible to estimate the β value of the chromophores in a special wavelength. It was reported that the β of 4-NA and DR1 measured at 1907 nm through EFISH method are 0.62×10^{-38} and 0.26×10^{-37} m^4/V,

respectively and the β_0 value of 4-NA and DR1 are 0.50×10^{-38} and 0.19×10^{-37} m^4/V, respectively [31]. It can be seen that the β values of 4-NA and DR1 from our calculation are basically the same with the data reported, which confirms that our experimental procedure and program are correct. From the data listed in Table 4-3, it can be seen that the $\Delta\mu_{eg}$ of 4-NA is slightly larger than that of DR1; however, the γ_{eg}^2 of DR 1 is almost 3 times of that of 4-NA. This means that the γ_{eg} is significant for the hyperpolarizability. The μ_g of DR1 is notably larger than that of 4-NA because DR1 has larger conjugated length than 4-NA.

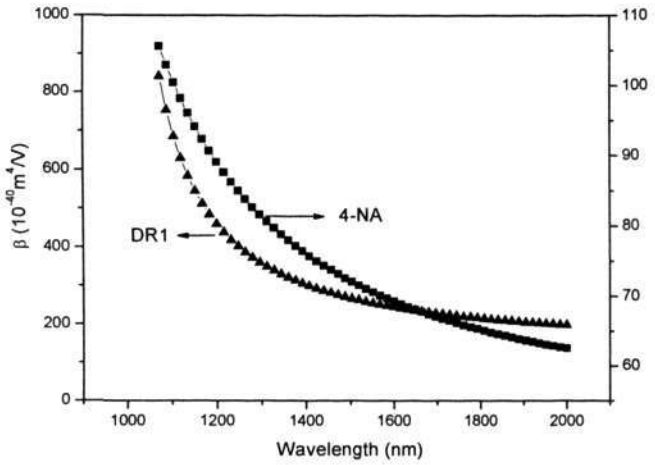

Figure 4-4 The dispersion of the hyperpolarizabilities of the 4-NA and DR1

4.4.2 Effects of Fluorine on Hyperpolarizabilities of Simple Analog Chromophores

In order to have a deep understanding on the effects of fluorine and fluorine position on the hyperpolarizabilities of the fluoronitroaryl diaminoazobenzene chromophores, the corresponding simple chromophores (3-NA, 2-F-5-NA and 4-F-3-NA) were selected as analogs. The UV-vis spectra of 3-NA, 2-F-5-NA and 4-F-3-NA in different

solvents are shown in Figure 4-5. Red shifts in λ_{max} were also found with the increase in the polarity of the solvent. The plots of Eq. (4-8) for 3-NA, 2-F-5-NA and 4-F-3-NA are shown in Figure 4-6. The linear correlation coefficients of 0.93, 0.92 and 0.95, indicated that the linear correlations are satisfied. The concentration dependences of the dielectric constants are shown in Figure 4-7. The parameters used for the calculation of the hyperpolarizabilities are listed in Table 4-4.

Formatted: Right

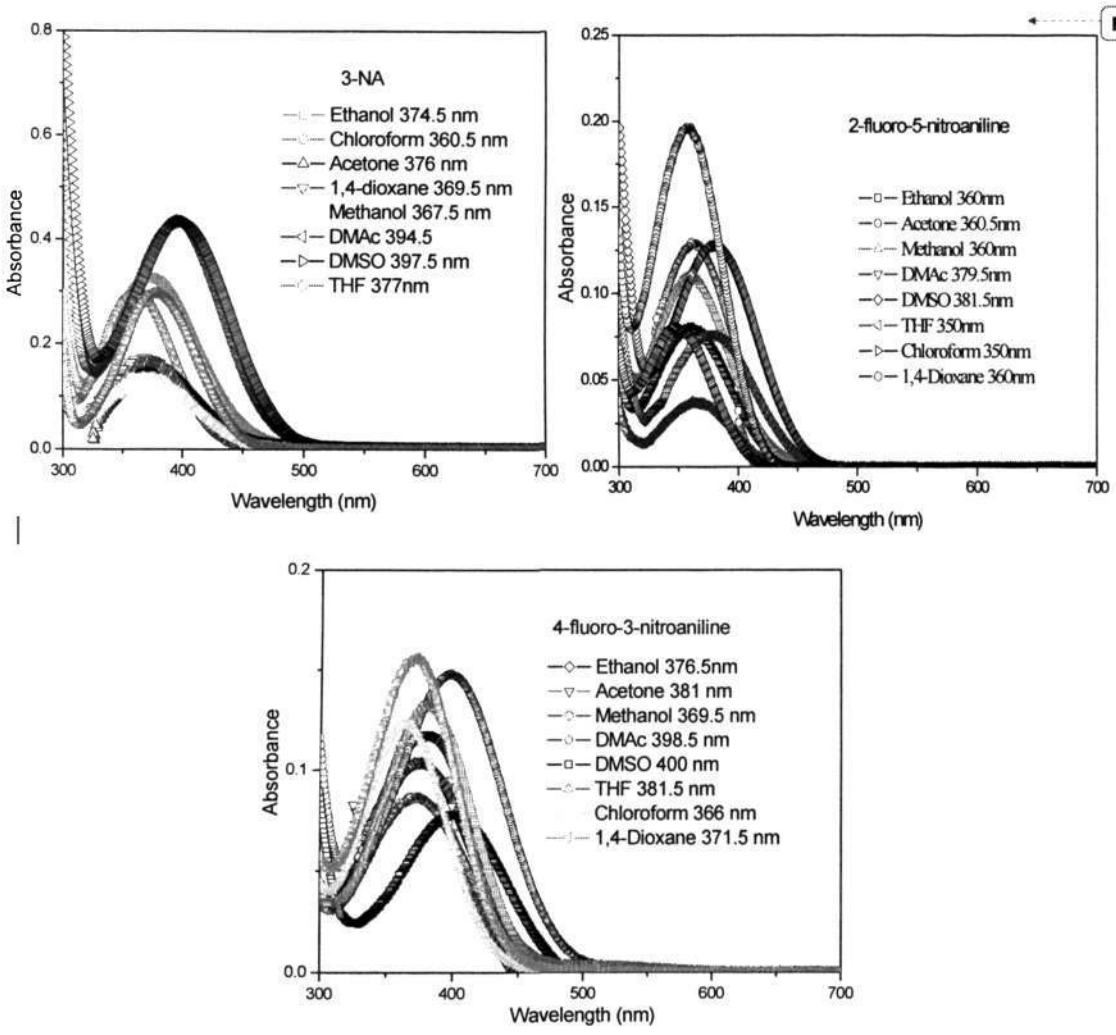

Figure 4-5 UV-vis spectra of 3-NA, 2-F-5-NA and 4-F-3-NA in different solvents

From the data listed in Table 4-4, it can be seen that μ_g of 4-F-3-NA is the largest and that of 3-NA is the smallest of the 3 selected chromophores. The incorporation of fluorine into 3-NA could increase the μ_g because the fluorine is a strong electronegative atom. The μ_g of 4-F-3-NA is larger than that of 2-F-5-NA possibly because of the fluorine at the para position that leads to the more concentrated distribution of negative charge in the same direction. However, the fluorine at the ortho position leads to the distribution of negative charge more evenly in two different directions. And results also show that 3-NA has smaller μ_g than 4-NA because of the nitro group at the meta position [7]. The hyperpolarizability β_0 of 3-NA, 2-F-5-NA and 4-F-3-NA are determined to be 4.97, 3.39 and 4.75, respectively. The dispersions of the hyperpolarizability derived from quantum-mechanical two-level model following the Eq. (4-2) are shown in Figure 4-8. In comparison with 4-NA, 3-NA displays smaller hyperpolarizability because the nitro group locates at the meta position. The nitro group at the meta position cannot form the conjugated system with the benzene ring so that the charge transfer resonance is forbidden for meta substituent as shown in Figure 4-9. It can be concluded that the β_0 of 3-NA is the largest one of 3 selected chromophores. Generally, the incorporation of fluorine into a molecule structure will lead to a decrease in hyperpolarizability because fluorine group is weak π-donors and strong δ-acceptors [20]. It can also be seen that the hyperpolarizability of 4-F-3-NA is larger than that of 2-F-5-NA. This reveals that the fluorine group in different position will lead to different electronic distribution of the charge-transfer states of the two molecules. This can be verified from the UV-vis spectra (Figure 4-5) and the measured transition dipole moments (Table 4-4).

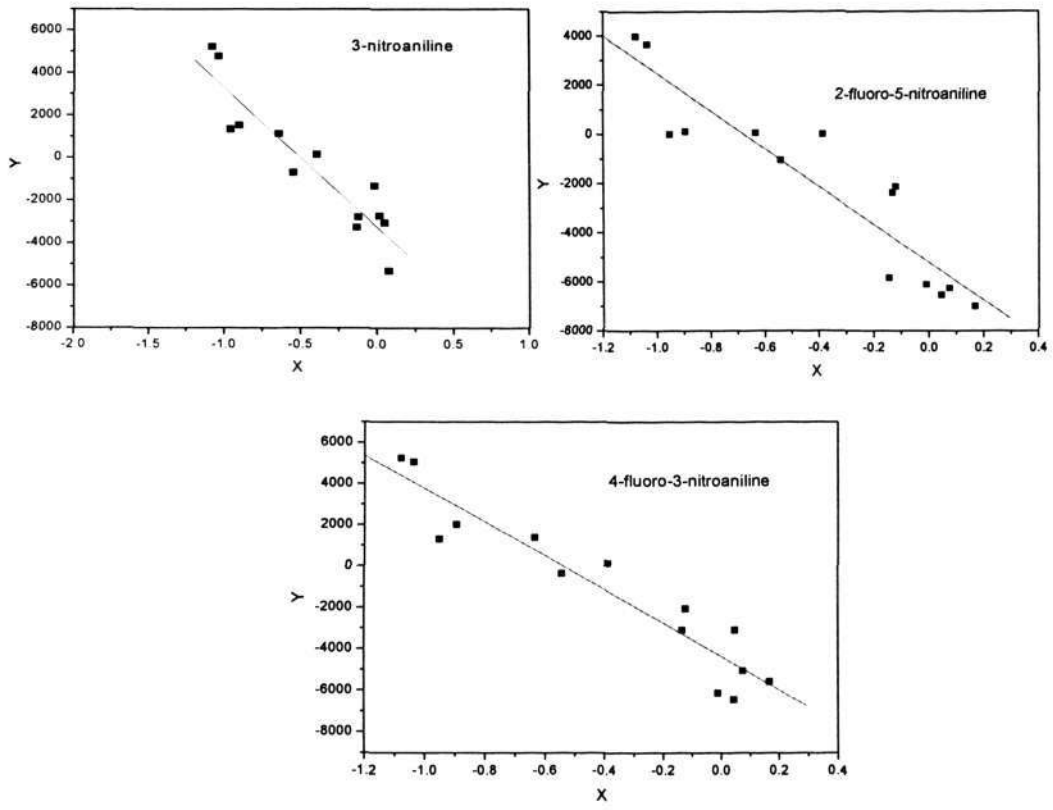

Figure 4-6 Plot of Eq. (4-8) for 3-NA (r = 0.93), 2-F-5NA (r = 0.92) and 4-F-3-NA (r = 0.95)

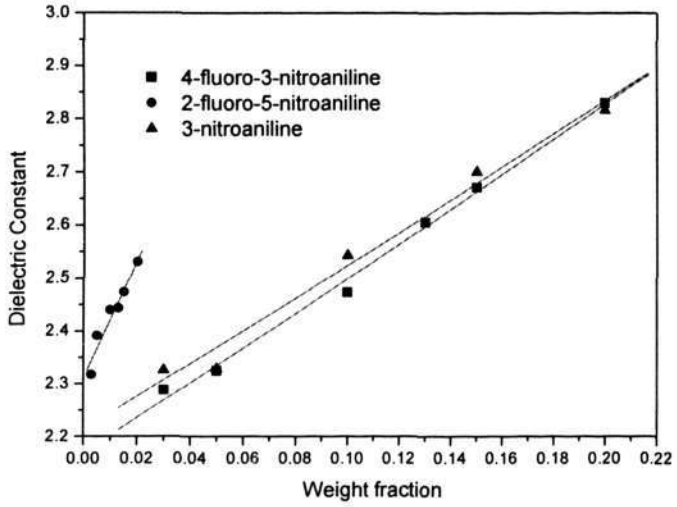

Figure 4-7 Concentration dependence of the dielectric constant of 3-NA, 2-F-5-NA and 4-F-3-NA in1,4-dioxane

Table 4-4 Parameters derived from the solvatochromic methods and values of hyperpolarizabilities for 3-NA, 2-F-5-NA and 4-F-3-NA

	3-NA	2-F-5-NA	4-F-3-NA
$(\partial\varepsilon/\partial w)_0$ *	24.0	38.6	42.3
μ_g ($\times 10^{-29}$ C m)	1.76	2.37	2.49
B	-3260.0	-5222.9	-4351.1
ρ (g/cm^3)	0.90	1.66	1.58
a (Å)*	5.56	4.94	5.03
$\Delta\mu_{eg}$ ($\times 10^{-29}$ C m) *	3.57	2.97	3.27
γ_{eg}^2 ($\times 10^{-36}$)*	2.16	1.85	2.22
β_0($\times 10^{-40}$m^4/V)*	4.97	3.39	4.75

* Measured in 1,4-dioxane

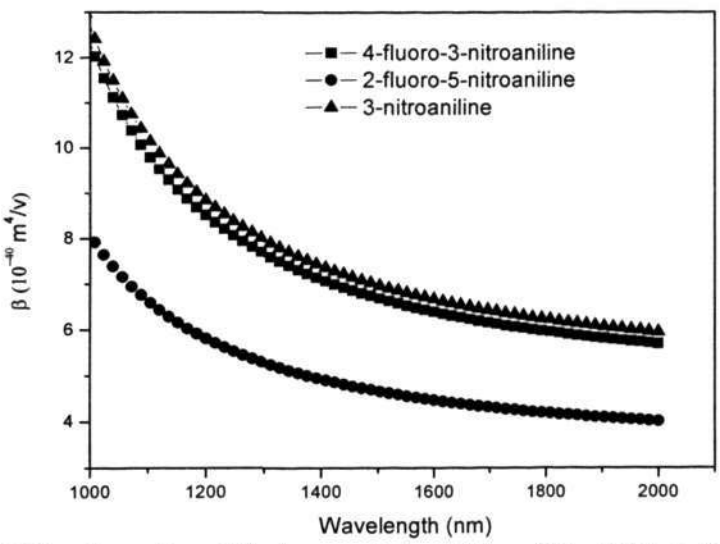

Figure 4-8 The dispersion of the hyperpolarizabilities of the 3-NA, 2-F-5-NA and 4-F-3-NA

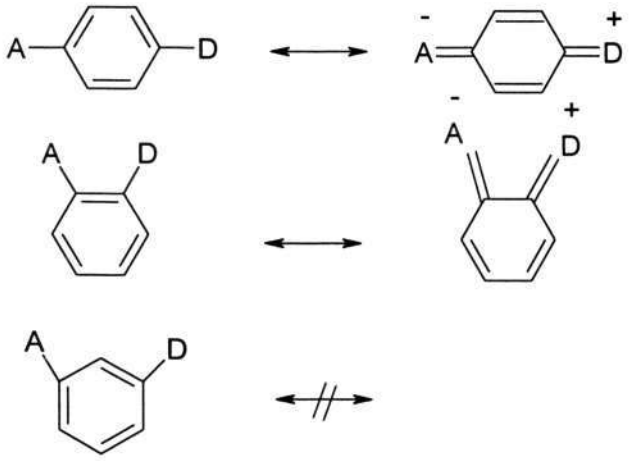

Figure 4-9 Ground-state and lowest energy polar resonance forms for para, ortho and meta substitution.

4.4.3 Hyperpolarizabilities of Diaminoazobenzene Chromophores

This section describes how the hyperpolarizabilities of diaminoazobenzene chromophores were determined. The UV-vis spectra of 2R-4N-DIAMINE, 2R-3N-DIAMINE, 2R-2F-5N-DIAMINE and 2R-4F-3N-DIAMINE in different solvents are shown in Figure 4-10. The λ_{max} in different solvents are listed in Table 4-5. It can be found that the λ_{max}s of these diaminoazobenzene chromophores also exhibit the positive solvatochromism. It is interesting to find that the λ_{max} of 2R-4F-3N-DIAMINE is larger than that of 2R-3N-DIAMINE in all solvents except NMP, whereas 2R-4F-3N-DIAMINE exhibits red shift λ_{max} in NMP compared with 2R-3N-DIAMINE. This is possibly because the interaction between 2R-4F-3N-DIAMINE and NMP is larger than that between 2R-3N-DIAMINE and NMP so that the energy gap between the $\pi \rightarrow \pi^*$ excitation for 2R-4F-3N-DIAMINE is smaller than that for 2R-3N-DIAMINE.

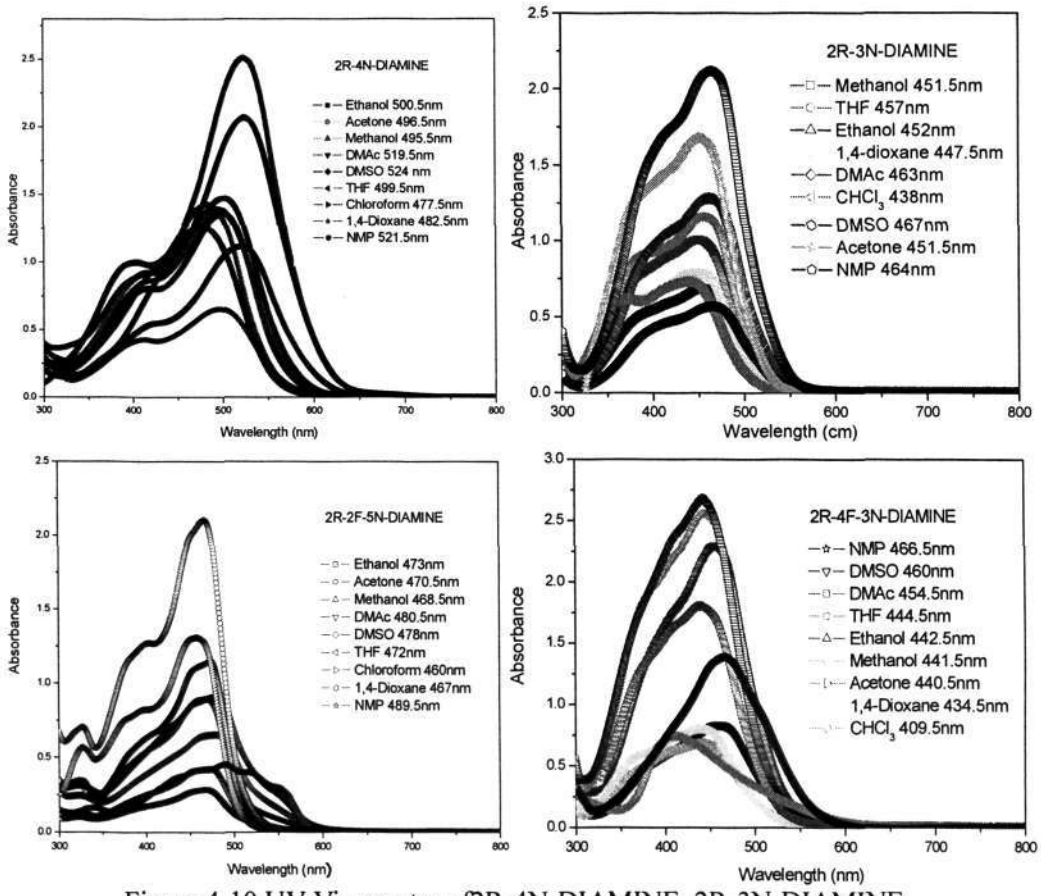

Figure 4-10 UV-Vis spectra of2R-4N-DIAMINE, 2R-3N-DIAMINE, 2R-2F-5N-DIAMINE and 2R-4F-3N-DIAMINE in different solvents

The plots of Eq. (4-8) for 2R-4N-DIAMINE, 2R-3N-DIAMINE, 2R-2F-5N-DIAMINE and 2R-4F-3N-DIAMINE are shown in Figure 4-11. Their linear correlation coefficients were 0.94, 0.92, 0.93 and 0.91, respectively, which show satisfactory linear correlations. Their concentration dependences of the dielectric constants are shown in Figure 4-12. The parameters used for the calculation of the hyperpolarizabilities are shown in Table 4-7. Figure 4-13 shows the dispersion of the hyperpolarizabilities derived from quantum-mechanical two-level model following the Eq. (4-2).

Table 4-5 λ_{max} of 2R-DIAMINE and 2R-2F-5N-DIAMINE in different solvents

λ_{max}	2R-4N-DIAMINE	2R-3N-DIAMINE	2R-2F-5N-DIAMINE	2R-4F-3N-DIAMINE
NMP	521.5 nm	464 nm	489.5 nm	466.5 nm
DMSO	524 nm	467 nm	478 nm	460 nm
DMAc	519.5 nm	463 nm	480.5 nm	454.5 nm
Ethanol	500.5 nm	452 nm	473 nm	442.5 nm
Methanol	495.5 nm	450 nm	468.5 nm	441.5 nm
Acetone	496.5 nm	451.5 nm	470.5 nm	440.5 nm
THF	472 nm	457 nm	472 nm	444.5 nm
1,4-dioxane	467 nm	447.5 nm	467 nm	434.5 nm
$CHCl_3$	460 nm	438 nm	460 nm	409.5 nm

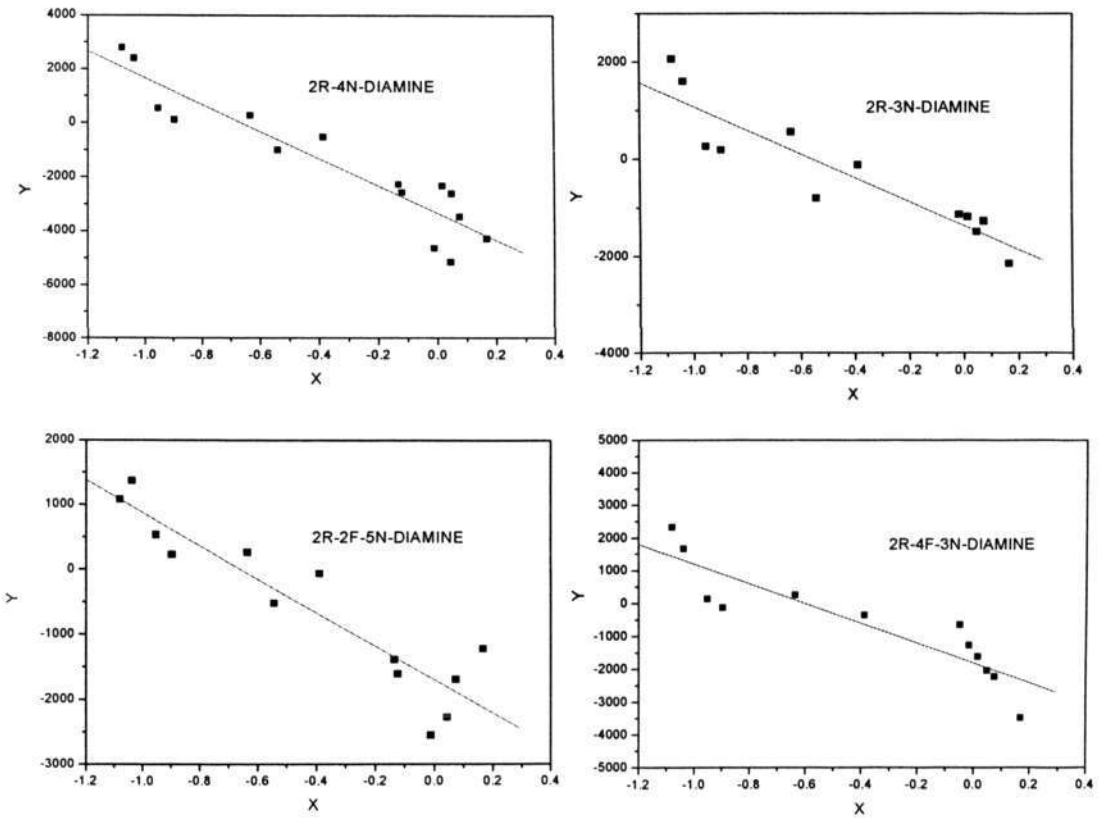

Figure 4-11 Plot of Eq. (4-8) for 2R-4N-DIAMINE (r = 0.94), 2R-3N-DIAMINE (r = 0.92), 2R-2F-5N-DIAMINE (r = 0.93) and 2R-4F-3N-DIAMINE (r = 0.91)

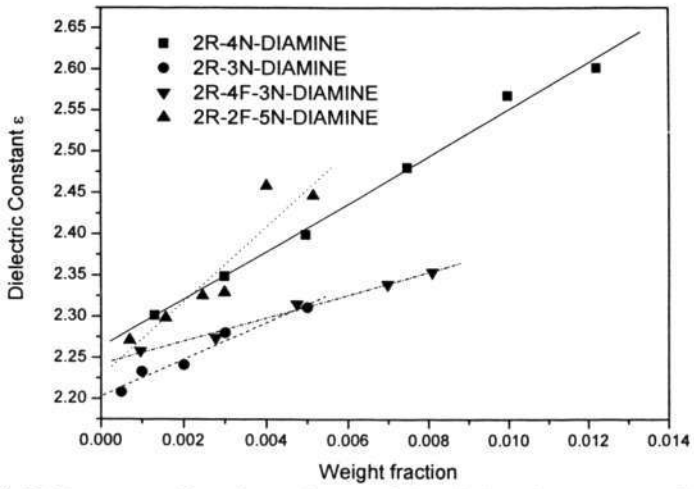

Figure 4-12 Concentration dependence of the dielectric constant of 2R-4N-DIAMINENE, 2R-3N-DIAMINE, 2R-2F-5N-DIAMINE and 2R-4F-3N-DIAMINE in 1,4-dioxane

Formatted: Centered

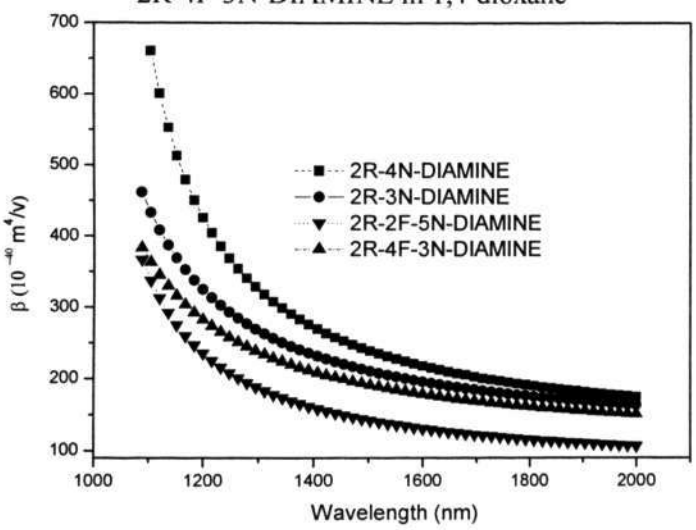

Figure 4-13 The dispersion of the hyperpolarizabilities of the 2R-4N-DIAMINE, 2R-3N-DIAMINE, 2R-2F-5N-DIAMINE, and 2R-4F-3N-DIAMINE

From the data listed in Table 4-6, it can be seen that μ_g decreases in the following sequence: 2R-4F-3N-DIAMINE > 2R-2F-5N-DIAMINE > 2R-4N-DIAMINE > 2R-4N-DIAMINE. Compared diaminoazobenzene chromophores with the selected simple analog chromophores, the similar effects of fluorine and fluorine position on μ_g were also found for the diaminoazobenzene chromophores. This further confirms that the

incorporation of fluorine into chromophore could increase μ_g because the fluorine is a strong electronegative atom and fluorine at different position will lead to different charge distribution. Results also show that 2R-4N-DIAMINE has larger μ_g than 2R-3N-DIAMINE because of the nitro group at the para position [7].

Table 4-6 Parameters derived from the solvatochromic methods and hyperpolarizabilities for 2R-4N-DIAMINE, 2R-3N-DIAMINE, 2R-2F-5N-DIAMINE and 2R-4F-3N-DIAMINE

	2R-4N-DIAMINE	2R-3N-DIAMINE	2R-2F-5N-DIAMINE	2R-4F-3N-DIAMINE
$(\partial\varepsilon/\partial w)_0$ *	46.00	40.85	72.51	81.04
μ_g ($\times 10^{-29}$ C m)	3.31	3.13	4.31	4.56
B	-3354.6	-1364.7	-1694.4	-1810.3
ρ (g/cm^3)	1.47	2.47	1.67	0.97
a (Å)*	5.74	5.08	5.67	6.46
$\Delta\mu_{eg}$ ($\times 10^{-29}$ C m) *	2.11	1.77	1.58	1.53
γ_{eg}^2 ($\times 10^{-35}$)*	5.42	7.98	4.85	7.79
β_0 ($\times 10^{-40}$ m^4/V)*	126	124.1	78.6	116.7

* Measured in 1,4-dioxane

The hyperpolarizabilities β_0 of 2R-4N-DIAMINE, 2R-3N-DIAMINE, 2R-2F-5N-DIAMINE and 2R-4F-3N-DIAMINE were determined to be 126, 124.1, 116.7 and 78.6 $\times 10^{-40}$ m^4/V, respectively. The hyperpolarizabilities were found to decrease in the same sequence with their simple analog chromophores. Similar effects of the nitro

group at the meta position, fluorine and fluorine position on the hyperpolarizabilities for these diaminoazobenzene chromophores were also found. From the β_0 value of 2R-3N-DIAMINE being smaller than that of 2R-4N-DIAMINE, it was further confirmed that the nitro group at the meta position could decrease β value because it cannot form the conjugated system with the benzene ring and results in the forbidden charge transfer resonance. The β_0 of 2R-3N-DIAMINE is the larger than that of 2R-4F-3N-DIAMINE and 2R-2F-5N-DIAMINE because of the incorporation of fluorine into chromophore. It can also be seen that 2R-4F-3N-DIAMINE has larger hyperpolarizability than 2R-2F-5N-DIAMINE. This also confirms that the fluorine group in different position will lead to different electronic distribution in the charge-transfer states of the two molecules. Compared with their corresponding simple analog chromophores, the diaminoazobenzenes chromophores exhibited larger hyperpolarizabilities because they have longer conjugated systems in their structures. It can also be concluded that although the β_0 values of these diaminoazobenzenes chromophores are slightly smaller than that of DR1, they are in the same order with DR1 and large enough for the development of polyimide with large second harmonic coefficient.

4.5 Summary

In this chapter, a solvatochromic method was used to characterize the hyperpolarizability of the chromophore. The calibration results through 4-NA and DR1 show that the experimental procedure and the programs based on the solvatochromic method are reliable.

In order to understand the effects of fluorine and position of the fluorine on the hyperpolarizabilities, 3-NA, 2-F-5-NA and 4-F-3-NA were studied first. The incorporation of fluorine into 3-NA could lead to an increase in dipole moment and decrease in hyperpolarizability. And the results reveal that the fluorine group in different position will lead to different electronic distribution in the charge-transfer states of the two molecules, different dipole moment and hyperpolarizability.

The hyperpolarizabilities of 2R-4N-DIAMINE, 2R-3N-DIAMINE, 2R-2F-5N-DIAMINE and 2R-4F-3N-DIAMINE were characterized. The hyperpolarizabilities β_0 of 2R-4N-DIAMINE, 2R-3N-DIAMINE, 2R-2F-5N-DIAMINE and 2R-4F-3N-DIAMINE were 126, 124.1, 116.7 and 78.6 $\times 10^{-40}$ m^4/V, respectively. The effects of fluorine and the fluorine position on the dipole moment and hyperpolarizability of the diaminoazobenzene chromophores are similar to those of their simple analog chromophores. Compared with their corresponding simple analog chromophores, the diaminoazobenzenes chromophores exhibited larger hyperpolarizabilities because they have longer conjugated systems in their structures. The β_0 values of the diaminoazobenzenes chromophores were slightly smaller than that of DR1 but were in the same order, and large enough for the development of polyimides with large second harmonic coefficient.

Chapter 5 Synthesis and Characterization of NLO Polyimides Based on Diaminoazobenzene Chromophores

5.1 Introduction

In Chapter 2, it was suggested that the device-quality NLO polymers need to meet some basic requirement such as large second-order nonlinearity, high thermal long-term stability and low optical loss. In past decades, a lot of research work concentrated on how to prepare NLO polymers with large nonlinear optical coefficient. Researchers found that these NLO polymers always display lower thermal stability (T_d <300 °C) and lower transparency (λ_{max} > 500 nm). Although large E-O coefficient have been demonstrated in several prototype EO modulator using guest-host poled polymers and the progress is encouraging, these prototype EO modulators cannot be used in actual device operation due to poor long term stability and high optical loss. Therefore, there is still a very strong need to improve thermal stability and transparency of these materials in order to fulfill the requirements for long-term device operation and substitute the NLO inorganic materials. Many researchers such as Dalton [64] have been concentrating on how to improve the thermal stability and transparency of the NLO polymer. Since chromophores were firstly incorporated into polyimide, researchers have focused their attention on this material because it possesses long-term stability [9,127,144,154]. In past decades, much more attention has been given to side-chain NLO polyimides as they can overcome some disadvantages of guest-host polymers and improve some properties such as thermal stability [145,149-150,153]. Although these side-chain NLO polyimides exhibit good properties, the long tails of the intrinsic absorption of the polyimides backbone and chromophore side chain can extend several hundreds nanometers into the operating

wavelength and could lead to low transparency and large optical loss because there are many aromatic conjugated structures and auxochrome group in polyimides backbone and chromophore side chain, which is the primary sources of optical loss. Therefore, their applications are limited. Hence, it is very important to optimize the comprehensive properties of the NLO polyimide especially transparency. It was reported that the optical loss from polyimide backbone can be decreased through fluorinated monomer such as 6FDA because of the reduction of in-planing packing and polymer deformation. However, the optical loss from the chromophore side chain still cannot be decreased. It has been found that the incorporation of fluorinated chromophores into polymer as guests could lead to good properties such as high transparency and low optical loss. However, guest-host NLO polymer materials have some fatal disadvantages such as the fast decay of NLO activity due to orientational relaxation. Hence, the design and synthesis of donor-embedded side-chain NLO polyimides based on fluorinated chromophore could be a new approach to improve the thermal and optical properties for meeting the requirement of the application. Based on the successful synthesis of fluorinated chromophore diamine monomers, this chapter reports the synthesis and characterization of two new polyimides containing fluorinated diaminoazobenzene as the NLO-active side chain and their corresponding analogues. The effects of fluorine and the fluorine position in NLO-active side chain on their properties have also been investigated. Possible mechanisms have been proposed based on the results of structure modeling of the polyimide.

5.2 Synthesis of NLO Polyimides Based on Diaminoazobenzene Chromophores

5.2.1 Materials

Table 5-1 lists the main raw materials used in the synthesis of polyimide. BTDA was purified through recrystallization from acetic anhydride and PMDA was purified

through sublimation. These dianhydrides (PMDA, BTDA and 6FDA) were dried under a vacuum at 150 °C overnight before use. 1-Methyl-2-pyrrolidone (NMP) was purchased from Clariant and stored over 4 Å molecular sieves. Other chemicals were purchased from Aldrich, Merck and Clariant and were used without further purification, unless otherwise stated.

Table 5-1 Main raw materials used in the synthesis of polyimide

Name	Molecular Formula	Supplier
3,3',4,4'-Benzophenonetetracarboxylic dianhydride (BTDA) 98%	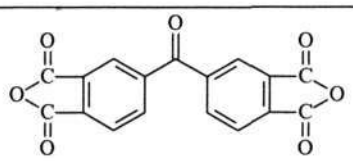	Clariant
4,4'-(Hexafluoroisopropylidene)diphthalic anhydride (6FDA) 99%	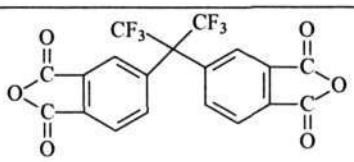	Clariant
Pyromellitic dianhydride 98%	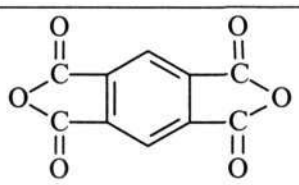	Clariant
1-Methyl-2-pyrrolidone (NMP) 99.5%	C_5H_9NO	Clariant

5.2.2 Characterization

^{1}H NMR, element analysis, FTIR spectroscopy, UV-visible spectra and TGA were used to characterize the synthesized polyimide as described in Chapter 3.

Glass transition temperature T_g of the polyimide was determined through DSC

analysis that was performed by a TA Instruments 2010 at a heating rate of 10 °C/min in nitrogen atmosphere (50 cc/min).

Intrinsic viscosity measurement was performed through a Cannon-Ubbelohde viscometer at a bath temperature of 25 °C to determine the relative molecular weights of PA in NMP. The solubility of polyimide were tested by immersing 10 wt% of the films into solvents and stored in a small capped glass vials for 24 hours. For soluble polyimides (series PI III), the molecular weight and its polydispersity can be characterized through gel permeation chromatography (GPC). The number-average molecular weights (M_n), weight-average molecular weights (M_w) and polydispersities (M_w/M_n) were determined using an Agilent series 1100 gel permeation chromatograph equipped with a differential refractometer detector. A mixed bed column (PLGel Mixed Bed C, 5μ, 300×7.5 mm, Polymer Laboratories) along with a guard column (50×7.5 mm, Polymer Laboratories) was employed. The mobile phase was a mixture of tetrahydrofuran (THF)/dichloromethane (DCM) in a volume ratio of 80/20. Molecular weights of samples were obtained relative to polystyrene standards. The flow rate of mobile phase was 1 ml/min and the temperature (both the column compartment and the flow cell of the refractive index detector) was 35±0.1°C.

The contact angle was measured using First Ten Angstroms system with automatic gain control camera with deionized water as reference liquid. The surface energy was automatically computed through Girifalco-Good-Fowkes-Young Model. In water absorption test, the polyimide films on glass slide were cut into 20×20 mm samples. The samples were dried at 105 °C for 1 hour and weighed. After that, they were kept in deionized water at 25 °C for 24 hours and weighed again.

The optimized polyimide unit structure simulation was carried out through AM1/VAMP model/Material Studio 3.0 software package (Accelrys Inc.).

The second harmonic coefficient d_{33} of the second-order NLO polymeric film was characterized by the Maker-fringe method. According to reference [118], a SHG measurement for measuring d_{33} through Maker-fringe method was set up. The typical setup for measurement of d_{33} is shown in Figure 5-1. The laser source was a Polaris II Q-switched Nd:YAG pulse laser with a 1064 nm p-polarized fundamental beam (4-5 ns pulse width, 20 Hz maximum Repetition rate, 50 mJ maximum energy, New Ware Research). The laser beam passed through the polymer sample mounted on a motorized rotating stage (DT-80, Micos) controlled by computer through an interface module (SMC Corvus, Micos). The fundamental laser beam was filtered off by a short pass filter. The interference filter only let the second harmonic light at 532 nm pass. The second harmonic signal was detected and amplified by a photomultiplier tube (PMT R928, Hamamatsu) and was then averaged in a boxcar integrator (Model SR250, Stanford Research System) and transferred to a computer through an interface module (Model SR245, Stanford Research System). The second harmonic signal was also monitored directly on a HP Model 54615B 500MHz digital oscilloscope. The film thickness was measured by an Alpha-step 500 Surface Profilometer. The refractive indexes at 532 nm and 1064 nm were measured by a M-2000® Spectroscopic ellipsometer (J. A. Woollam Co. Inc.).

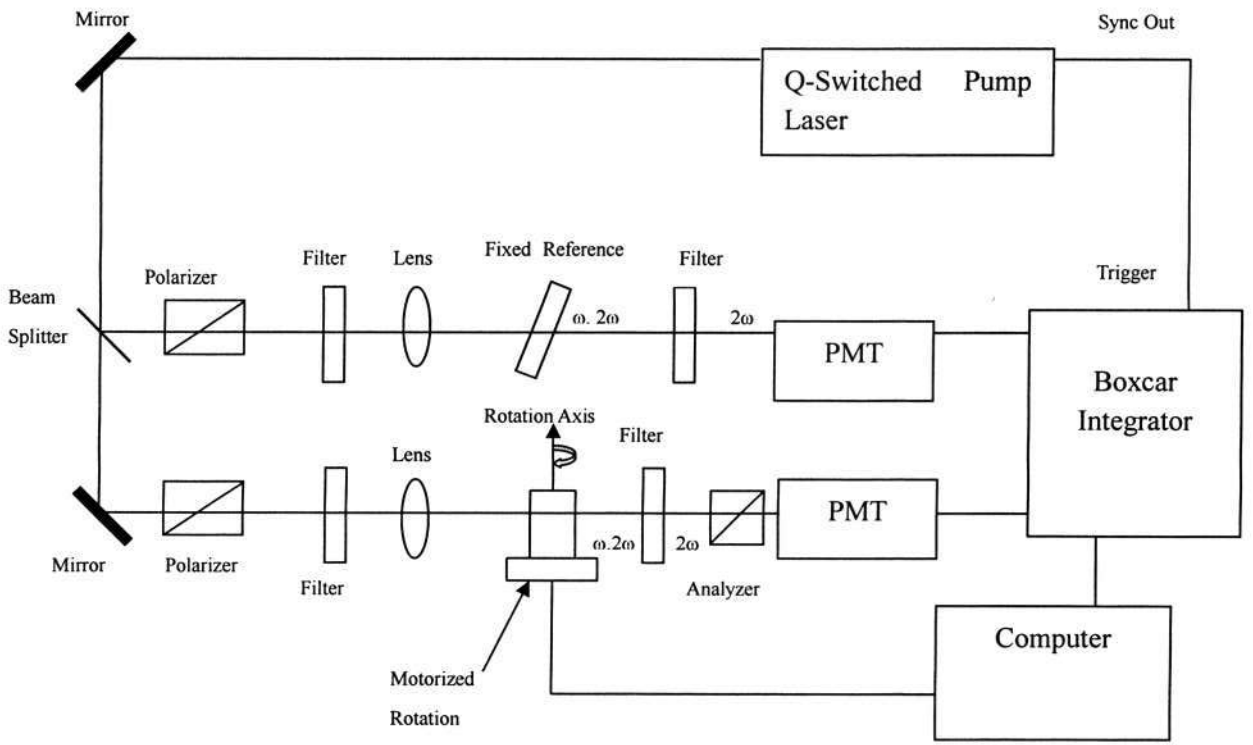

Figure 5-1 Experimental configuration for measuring d_{33} by the Maker fringe method

5.2.3 Polymerization of Poly(amic acid) and Mechanism

5.2.3.1 Polymerization of Poly(amic acid)

A general polymerization procedure for NLO poly(amic acid) (PA) is shown in Figure 5-2. The diamine chromophore monomer (2.0 mmol) was dissolved in 7 ml anhydrous NMP at 0 °C, followed by the addition of the dianhydride monomer (2.08 mmol) at once. After stirring at a temperature between 0 and 5 °C for 4 hours, the solution was then stirred at room temperature for 20 hours. The resulting polymer solution was filtered through a 0.2 μm Teflon membrane filter and was spin-coated on a substrate at various speeds ranging from 500 rpm to 4000 rpm for different durations from 5 to 30 second in clean room. After the films were dried in a vacuum oven at 65 °C for 12hr to remove the solvent, they were subjected to imidization or in-situ poling and imidization at different temperatures.

The synthesized poly(amic acid) and polyimides, and the corresponding monomers used in the experiment are summarized in Table 5-2, where the names of the poly(amic acid)s and polyimides are simplified.

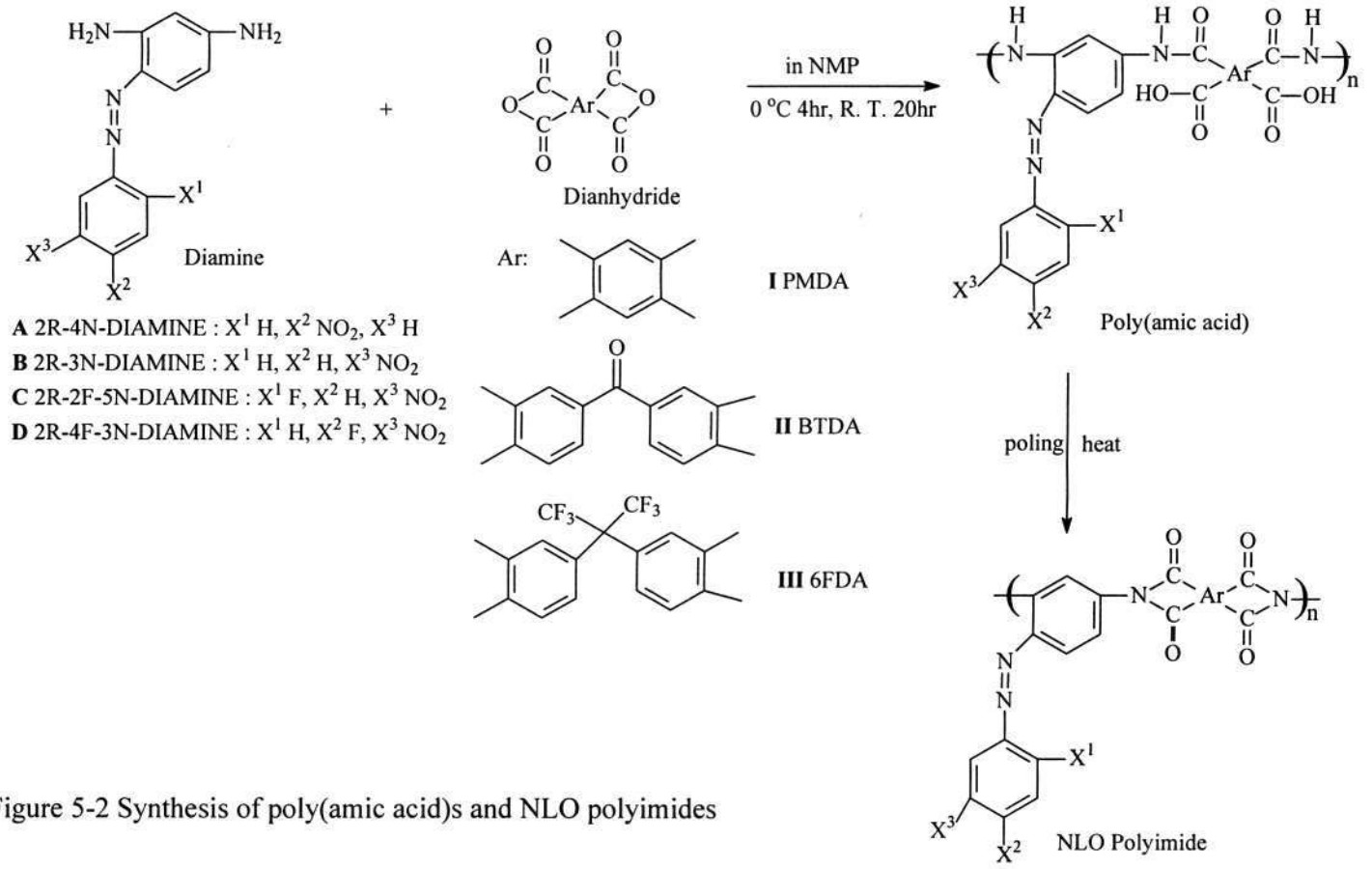

A 2R-4N-DIAMINE : X^1 H, X^2 NO_2, X^3 H
B 2R-3N-DIAMINE : X^1 H, X^2 H, X^3 NO_2
C 2R-2F-5N-DIAMINE : X^1 F, X^2 H, X^3 NO_2
D 2R-4F-3N-DIAMINE : X^1 H, X^2 F, X^3 NO_2

Figure 5-2 Synthesis of poly(amic acid)s and NLO polyimides

Table 5-2 Symbols of poly(amic acid), polyimide and their monomers

Poly(amic acid)	Polyimide	Diamine chromophore	Dianhydride
PA **A-I**	PI **A-I**	2R-4N-DIAMINE (A)	PMDA (I)
PA **A-II**	PI **A-II**	2R-4N-DIAMINE (A)	BTDA (II)
PA **A-III**	PI **A-III**	2R-4N-DIAMINE (A)	6FDA (III)
PA **B-I**	PI **B-I**	2R-3N-DIAMINE (B)	PMDA (I)
PA **B-II**	PI **B-II**	2R-3N-DIAMINE (B)	BTDA (II)
PA **B-III**	PI **B-III**	2R-3N-DIAMINE (B)	6FDA (III)
PA **C-I**	PI **C-I**	2R-2F-5N-DIAMINE (C)	PMDA (I)
PA **C-II**	PI **C-II**	2R-2F-5N-DIAMINE (C)	BTDA (II)
PA **C-III**	PI **C-III**	2R-2F-5N-DIAMINE (C)	6FDA (III)
PA **D-I**	PI **D-I**	2R-4F-3N-DIAMINE (D)	PMDA (I)
PA **D-II**	PI **D-II**	2R-4F-3N-DIAMINE (D)	BTDA (II)
PA **D-III**	PI **D-III**	2R-4F-3N-DIAMINE (D)	6FDA (III)

It should be noted that only one layer of the film was spun onto the substrate. The film thickness was controlled by changing the concentration of the PA solution, spin speed and spin time. Microscope glass slide or indium tin oxide (ITO) glass was used as substrate for different characterization purposes. It is very important to clean the substrate for preparing the good films. The glass was ultrasonically cleaned with NMP, deionized water, acetone, ethanol and isopropanol (IPA) for 15 minutes, respectively. Finally, it was rinsed with deionized water and purged with pure nitrogen gas for drying the surface.

5.2.3.2 Mechanism of Polymerization of Poly(amic acid)

Synthesis of polyimide can be carried out in one- or two-stage method. In our

experiments, two-stage method via poly(amic acid) was used to synthesize polyimide because both the soluble and insoluble polyimide in organic solvents can be synthesized by this method. Another advantage is that this method allows the diffusion of by-product and solvent without forming bristles and voids in the final polyimide products and, hence, is suitable for preparation of thin objects such as films, fibers, coatings, modeling powder. The first stage of the synthesis is the formation of intermediate, poly(amic acid). The second stage of synthesis, called imidization, is carried out in cast products by thermal treatment of poly(amic acid) or by treating poly(amic acid) with water-capturing agents in the presence of catalysts. There are many factors influencing the polymerization of poly(amic acid), such as chemical and physical natures of monomers and intermediate as well as solvents.

a) Effects of Temperature and Concentration of Monomers

When a diamine and a dianhydride are added into a dipolar aprotic solvent such as NMP, PA is rapidly formed at ambient temperatures. The reaction mechanism involves in the nucleophilic attack of the amino group on the carbonyl carbon of the anhydride group, and the opening of the dianhydride ring to form amic acid groups (Figure 5-3) [185]. The most important aspect of this reaction is that it is an equilibrium reaction. It should be noted that the acylation reaction of amines is an exothermic reaction and that the equilibrium is favored at lower temperatures. The forward reaction in dipolar solvents is a second-order reaction and the reverse reaction is a first-order reaction. Therefore, the equilibrium is favored at high monomer concentrations to form higher molecular weight of poly(amic acid). Lower reaction temperature especially at the beginning of the synthesis reaction (< 5 ^{o}C, first 4 hours

and then room temperature) and high monomers concentration (>10%)were used to yield high molecular weight of PA solution.

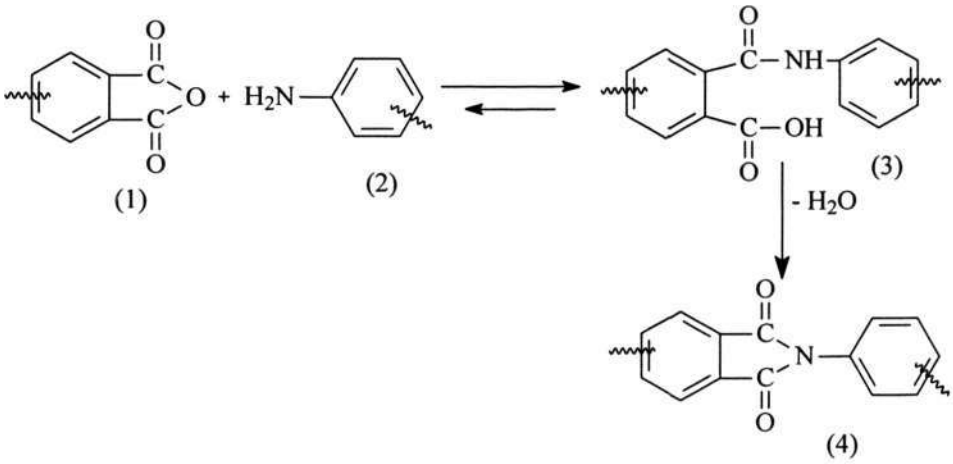

Figure 5-3 Reaction mechanism of imide formation

b) Effect of Reactivity of Monomer

According to the nucleophilic substitution reaction mechanism, the reaction rate is primarily governed by the electrophilicity of the carbonyl groups of the dianhydride and the nucleophilicity of the amino nitrogen atom of the diamine. Among commonly available dianhydrides, PMDA, BTDA and 6FDA are more reactive because they have large electron affinity [185]. These dianhydrides must be handled under strictly moisture-free conditions at all times due to their high activity. The structure of diamine seems to influence the rate of acylation reaction more than the variation in dianhydride structure. The reactivity of diamine is related with its basicity [185]. Although there is fluorine group located in the new designed chromophores leading to a decrease in basicity, the nitro group located at the meta position cannot form the conjugated system with the

benzene ring and lead to an increase in the basicity. Therefore, the new fluorinated diaminoazobenzene chromophores can also have enough reactivity so that high enough molecular weight of poly(amic acid) can be synthesized.

c) Effect of Solvents

Solvents used in the polymerization of poly(amic acid) play an important role. Most commonly used solvents are dipolar aprotic solvents such as N,N-dimethylformamide (DMF), N,N-dimethylacetamide (DMAc), N-methylpyrolidinone (NMP) and tetramethylurea (TMU). Solvent choice also influences the molecular weight of poly(amic acid). The molecular weight of poly(amic acid) increased with the thermodynamic quality of the solvent in the order of DMAc > NMP > DMF [186]. As DMAc is more poisonous than NMP, NMP was selected as the solvent. In the presence of water, the side reaction that the dianhydride group is hydrolyzed to form ortho dicarboxylic group will happen. The common source of the water in the reaction is the water which exists in the solvent. Therefore, anhydrous NMP should be used. In our experiments, anhydrous NMP were stored with 4 Å molecular sieves in order to get rid of the moisture in NMP.

d) Effects of Molar Ratio of the Monomer and Addition Sequence of the Monomer

In the polycondensation reaction, the exact stoichiometry is very important to obtaining high molecular weight. However, a slight excess of dianhydride is found to be useful in attaining higher molecular weight of poly(amic acid) because the side reaction always consume a small part of dianhydride [187]. The addition sequence of

the monomers is another important factor that influences the molecular weight of poly(amic acid). Generally, addition of a diamine to a PMDA solution produced a lower molecular weight poly(amic acid) solution than when it was prepared in the reverse order of addition [188]. Therefore, in our experiments, the molar ratio of dianhydride to diamine was selected to be 1.04:1 and the addition of dianhydride to diamine solution method was chosen.

5.2.4 In-situ Poling and Imidization of Poly(amic acid) Films

5.2.4.1 In-situ Poling and Imidization of Poly(amic acid) Films

In this study, the corona poling was used to pole the films. The advantages of the corona poling are that only the film surface is charged and the defects in the film such as impurities and pinholes, do not produce enough local current to lead to short circuiting in the samples. A corona poling in a wire-to-plane geometry at elevated temperatures was selected in our study, since this configuration can impose a large orientation order on a material and results in higher second-order NLO effects. According to the reference [189], a simple in-situ poling and imidization system was set up and the schematic figure is shown in Figure 5-4. Poly(amic acid) films were poled in a temperature-controlled oven under a corona discharge field using 75 μm diameter tungsten wire in a wire-to-plane geometry of 1.5 cm above a Teflon protected, grounded copper block. High voltage power supply (Glass Man Voltage) was controlled and monitored by a picoammeter/voltage source (KEITHLEY Model 487). The positive voltage applied to the tungsten wire was as high as 7 kV while the copper substrate was grounded. Beyond 7 kV, the dielectric breakdown happened and the film would be damaged by the dielectric breakdown.

A two-step corona poling process was employed to orient the NLO chromophore. While a high voltage was applied to a corona wire simultaneously, the sample was first heated to 200~260 °C, at a rate of 5 °C/min and successively held at this temperature for 1 hr. The sample was then cooled to room temperature in the presence of the poling field.

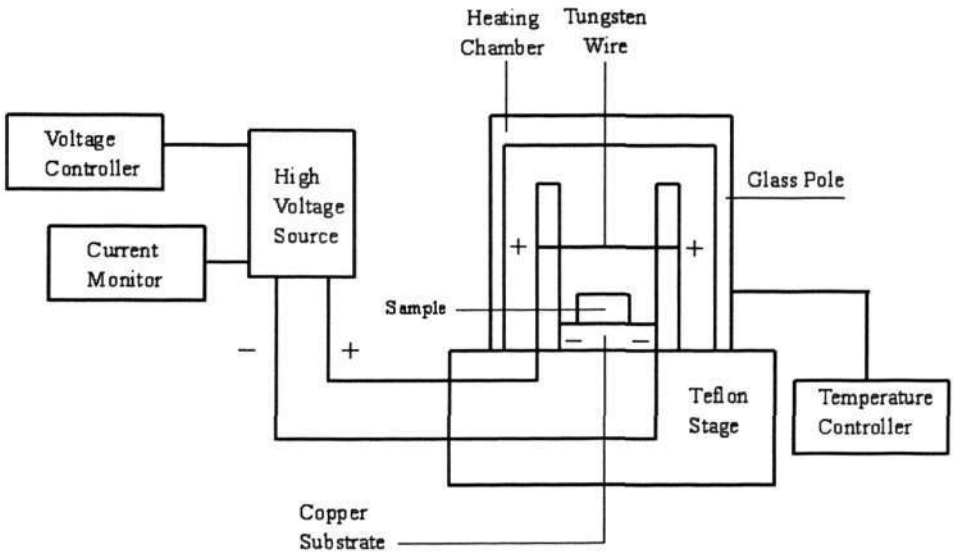

Figure 5-4 Poling setup scheme

5.2.4.2 Optimized Imidization and Poling Conditions

It is important to choose the imidization and poling conditions (poling voltage and imidization temperature) to obtain the best properties such as a maximum SH signal. Extra high poling voltage and imidization temperature will lead to the decrease in properties due to material damage and chromophore bleaching. Furthermore, material damage is also the most serious source of optical loss associated with electric field poling. In this study, the imidization and poling conditions were chosen by using series PA III as representative through monitoring spectroscopies (FTIR, UV), T_g and d_{33}.

a) Optimized Imidization Temperature

The aim of the imidization is to remove any residual solvents and to complete the conversion of the precursor into polyimide. The poly(amic acid) film was dried and heated gradually up to 200~350 °C depending on the stability and T_g of the polyimide. Too rapid a heating may cause the formation of bubble sample. A ramped cure cycle is generally used to facilitate solvent removal and complete conversion of the precursor to the polyimide. The first step is typically carried out at a low temperature to remove most of the solvent. In the subsequent heating to a high temperature around the boiling point of solvent (205 °C for NMP), the imidization is carried out. Finally, it was annealed at this temperature for some time to remove residual solvent, and to achieve full imidization and dense packing structures. Generally, at higher temperatures, a higher degree of imidization and more dense packing structure is attained. Yu [136] reported that his samples were fully imidized at 200 °C for 1 hour. Based on the above analysis and the decomposition temperature of our polyimides, we selected a slow heating rate (5 °C/min) to the final imidization temperatures (200, 230 and 260 °C) and keep the final imidization temperature for 1 hour. It was reported that there is a best imidization or cured temperature for better comprehensive properties of the polymer, especially large d_{33}, even if the imidization were fully completed [190]. Therefore, the imidization temperature was optimized through monitoring spectroscopies (FTIR, UV), T_g and d_{33} to achieve dense packing structure and better comprehensive properties under the guarantee of full imidization and no decomposition, especially chromophore decomposition.

Figure 5-5 shows FTIR spectra of the series PA III imidized at different temperatures. It was found that for the poly(amic acid) film imidized at 65 °C, the characteristic

absorption peak of carboxylic carbonyl group appeared at 1660 cm^{-1} whereas the characteristic absorption peak of the imide group at 1780 cm^{-1} does not emerge in the FTIR spectra. Therefore, the imidization basically does not begin at 65 °C. In contrast, the characteristic absorption peak of the imide group at 1780 cm^{-1} appeared in the FTIR spectra of PA imidized at the temperature of 200, 230 and 260 °C. Results also show that the characteristic absorption peak of carboxylic carbonyl group at 1660 cm^{-1} disappeared and the carbonyl group of imide ring absorption at 1720 cm^{-1} and 720 cm^{-1} become much stronger in comparison with the FTIR spectra of PA imidized at 65 °C. The results indicates that the imidization should be basically completed as evidenced by the appearance of absorption peak at 1780 cm^{-1} and the disappearance of the carboxylic carbonyl absorption at 1660 cm^{-1} when imidized at 200, 230 and 260 °C.

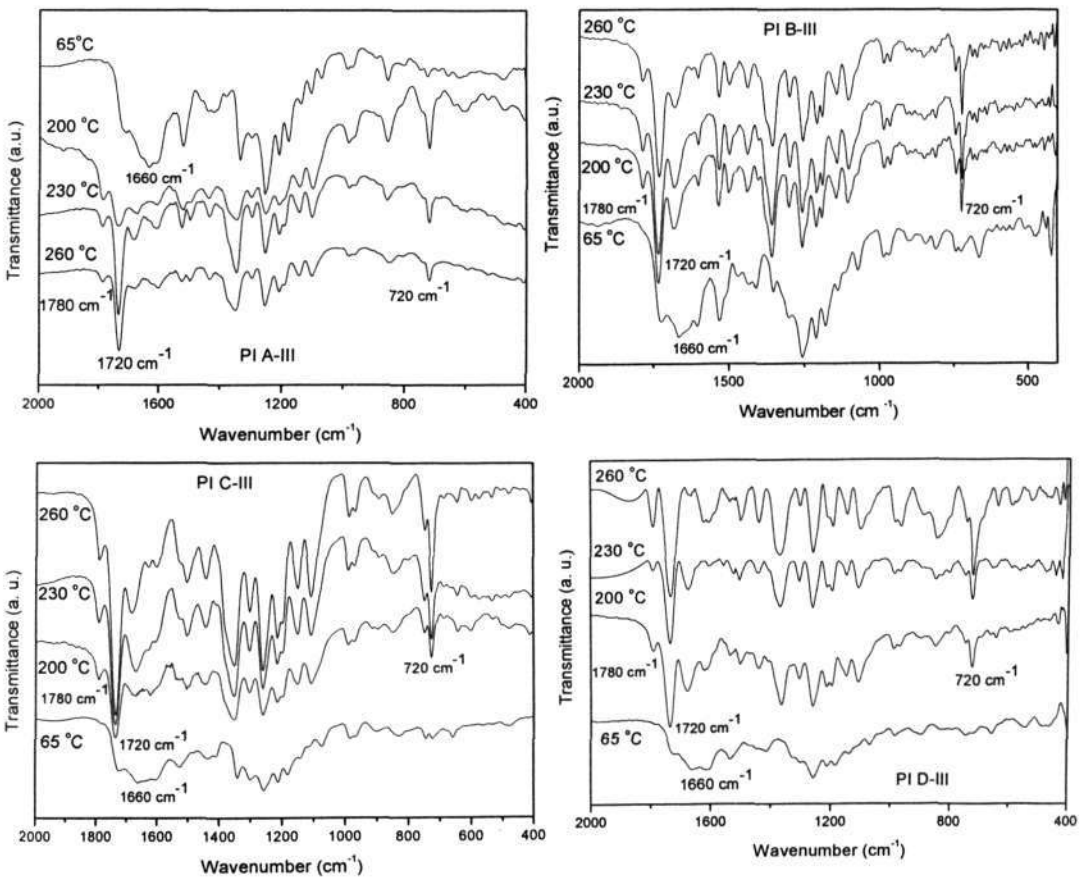

Figure 5-5 FTIR spectra of series PA III imidized at different temperatures

The UV-Vis absorption spectra of series PA III imidized at different temperatures are shown in Figure 5-6. The maximum absorption wavelength λ_{max}s are listed in Table 5-3. Results show that in comparison with PA imidized at 65 °C, PA imidized at 200, 230 and 260 °C exhibited the significant blue-shift of λ_{max}, which is ascribed to the reduction of the electron-donating ability of amide (-NHCO-) groups upon conversion to the imide group (-$N(CO)_2$-). And it was also found that the λ_{max} of PA imidized at 230 °C is basically the same with that of PA imidized at 260 °C and is smaller than that of PA imidized at 200 °C. This is attributed to the more complete imidization and less residual solvent when imidized at 230 and 260 °C. The imperfect polyimide structure such as the residual solvent generally leads to a larger λ_{max}.

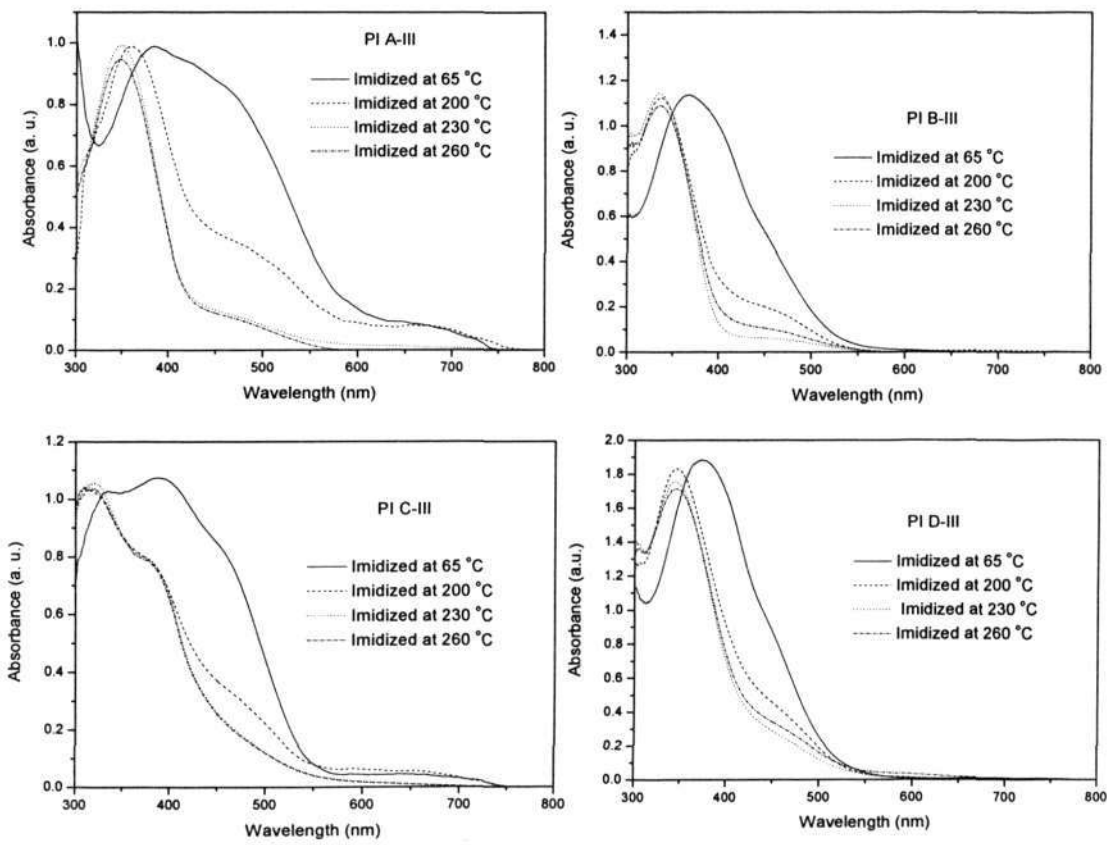

Figure 5-6 UV-Vis spectra of series PA III imidized at different temperatures

DSC of series PA III imidized at different temperatures are shown in Figure 5-7 and the values of T_g are listed in Table 5-3. These polyimides were found to possess high T_g (> 200 °C) and exhibit high thermal stability. Results reveal that the increase in imidization temperature leads to an increase of the T_g value. This is because the imidization at higher temperature will lead to less residual solvent as plasticizer, more complete imidization, denser packing structures and less free volume.

Table 5-3 Properties of series PA III imidized and poled at different temperatures

Sample	Imidization Temperature (°C)	λ_{max} (nm)	T_g (°C)	d_{33} (pm/V)
PA A-III	65	387.5	-*	-
	200	360.5	207.2	10.93
	230	348	208.8	11.73
	260	348	228.6	11.1
PA B-III	65	373.5	-	-
	200	336.5	201.3	9.17
	230	334.5	218.6	10.91
	260	334.5	251.2	10.3
PA C-III	65	379.5	-	-
	200	331.5	232	8.51
	230	298.5	263.6	10.52
	260	298.5	278.3	8.61
PA D-III	65	368	-	-
	200	347	214.2	6.17
	230	343.5	242.7	8.34
	260	343.5	274.2	8.32

*: Not measured

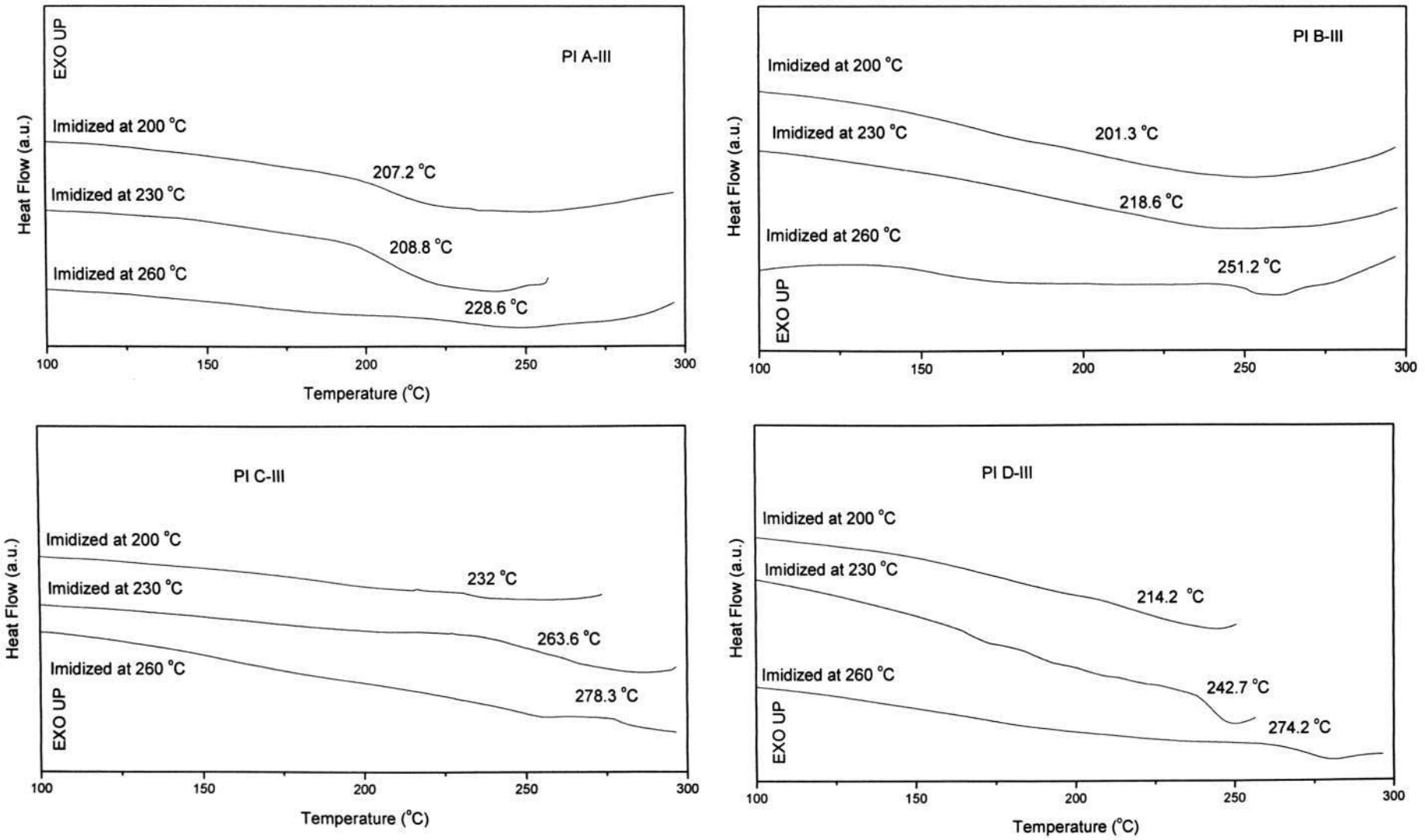

Figure 5-7 DSC of series PA III imidized at different temperatures

Figure 5-8 shows the d_{33} values of PA imidized at different temperatures and poled under a voltage of 6 kV. It can be seen that the d_{33} values initially increased with temperature and then decrease. The d_{33} values are largest when imidized at 230 °C. PA III imidized at 200 °C possessed a lower d_{33} values possibly because the ionic impurities from residual solvent and imperfect polyimide structure can dramatically reduce the effective electric field when poled and imidized at 200 °C [191]. As shown in Figure 5-5, the chromophore moieties didn't decompose evidently during the imidization at 260 °C. Hence, the lower d_{33} values of PA III imidized at 260 °C could be mainly attributed to the denser packing structures and less free volume so that the chromophore has difficulty reorienting again [190].

Based on the above results, the best imidization temperature is at 230 °C.

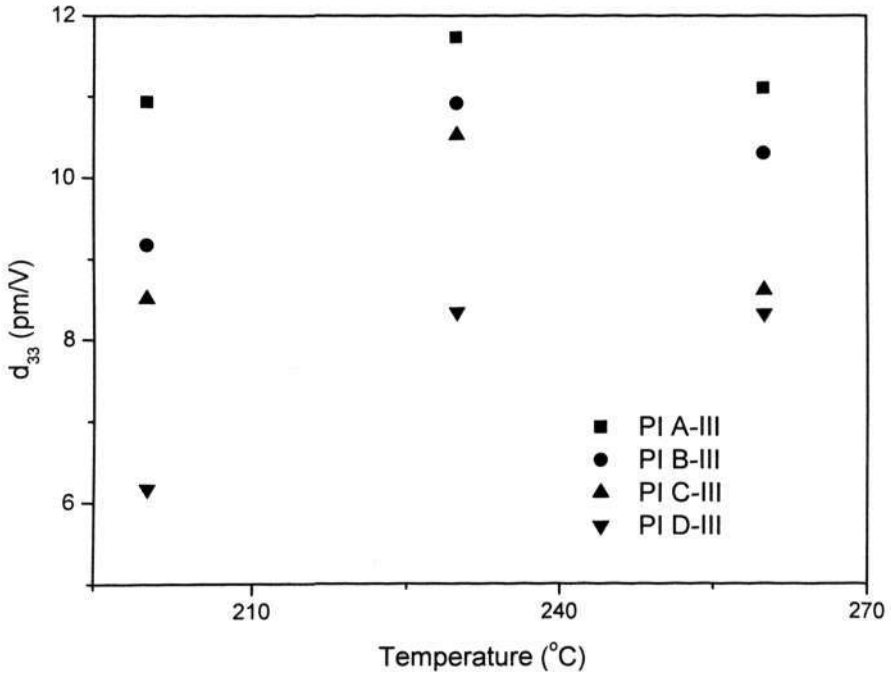

Figure 5-8 d_{33} values of series PA III imidized at different temperatures under 6 kV poling voltage

b) Optimized Poling Voltage

According to the one-dimensional rigid oriented gas model (1D ROGM), the macroscopic second harmonic coefficient d_{33} can be written as [88]:

$$d_{33} = \frac{1}{2} N\beta f^{2\omega} (f^{\omega})^2 \frac{\mu E_p}{5kT} \qquad 5\text{-}1$$

where N is the number density of the chromophore in the polymer, f^{ω} and $f^{2\omega}$ are the Onsager type local field factors at the fundamental and doubling frequency, μ is the dipole moment of the chromophore, and E_p is the poling field. It is clear that according to this equation, d_{33} is linear dependent on the poling field. Therefore the d_{33} values initially increased with poling voltages. As the breakdown might happen when poling voltage exceeds 7 kV, three poling voltages (5, 6 and 7 kV) were selected in our experiment. The d_{33} values of PA poled at different voltages at 230 °C are shown in Figure 5-9. It was found that the d_{33} values initially increased with poling voltages and then decreased. The maximum d_{33} values were obtained when poling at 6 kV. The decrease is possibly due to electric discharge in the air gap between the electrode and the samples so that the sample surface could be damaged [192-193]. When poling at 7 kV, some sample surfaces were found to have some small cracks.

According to the above experimental results, the optimized imidization temperatures and poling voltage was determined to be 230 °C and 6 kV, respectively.

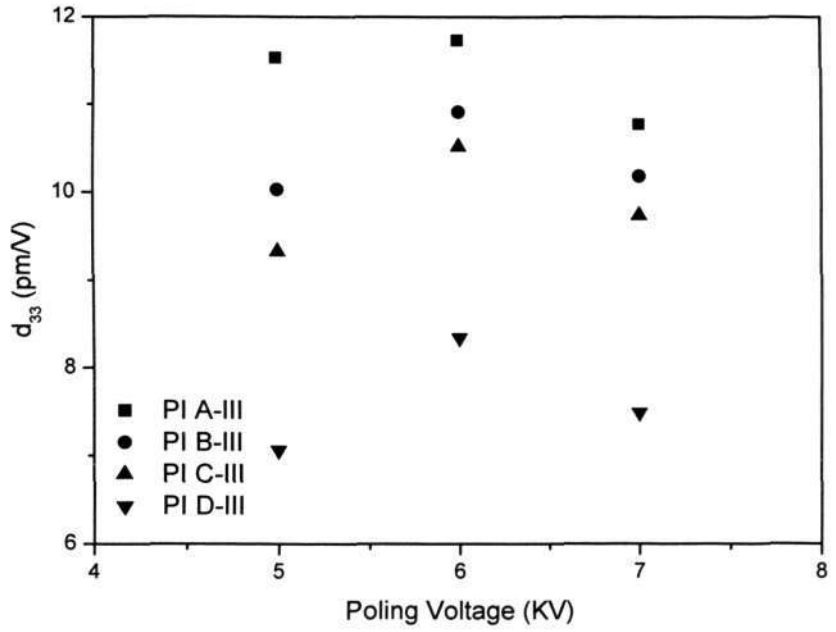

Figure 5-9 d_{33} values of series PA III poling at different voltages under 230 °C

5.3 Structures of NLO Polyimides Based on Diaminoazobenzene Chromophores

5.3.1 Molecular Weight

The solubilities of PIs in THF, DMSO and NMP are listed in Table 5-4. Only series PI III was found to be soluble in THF, DMSO and NMP. The good solubility of series PI III can be attributed to the hexafluoroisopropylidene moiety in the main chain. Series PI I exhibits the worst solubility because it has the most rigid structure. Series PI II can be partly soluble in DMSO and NMP, and insoluble in THF due to the -CO- group in the

main chain. Because only series PI III can be soluble in THF, their molecular weight can be characterized through GPC. For the other two series, viscosities of poly(amic acid)s were used to characterize the molecular weights.

Table 5-4 Viscosities of PA solutions, Mn, Mw, Mw/Mn and solubilities of PIs in THF, DMSO and NMP

Polyimide	Viscosity of PA (dl/g)	M_n 10^3(g/mol)	M_w 10^4(g/mol)	M_w/M_n	Solubility [b]		
					THF	DMSO	NMP
PI A-I	0.19	----	----	----	I	I	I
PI A-II	0.10	----	----	----	I	P	P
PI A-III	0.101	8.61	1.48	1.72	S	S	S
PI B-I	0.319	----	----	----	I	I	I
PI B-II	0.219	----	----	----	I	P	P
PI B-III	0.1329	8.75	1.44	1.65	S	S	S
PI C-I	0.1145	----	----	----	I	I	I
PI C-II	0.0893	----	----	----	I	P	P
PI C-III	0.0848	8.60	1.39	1.63	S	S	S
PI D-I	0.0893	----	----	----	I	I	I
PI D-II	0.0593	----	----	----	I	P	P
PI D-III	0.0719	8.21	1.38	1.68	S	S	S

[a] ---- : the molecular weight of polyimide can not be obtained.

[b] S: soluble, P: partially soluble, and I: insoluble.

Molecular weight is an important parameter for polymer. Molecular weight could affect the properties of the polymer. In Table 5-4, which lists the viscosities of PA solutions, M_n, M_w, M_w/M_n of PIs, series B exhibited larger viscosities or M_n than Series A. According to

the mechanism of PA synthesis reaction, this can be attributed to the stronger basicity of 2R-3N-DIAMINE compared with 2R-4N-DIAMINE. For 2R-3N-DIAMINE, the nitro group at the meta position cannot form conjugation with the benzene ring in comparison with 2R-4N-DIAMINE so that 2R-3N-DIAMINE has stronger basicity than 2R-4N-DIAMINE. Series C and D displayed smaller viscosity or M_n than series B because of the incorporation of fluorine in chromophore diamine. The incorporation of fluorine into 2R-3N-DIAMINE leads to a decrease in the basicity because fluorine is a strong electronegative group. Series D display smaller viscosity than series C because the fluorine in para position can form stronger conjugation than that in ortho position so that 2R-4F-3N-DIAMINE has lower basicity than 2R-2F-5N-DIAMINE. Series I also displayed largest viscosities because PMDA has the strongest electron affinity [185].

5.3.2 Confirmation of Polyimide Structure

The FTIR spectra of NLO polyimides are shown in Figure 5-10. The characteristic imide peaks around 1780 cm^{-1} (C=O asymmetrical stretching), 1720 cm^{-1} (C=O symmetrical stretching) and 725 cm^{-1} (C=O bending) were clearly shown in these spectra. The peaks around 1525 cm^{-1} (NO_2 asymmetrical stretching) and 1344 cm^{-1} (NO_2 symmetrical stretching) are attributed to the nitro group in chromophore side chain. The peak around 1425 cm^{-1} (N=N stretching) is attributed to the N=N group in the chromophore side chain.

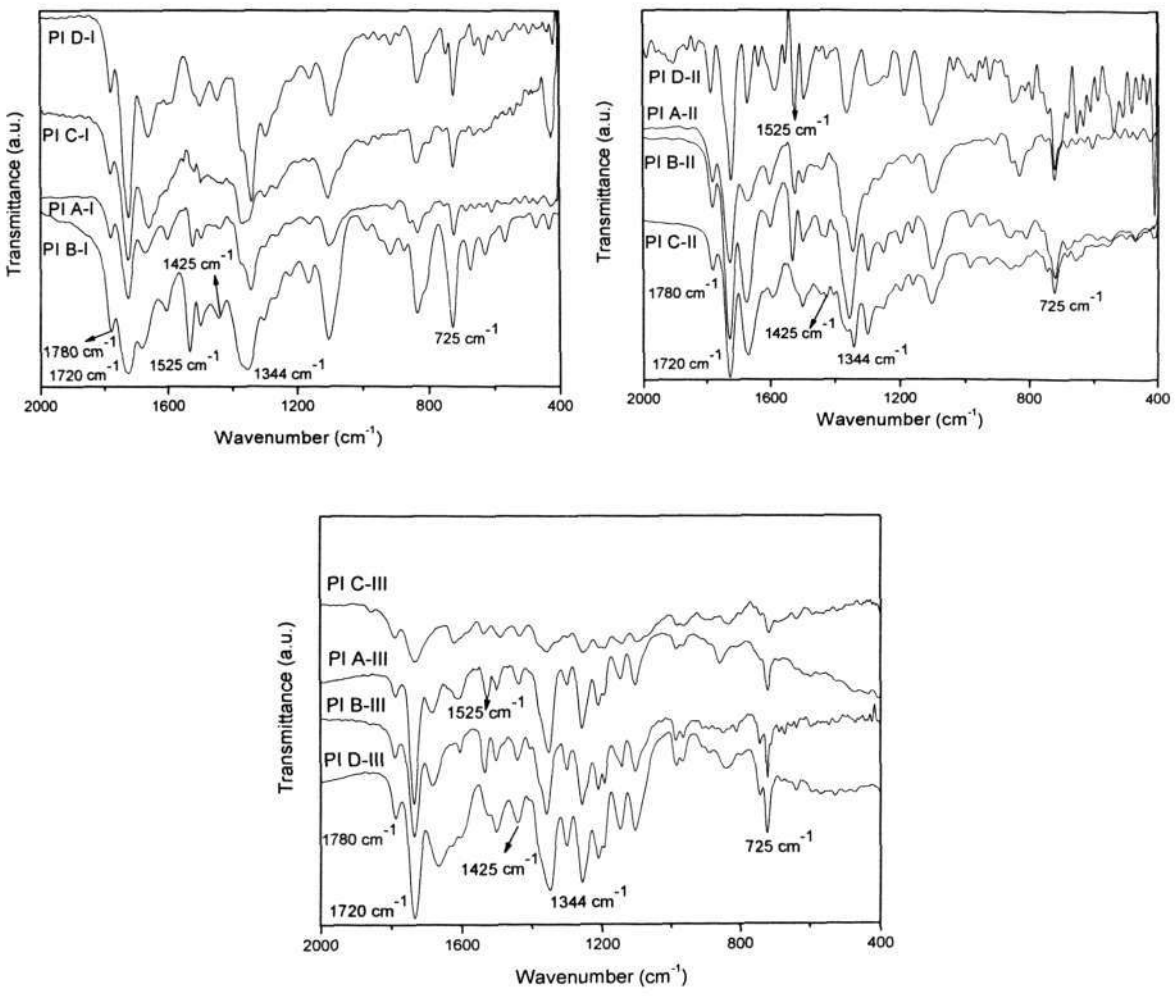

Figure 5-10 FTIR spectra of NLO Polyimide

The structures of the soluble polyimides can be also characterized by ^{1}H NMR. ^{1}H NMR spectra of PI A-III, B-III, C-III and D-III are shown in Figure 5-11, 5-12, 5-13 and 5-14, respectively. The chemical shifts in NMR spectra were assigned based on the comparison with those of corresponding chromophores. For PI A-III, the peaks at 8.35, 7.93, 7.9 and 7.8 ppm are attributed to the H_1, H_5, H_3 and H_4 in the chromophore moieties, respectively. The H atom 2 and 6 overlapped at the peak of 8.26 ppm. The H atom 7 and 8 also overlapped at the peak of 8.15 ppm. For PI B-III, the peaks at 8.37, 8.05, 7.87, 7.82 and

7.37 ppm are ascribed to H_4, H_2, H_5, H_6 and H_7 in the chromophore moieties, respectively. The proton of H_1, H_{13}, and H_8 overlapped at peak of 8.25 ppm. The peaks at 8.1 and 7.95 ppm are attributed to H_9 and H_{10}, respectively. For PI C-III, the peaks at 8.05, 7.9, 7.85, 7.8 and 7.24 ppm are ascribed to H_2, H_3, H_6, H_4 and H_5 in the chromophore moieties, respectively. The peaks at 7.96 and 7.95 ppm are ascribed to H_8 and H_9, respectively. The peak at 8.25 ppm is attributed to the overlapping of H_1 and H_7. For PI D-III, the peaks at 8.12 and 7.22 ppm are ascribed to H_1 and H_5 in the chromophore moieties. The peaks at 8.2, 8.04 and 7.85 ppm are attributed to the H_7, H_8 and H_9, respectively. H_2 and H_3 overlapped at the peak of 7.9 ppm. And H_4 and H_6 also overlapped at the peak of 7.83 ppm. These spectral assignments clearly support the proposed structures. The absence of downfield signal corresponding to poly(amic acid) proton suggested that the imidization is completed. The characteristic peaks of chromophores moieties assigned with the chromophores clearly indicated the chromophores existed in the corresponding PI structures and did not decompose during the imidization.

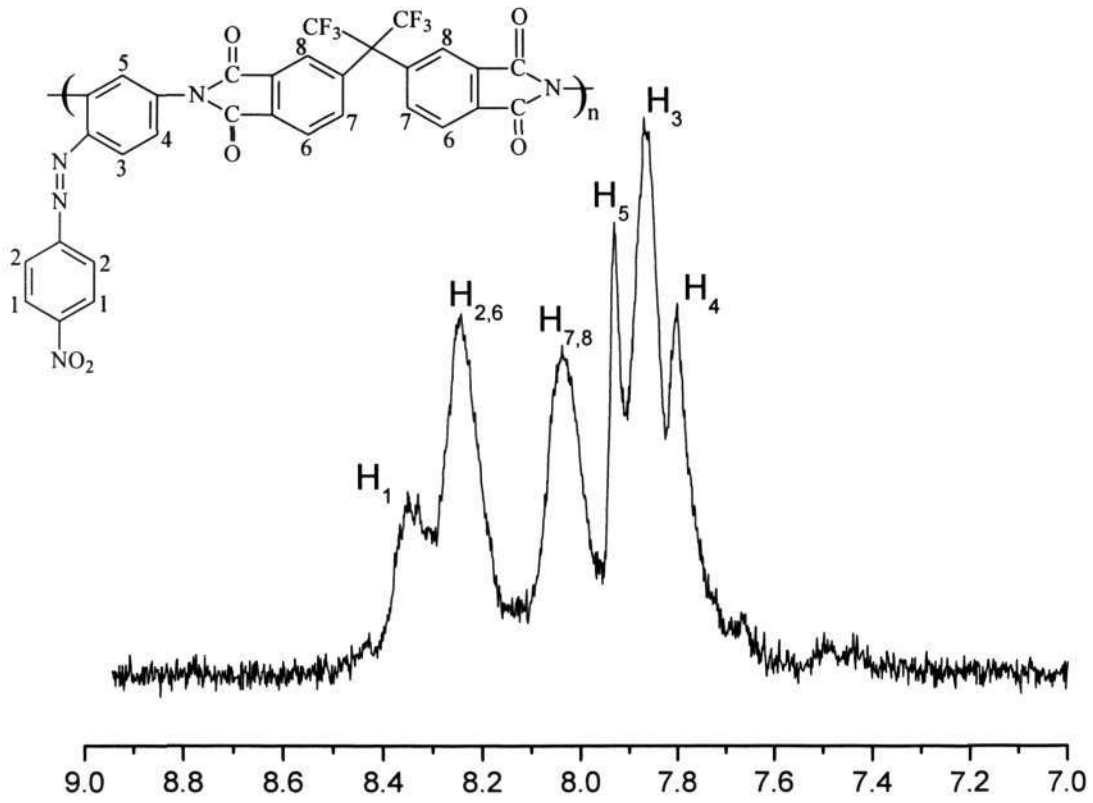

Figure 5-11 ^{1}H NMR of PI A-III in DMSO-d_6

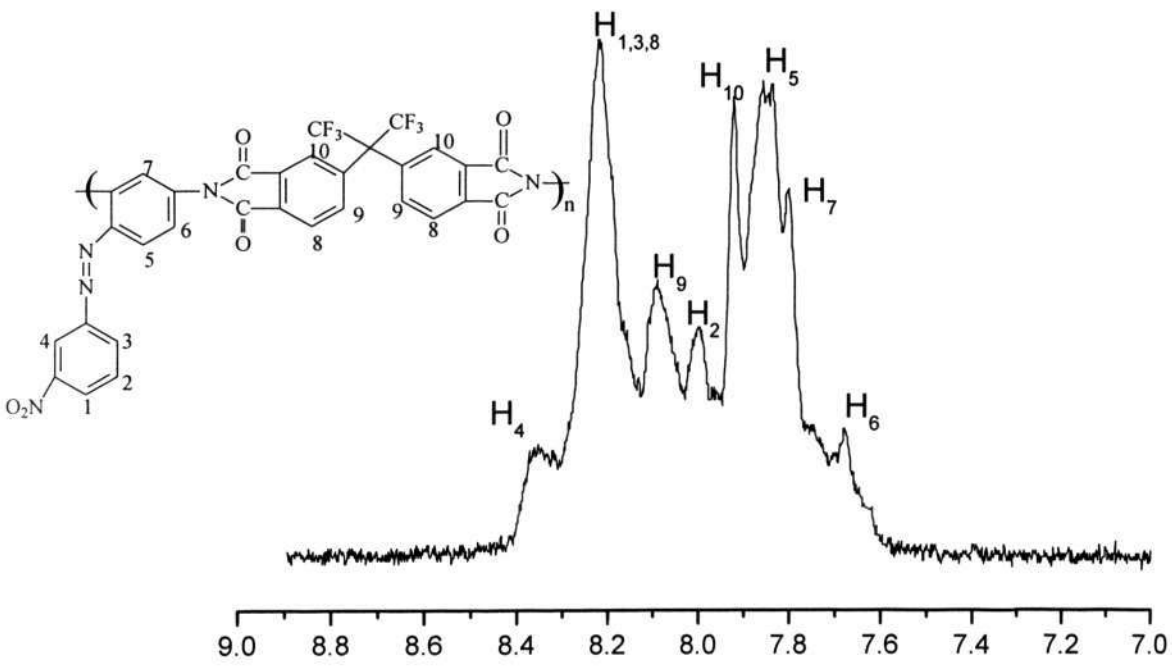

Figure 5-12 ^{1}H NMR of PI B-III in DMSO-d_6

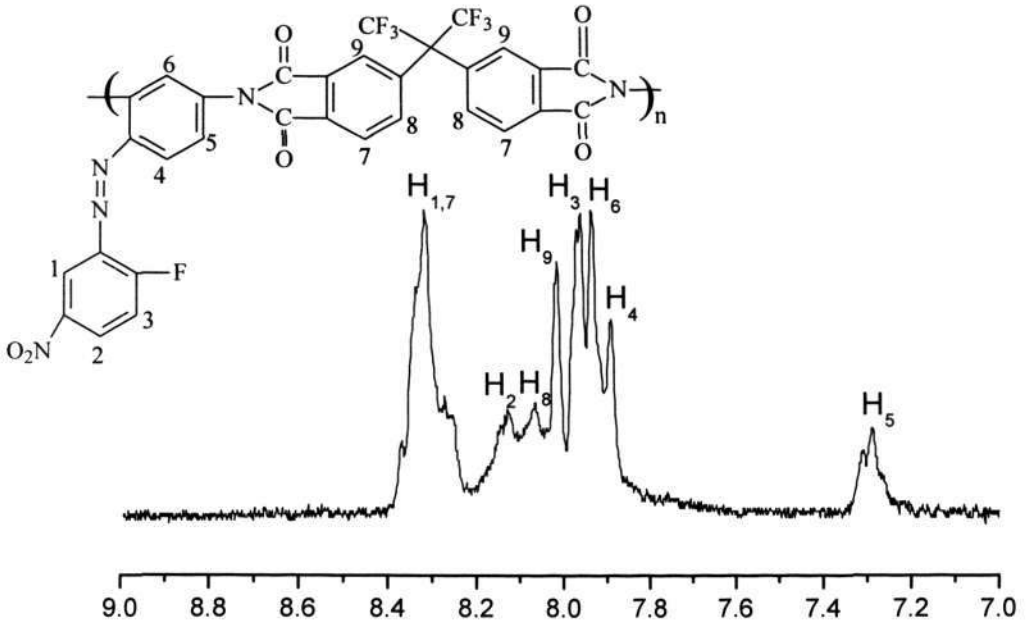

Figure 5-13 ^{1}H NMR of PI C-III in DMSO-d_6

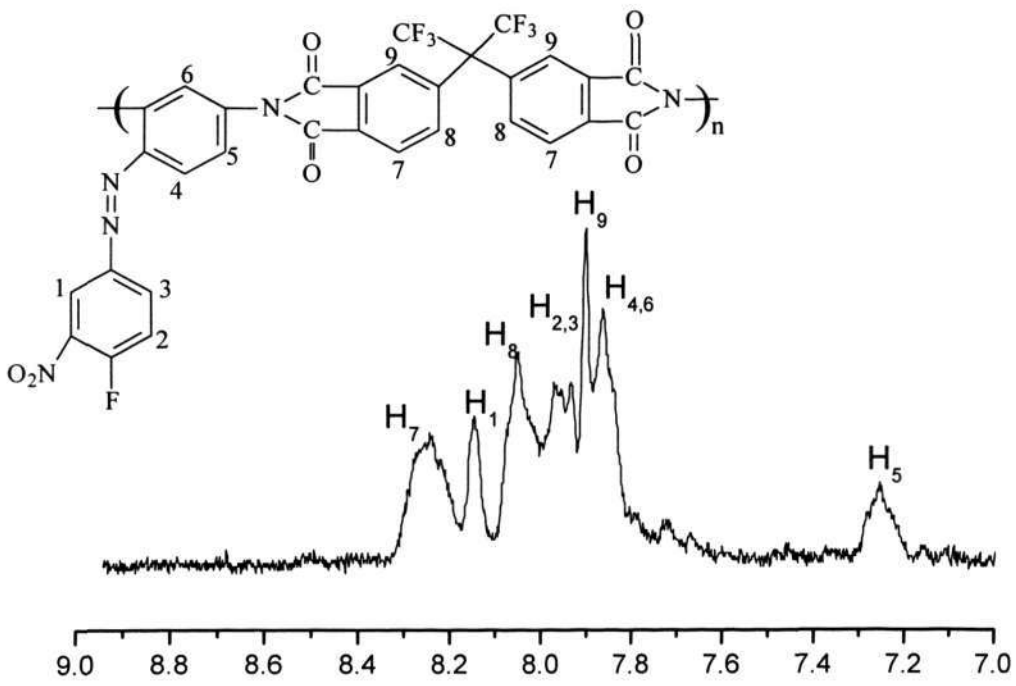

Figure 5-14 ^{1}H NMR of PI D-III in DMSO-d_6

For the series PI III, elemental analysis was also used to confirm the structures. The results of elemental analysis as listed in Table 5-5 confirm the polyimide structures.

Table 5-5 Elemental analysis results of series PI III

Sample		C	H	N	O
PI A-III	Calculated	55.95	1.97	14.42	10.52
	Experimental	55.82	1.94	14.17	10.69
PI B-III	Calculated	55.95	1.97	14.42	10.52
	Experimental	55.71	1.91	14.21	10.68
PI C-III	Calculated	54.48	1.77	14.04	10.25
	Experimental	54.13	1.81	14.29	10.38
PI D-III	Calculated	54.48	1.77	14.04	10.25
	Experimental	54.21	1.87	14.11	10.37

5.3.3 Optimized Unit Structures of NLO Polyimides

The optimized unit structure of polyimide was modeled using AM1 model/Material Studio 3.0 software package (Accelrys Inc.), which took a unit of series PI I as representative. The semi-empirical quantum mechanical molecular modeling techniques used in this research are based on the molecular orbital theory through parameters selection to approximate the solution of the Schrödinger equation for a molecule [194]. By using the Born-Oppenheimer approximation to separate electronic and nuclear motion, the Schrödinger equation maybe written as:

$$E_{tot}\psi = E_{nuc}\chi + E_{elec}\phi \qquad 5\text{-}2$$

where ψ is the wavefunction of a molecule, χ is the nuclei wavefunction for a molecule and ϕ is electronic wavefunction for a molecule.

Subsequently the electronic and nuclear Schrödinger equations may be solved independently of one another. Solution of the electronic wavefunction (ϕ) for a molecule with n electrons is performed by breaking the wavefunction into n one-electron equations (ϕ_i, i=1 to n) each representing an orbital. The molecular electronic wavefunction (ϕ) is then the product of these one-electron wavefunctions. The self-consistent field (SCF) approach is used to account for the electron-electron interactions which have been neglected in the breakdown of the electronic wavefunction into multiple one-electron problems.

The molecular orbitals are created from the atomic orbitals centered on the component atoms in the molecule by using the LCAO (linear combination of atomic orbital) approach. LCAO simplifies the molecular orbital equations by finding the combination of atomic orbitals which have the proper symmetry and the lowest electronic energy. Semi-empirical methods further simplify this problem by assuming the closed shell electrons to be "core" electrons which are absorbed into nucleus and only solving ϕ_i for the valence electrons in the molecules.

The orbitals (ϕ_i) are solved by initially creating a set of orbitals from the starting molecular conformation and iteratively improving the orbitals by solving a set of

differential equations until the electronic energy is at a constant minimum. For an electron in any given orbital, the SCF approach creates an average electric field associated with the remaining electrons in the molecule. The electron energy is calculated based on the position of an electron in a single orbital interacting with the mean field, the orbitals are improved, and the electronic energy decreased until such time the field of the electrons is considered to be static and "self-consistent".

AM1 is a *s* and *p* orbital based MNDO-like method, but differs from MNDO (Modified neglect of differential overlap) in that extra Gaussian potentials are added to the core-core repulsion energy to allow it to form hydrogen bonds [194]. AM1 is parameterized for the following elements: H, B, C, N, O, F, Na, Mg, Al, Si, P, S, Cl, Zn, Ge, Br, Sn, I, Hg. AM1 is the default Hamiltonian when VAMP is run from the MS Modeling user interface. Of the *s* and *p* orbital based methods, AM1 is a good general method for organic compounds especially for many applications involving π-systems, including amides.

Figure 5-15 shows the optimized unit structures of PI A-I, PI B-I, PI C-I and PI D-I, where red line is for oxygen atom, blue line is for nitrogen atom, white line is for hydrogen atom, gray line is for carbon atom and cyan line is for fluorine atom. Results show that the torsion angles between the benzene rings of PMDA and that of chromophore (including the angles in red, blue, green and orange) were basically the same. It indicates that the conformation structures of the main chain were basically the same. However, it is interesting to find that the torsion angles between the benzene rings in

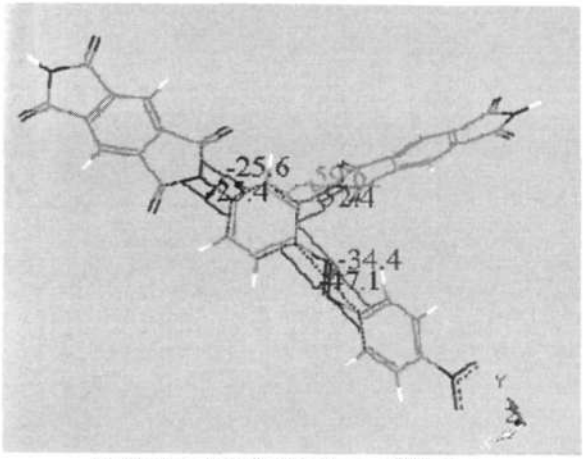

Optimized unit structure of PI A-I

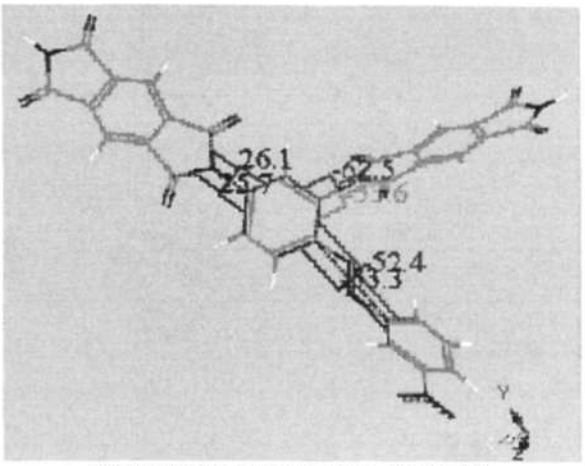

Optimized unit structure of PI B-I

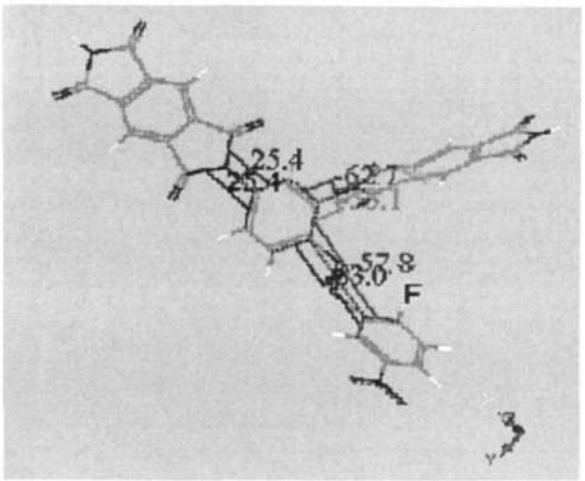

Optimized unit structure of PI C-I

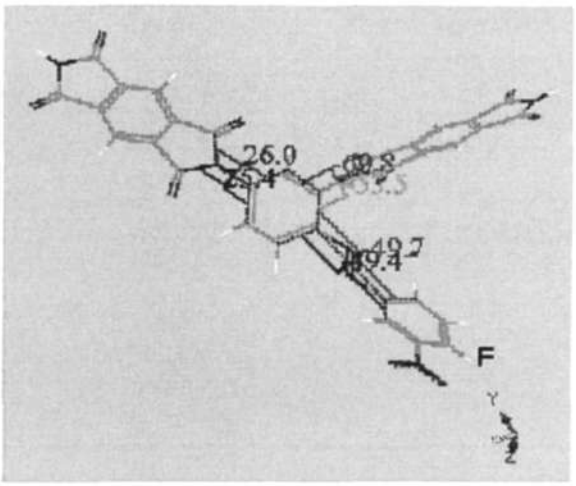

Optimized unit structure of PI D-I

Figure 5-15 Optimized series PI I structures and torsion angles (red line for oxygen atom, blue line for nitrogen, white line for hydrogen, gray line for carbon and cyan line for fluorine)

chromophore (including the angles in brown and purple) were different. The brown torsion angles of PI A-I, PI B-I, PI C-I and PI D-I were 47.1, 53.3, 63.0 and 49.4, respectively and the purple torsion angles of PI A-I, PI B-I, PI C-I and PI D-I were 34.4, 52.4, 57.8 and 49.7, respectively, which reveals that the torsion angles between two benzene rings in the chromophore moiety are different. In comparison with PI A-I, PI B-I

possesses larger torsion angle because of the nitro group at the meta position. PI C-I exhibits larger torsion angle than PI D-I due to the different position of fluorine group in the chromophore side chain. The larger torsion angle can decrease the planarity of the benzene rings and the degree of conjugation in chromophore side chain. Results clearly reveal that the nitro group and the fluorine group in chromophore side chain can affect the conformation structure of PI especially chromophore side chain so that they can lead to different properties.

5.4 Thermal Properties

Thermal properties of the NLO polyimides were characterized by DSC and TGA. The glass transition temperature T_g of the linear aromatic polyimides is strongly influenced by the chemical structure of the polyimide, which include the main chain stiffness, attachments of flexible/rigid groups, presence of bulky or polar side group. Other factors like presence of crystallinity, molecular weight and chain-chain interactions can also influence the T_g.

In the DSC study, the T_g of series PI I was not observed before they decomposed, implying that the glass transition temperature could be higher than the decomposition temperature. Generally, the dianhydride PMDA always leads to very rigid main chain because there is only benzene ring in its structure. However, there are flexible and swivel groups in PI II (-CO-) and PI III (-$C(CF_3)_2$-), which can result in flexible main chain of series PI II and PI III in comparison with series PI I. Hence, T_g of series PI II and III can

be observed and are shown in Figure 5-16 and Figure 5-17, respectively. Results reveal that the series PI II and III all exhibited high T_g (> 200 °C) and the T_g of the series PI II was higher than that of series PI III because the (-$C(CF_3)_2$-) group was more flexible and swivel group than the (-CO-) group. Results also show that T_g of the series PI B was higher than that of series PI A possibly because the nitro group was located at different position. According to the results of optimized unit structure, in comparison with series PI A, series PI B possesses larger torsion angle in chromophore side chain and strong steric hindrance effect, which can lead to higher T_g [196]. Series PI C and D were found to exhibit higher T_g than series PI B because of the presence of the fluorine. The incorporation of fluorine into the chromophore moiety could increase the polarity of the side group. Generally, the stronger the polarity, the higher the T_g [196]. PI C-II and PI C-III have higher T_g than PI D-II and PI D-III, respectively, possibly due to the different position of the fluorine in the chromophore side chain. Optimized unit structure results also show that the different fluorine position in chromophore side chain could lead to different steric hindrance effect. Series PI C exhibited larger torsion angle in chromophore side chain than series PI D indicating that series PI C possesses stronger steric hindrance effect that could hinder the movement of the polyimide more strongly and higher T_g due to the fluorine in ortho position in chromophore side chain.

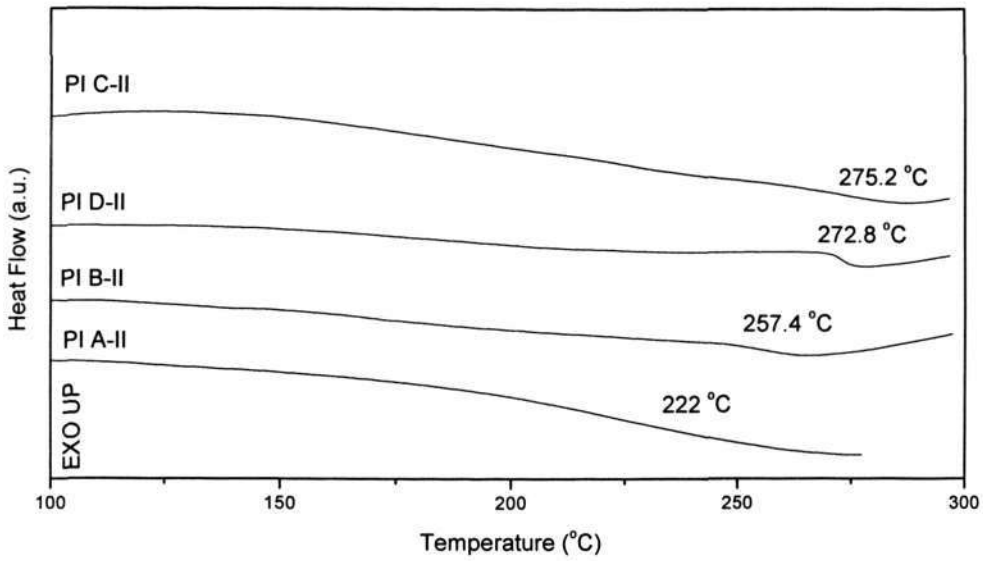

Figure 5-16 DSC of series PI II imidized at 230 °C

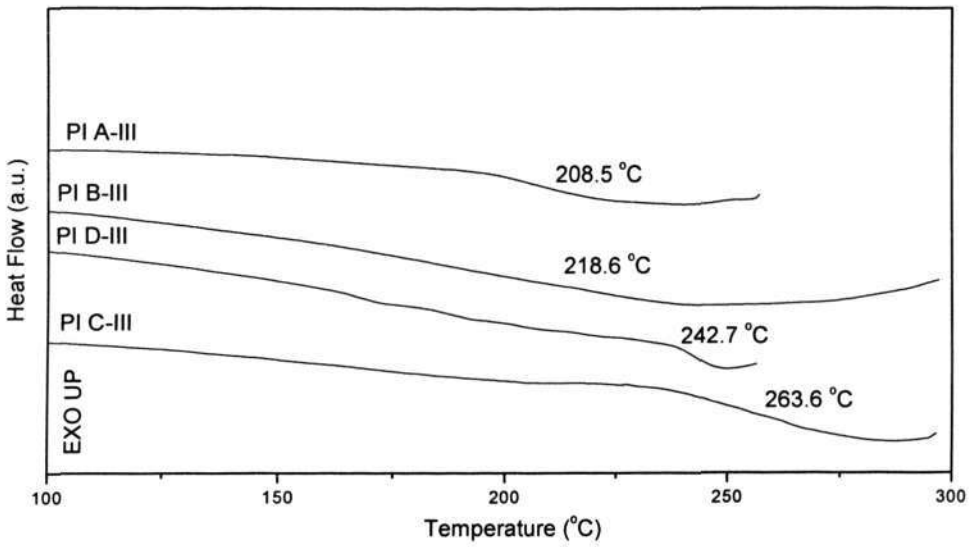

Figure 5-17 DSC of series PI III imidized at 230 °C

TGA curves of NLO polyimides are shown in Figure 5-17, from which the decomposition temperatures were determined and listed in Table 5-6. It can be found that these PIs all

display multi-step decomposition. The weight loss of PI at 240~290 °C is caused by the decomposition of chromophore. Aromatic polyimide backbones is known to decompose above 400 °C [121], which suggests that the thermal properties of the NLO polyimide systems can be greatly enhanced if the NLO chromophores stable at high temperatures are properly chosen [136].

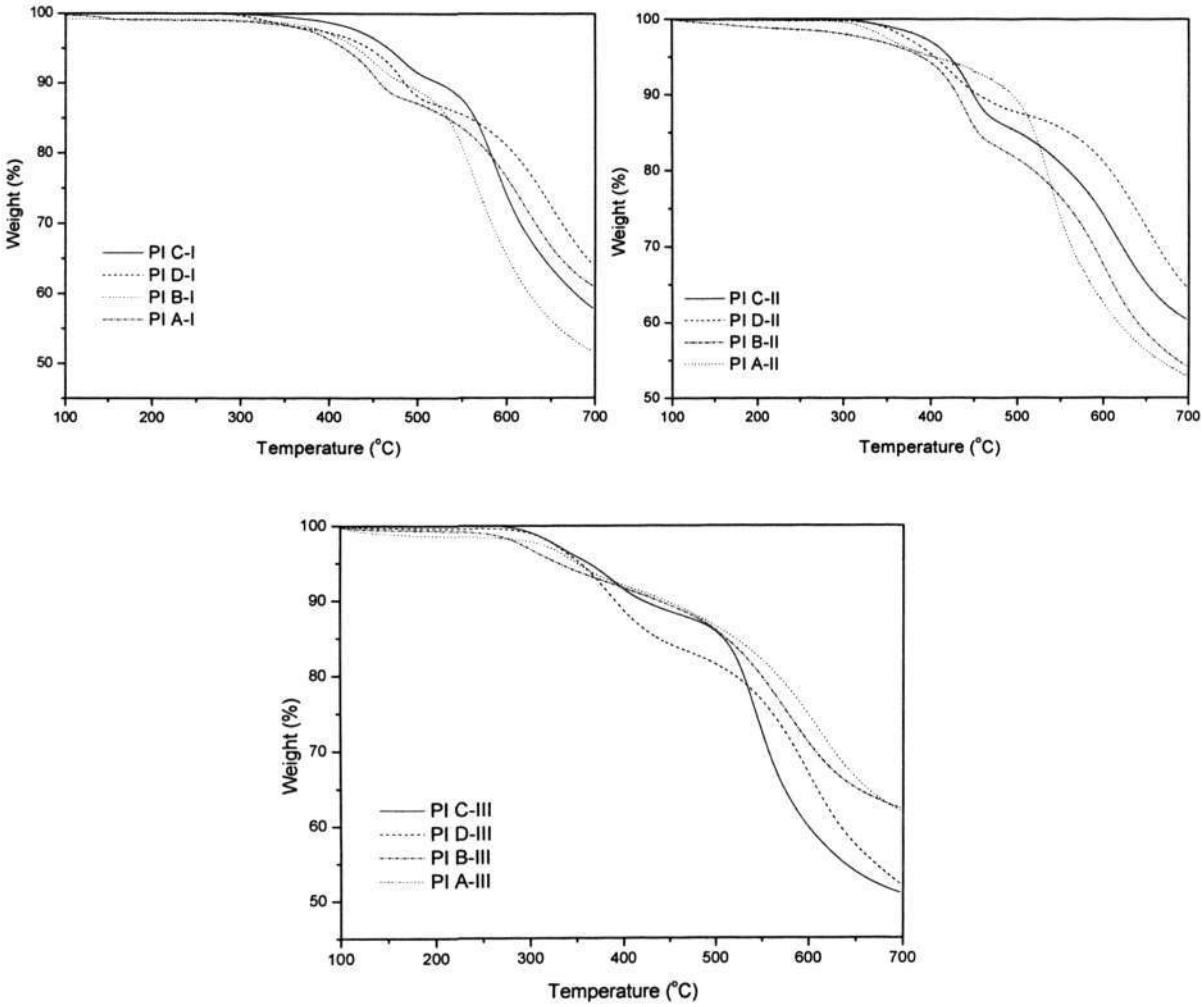

Figure 5-18 TGA of polyimide

Table 5-6 Thermal properties of NLO polyimides and other reported polymers

PI	T_g	T_{d5}[a]	T_{d1}[b]	T_{d2}[c]	R_w (%)[d]
PI A-I	-[e]	419.1	268.9	487.3	61.14
PI B-I	-	438.7	275.1	489.9	51.93
PI C-I	-	465.2	288.6	513.8	57.05
PI D-I	-	439.0	277.2	520	62.59
PI A-II	222	389.4	264.7	473.7	54.14
PI B-II	257.4	401.8	266.6	432.6	51.13
PI C-II	275.2	402.2	278.2	508.5	59..4
PI D-II	272.8	412.1	288	483.8	63.28
PI A-III	208.5	331.7	264.8	378.7	60.13
PI B-III	218.6	350.5	268.2	407	62.21
PI C-III	242.7	358.0	274	463.5	52.14
PI D-III	263.6	351.9	273.6	460.5	49.79
PC-1[30]	-	265	-	-	-
PM-1[197]	152	210	-	-	-

[a]: T_{d5} the decomposition temperature at 5% weight loss

[b]: T_{d1} the first decomposition temperature

[c]: T_{d2} the second decomposition temperature

[d]: R_w, Residual weight retained at 700 °C

[e]: Not observed

Results also show that the T_{d5} of series PI I was larger than that of the series PI II and PI III because PI I was more rigid than PI II and PI III. T_{d5} of PI increased with the sequence of PI C > PI D > PI B > PI A. This can be ascribed to the thermal stabilities of the

chromophore diamine monomers that increase in the sequence of 2R-2F-5N-DIAMINE (C) > 2R-4F-3N-DIAMINE (D) > 2R-3N-DIAMINE (B) > 2R-4N-DIAMIE (A).

In comparison with other research work, the T_g and T_{d5} of the reported NLO polymers by other research groups were also listed in Table 5-6 [30, 197]. Results show that our NLO polyimides showed higher T_g and T_{d5}, and hence might exhibit higher thermal stability than that of PC-1 and PM-1. This is because the chromophores in PC-1 and PM-1 lack of active group such as amino group and could not be incorporated into high T_g polyimide.

5.5 UV-Vis Absorption

UV-Vis absorption was used to characterize the transparency of NLO polyimide. The UV spectra of PI imidized and poled at 230 °C and 6 kV are shown in Figure 5-19. It can be seen that the λ_{max} of series PI III was smaller than that of series PI I and PI II. Series PI III exhibited higher transparency because the bulky -$C(CF_3)_2$- moieties in the main chain could separate and cut off the interactions between the electronic conjugation in the main chain and increase the energy gap between HOMO and LUMO. Generally, all polyimides based on 6FDA display higher transparency than polyimides based on BTDA and PMDA [198]. The λ_{max} of series PI I was the largest because PI based on PMDA has stronger electronic conjugation in the main chain and lower energy gap between HOMO and LUMO. It can be concluded that series PI B possess smaller λ_{max} than series PI A and exhibit higher transparency because the nitro group located at the meta position can lead to larger torsion angle, a decrease in the non-planarity of benzene ring and a degree of conjugation in chromophore side chain and increase the energy

gap between HOMO and LUMO. It is interesting to note that in comparison with series PI B, series PI C exhibited significantly blue-shift of λ_{max} and series PI D exhibit red-shift of λ_{max}. Based on the optimized unit structure, series PI C had larger torsion angle in chromophore side chain than series PI D, which can decrease the planarity of benzene ring and the degree of conjugation in chromophore side chain. From this analysis, it is possible to conclude that series PI C have smaller λ_{max} and larger energy gap between HOMO and LUMO. However, according to our previous studies on chromophores, the values of the λ_{max} of the chromophores are in the sequence of 2R-4F-3N-DIAMINE (D) <2R-3N-DIAMINE (B) <2R-2F-5N- DIAMINE (C).

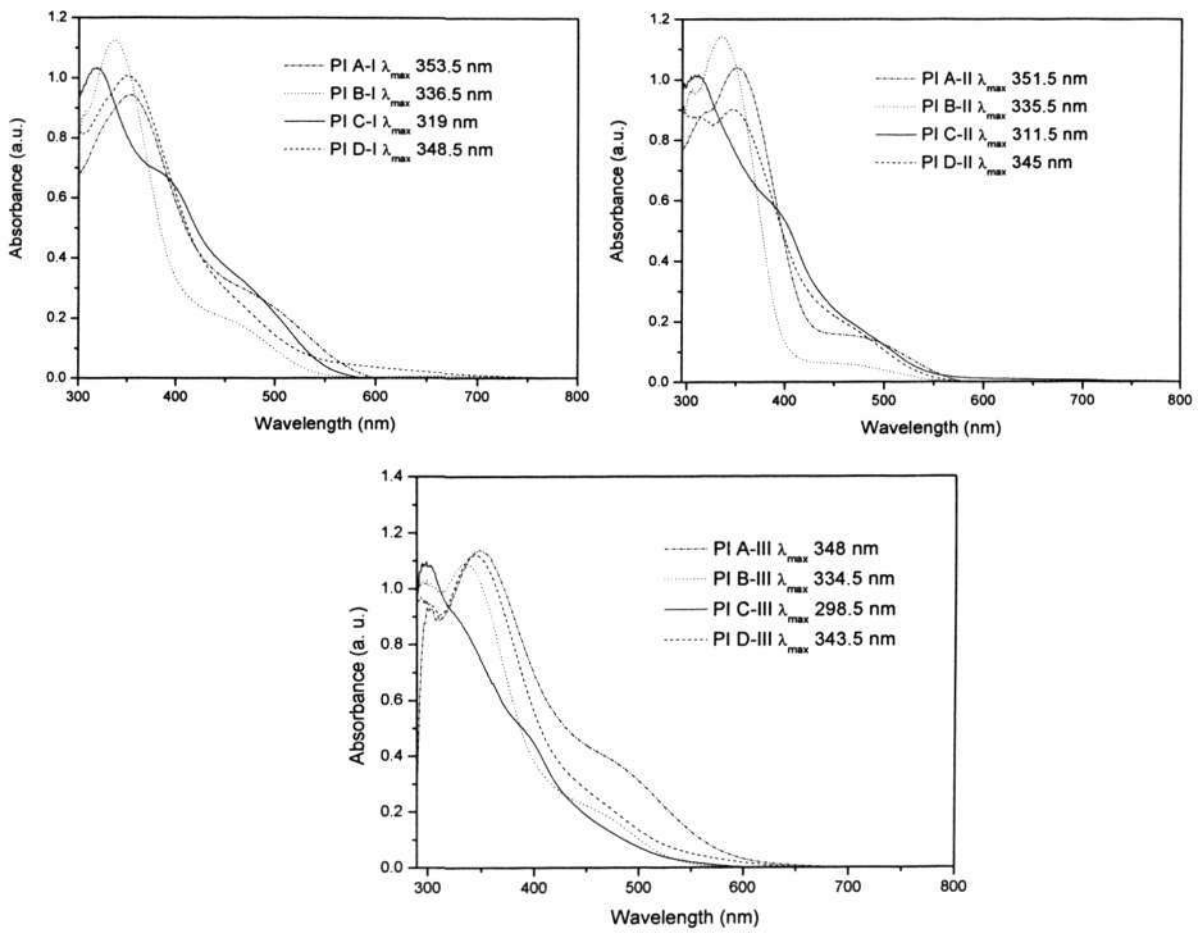

Figure 5-19 UV spectra of PI imidized and poled at 230 °C, 6 kV

Based on the results, it is reasonable to conclude that the λ_{max} of the PI films should be in the same order as well. However, our experiment revealed that λ_{max} of the PI films was actually in the sequence of series PI C < PI B < PI D.

In order to study this phenomena, the UV spectra of poly(amic acid) (PA) films imidized at 65 °C were also measured. The λ_{max} of the PA films imidized at 65 and 230 °C are listed in Table 5-7. It is worth mentioning that the λ_{max} of PA films imidized at 65 °C still decreased in the same sequence with the chromophore, i.e. PA C > PA B > PA D. However, λ_{max} of PI films imidized at 230 °C decreased in the reverse sequence, i. e. PI D > PI B > PI C. According to the above analysis, the imidization does not begin when cured at 65 °C. The sequence change of the λ_{max} should happen during the imidization. Jeng et al also reported a similar phenomena, where a silicon dye containing amino group was incorporated into the poly(amic acid) and polyimide, respectively [165,199]. This implies that the polymer and perhaps the dye moieties possibly undergo a certain extent of conformation change during the curing process. It was reported that an unfavorable conformation (b shown in Figure 5-20) has to rearrange to conformation (a shown in Figure 5-20) before ring closure during the imidization [200-201]. This confirmed that the sequence change of λ_{max} happened during the imidization.

The λ_{max} of the reported NLO polymers by other research group were also listed in Table 5-7 [30, 197] for comparison. Results revealed that our polyimides show a much smaller λ_{max} than other groups, especially PI C-III displayed 298.5 nm of λ_{max}. According to our knowledge, NLO polymers with λ_{max} smaller than 300 nm were very rarely reported.

Table 5-7 λ_{max} of PA imidized and poled at 65 and 230 °C and other reported polymers

Samples	λ_{max} (nm) PA Imidized at 65 °C	λ_{max} (nm) PA imidized at 230 °C
PA A-I	393	353.5
PA B-I	371.5	336.5
PA C-I	380	319
PA D-I	365	348.5
PA A-II	394.5	351.5
PA B-II	375	335.5
PA C-II	385	311.5
PA D-II	359	345
PA A-III	387.5	348
PA A-III	373.5	334.5
PA A-III	379.5	298.5
PA A-III	368	343.5
PC-1[30]	-	596.0
PM-1[197]	-	710.0

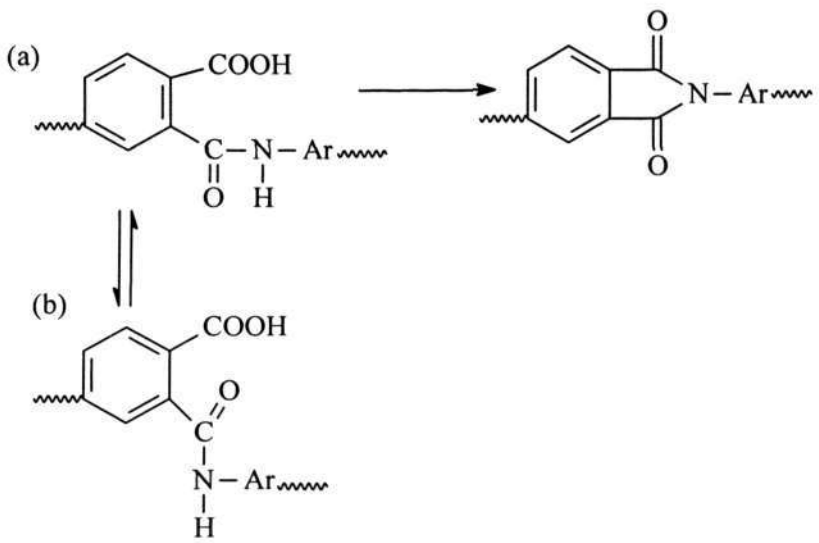

Figure 5-20 Mechanism of thermal ring closure of amic acid to imide

5.6 Hydrophobic Properties

It is important for the optoelectronic industry that the insulating polymers possess low water/moisture absorption rates. It was reported that the moisture can significantly influence the dielectric properties, such as dielectric constant and it can cause increased conductivity of dielectric insulator and promote corrosion of metal conductor, which could lead to the failure of optoelectronic device [202-203]. Generally, polyimides have relatively

high uptakes of water (at most 3.5 wt%) because many hydrophilic groups such as -CO-, -SO_2-, and -COOH exist in their structures. Especially for side-chain NLO polyimides, there are more hydrophilic groups in the main chain and chromophore moiety. Therefore, how to decrease the water absorption is a very important task. It was reported that the incorporation of hydrophobic fluorine or fluorine substituent group into polymer structure is an effective method to increase contact angle and decrease the water absorption because the hydrophobic group have lower surface energy [205].

The contact angle of PI dependence of time is shown in Figure 5-21. The average contact angle, water absorption and surface energy are listed in Table 5-8. Series PI III were found to possess higher contact angle and lower surface energy and water absorption than the other two series PI because they possess the hydrophobic fluorine-containing moieties -$C(CF_3)_2$- in main chain. Incorporation of hydrophobic -$C(CF_3)_2$- group causes a decrease of concentration of the highly hydrophilic carbonyl group (-CO-). Series PI II show smaller contact angle and higher water absorption than series PI I possibly because more hydrophilic carbonyl group existed in series PI II. It is interesting to note that series PI C and PI D all displayed higher contact angle and lower water absorption and surface energy than series PI B because of the hydrophobic fluorine in the side chain of series PI C and PI D. Generally, the higher content the fluorine, the higher the contact angle and the lower the water absorption [187]. Series PI C have different hydrophobic properties with series PI D possibly because the different fluorine position in the chromophore side chain results in different polymer conformation structure especially chromophore moiety. Series PI A also exhibited different hydrophobic properties with series PI B possibly because the different polymer structures results from the nitro group in different position. Loose packing structure could lead to high water/moisture pervasion and diffusion in the polyimide film. It was reported that the different polymer structure could lead to different contact angle and water absorption [187,205]. Although different positions of NO_2 or

fluorine in the chromophore side chain could lead to different hydrophobic properties, the difference in hydrophobic properties especially water absorption between them is smaller. Water absorption of polyimide could be divided into 2 steps: water/moisture absorption on the surface of polyimide and water/moisture pervasion and diffusion in the polyimide. Water absorption of polyimide was mainly controlled by the water/moisture absorption on the surface of polyimide. These results imply that the hydrophobic properties mainly depend on the fluorine content.

Table 5-8 Average contact angles, water absorptions and surface energy of PI

PI	Average contact	Water absorption (%)	Surface Energy (m N m^{-1})
PI A-I	73.34	0.36	30.13
PI B-I	73.16	0.36	30.27
PI C-I	76.14	0.31	27.96
PI D-I	75.81	0.34	28.22
PI A-II	69.82	0.42	32.92
PI B-II	69.61	0.42	33.09
PI C-II	73.59	0.40	29.94
PI D-II	71.67	0.40	31.45
PI A-III	79.02	0.29	25.79
PI B-III	77.41	0.31	27.00
PI C-III	82.08	0.21	23.56
PI D-III	81.15	0.21	24.23

5.7 Nonlinear Optical Properties and Stability

5.7.1 Theory

The second harmonic coefficient of the polymer film was measured by maker-fringe

method with the reference of the Y-cut quartz crystal (d_{11}= 0.5 pm/V). The transmitted second harmonic power P_2 is given by [206]:

$$P_2 = [\frac{512\pi^2}{c\,\omega^2}] d^2 P_1^2 [\frac{1}{n_1^2 - n_2^2}]^2 T_1^4(\theta)\ T_2(\theta)\ R(\theta)\ p^2(\theta)\ \beta(\theta) \sin^2\psi \quad (5\text{-}3)$$

where c is the speed of light in air, ω is the spot radius of the Gaussian beam, d is the second harmonic coefficient or NLO coefficient, P_1 is the incident fundamental laser power, n_1 and n_2 are the refractive indices of the sample at the fundamental and second harmonic wavelengths respectively, θ is the incident angle, $T_1(\theta)$ and $T_2(\theta)$ are the transmission factors for the incident fundamental and second harmonic light, respectively, $R(\theta)$ is the multiple reflection correction, $p(\theta)$ is the project factor, $\beta(\theta)$ is beam size correction factor, $sin^2\psi$ is the oscillating factor. Ψ can be expressed as:

$$\psi = \frac{\pi L}{2l_c(\theta)} \quad \text{So, } \sin^2\psi = \sin^2[\frac{\pi L}{2l_c(\theta)}] \quad (5\text{-}4)$$

$$l_c(\theta) = \frac{\lambda}{4|n_1 \cos\theta_1 - n_2 \cos\theta_2|} \quad (5\text{-}5)$$

where λ is the wavelength of the fundamental laser beam, L is the film thickness, $l_c(\theta)$ is the coherence length.

According to Snell's law we have

$$\sin\theta_1 = \frac{\sin\theta}{n_1} \quad \sin\theta_2 = \frac{\sin\theta}{n_2} \quad (5\text{-}6)$$

For p-polarized fundamental light, the transmission factor for the incident fundamental light is defined as:

$$T_1(\theta) = \frac{2\cos\theta}{n_1\cos\theta + \cos\theta_1} \quad (5\text{-}7)$$

For p-polarized second harmonic light,

$$T_2(\theta) = 2n_2 \cos\theta_2 \frac{(n_1 \cos\theta + \cos\theta_1)(n_2 \cos\theta_1 + n_1 \cos\theta_2)}{(\cos\theta_2 + n_2 \cos\theta)^3} \quad (5\text{-}8)$$

The multiple reflection correction $R(\theta)$ is defined as

$$R(\theta) = 1 + [\frac{(n_2 - 1)}{(n_2 + 1)}]^4 \text{ and } p(\theta) = 1 \quad (5\text{-}9)$$

Beam size correction factor $\beta(\theta)$ is defined as

$$\beta(\theta) = \exp[-(L^2/\omega^2)\cos^2\theta\ (\tan\theta_1 - \tan\theta_2)^2] \quad (5\text{-}10)$$

Let

$$[\frac{1}{n_1^2 - n_2^2}]^2 T_1^4(\theta)\ T_2(\theta)\ R(\theta)\ P^2(\theta)\ \beta(\theta) \sin^2\psi = C \quad (5\text{-}11)$$

For reference sample Y-cut quartz crystal, the equation (5-3) can be written as:

$$P_{2\,Quartz} = [\frac{512\ \pi^2}{c\ \omega^2}]\ P_1^2 \cdot C_{Quartz} \cdot d^2_{Quartz} \quad (5\text{-}12)$$

For Polymer, the equation (5-3) can be written as:

$$P_{2\,poly} = [\frac{512\,\pi^2}{c\ \omega^2}]\ P_1^2 \cdot C_{poly} \cdot d^2_{poly} \quad (5\text{-}13)$$

From equation (5-12) and equation of (5-13), the ratio of the transmitted powers of polyimide and reference quartz can be obtained:

$$\alpha = \frac{P_{2\,poly}}{P_{2Quartz}} = \frac{C_{poly} \cdot d^2_{poly}}{C_{Quartz} \cdot d^2_{quartz}} \quad (5\text{-}14)$$

Hence,
$$d_{poly} = \sqrt{\frac{\alpha\, C_{Quartz}}{C_{poly}}} \cdot d_{Quartz} \quad (5\text{-}15)$$

In order to determine d_{33} of the sample, the following parameters have to be determined: the thickness of the film (L), the incident angle (θ), the refractive index at the fundamental and second harmonic wavelengths (n_1 and n_2), the laser intensity of

fundamental and second harmonic lights (I_1 and I_2) which are proportional to the laser powers. The experimental error of the d_{33} value comes from the measurements of L, n_1, n_2, and the instability of the laser power.

5.7.2 Nonlinear Optical Property

The refractive index at 532, 1064 nm, the thickness and the d_{33} value of the polyimide films were measured and listed in Table 5-9. Results show that series PI III exhibited higher d_{33} values than other two series because more flexible series PI III have higher efficient reorientation of the chromophore due to their lower T_g and larger free volume. The series PI I exhibited lower d_{33} because the structures of PI I series are more rigid, has denser packing structures and have smaller free volume, which could lead to lower efficient reorientation. The d_{33} values of series PI B are smaller than that of PI A series as expected because the nitro group located at the meta position leads to smaller hyperpolarizability of 2R-3N-DIAMINE. Series PI C and PI D exhibited smaller d_{33} value than series PI B as expected. Generally, incorporation of fluorine into chromophores leads to the decrease in hyperpolarizabilities in comparison with their non-fluorinated analogue because fluorine is a weak π-donors and strong δ-acceptors [207]. On the other hand, results also revealed that the fluorine position in the chromophore side chain might have affected their nonlinear optical properties. The hyperpolarizabilities of the chromophores determined by solvatochromic method showed that 2R-4F-3N-DIAMINE has larger hyperpolarizability than 2R-2F-5N-DIAMINE [207]. Nevertheless, from Table 5-9, it can be seen that series PI C has larger d_{33} than series PI D. This change can be attributed to detrimental aggregation effects between the high polar chromophores, which effectively decrease the nonlinear optical effect. According to the simulation results obtained in previous section, series PI C have larger torsion angles in the

chromophore moiety than series PI D implying that series PI C could have more bulky 3D chromophore moiety than series PI D. It was reported that the more bulky 3D chromophore moiety could effectively hinder the detrimental aggregation effect [10]. Therefore, series PI C have larger d_{33} values due to their more bulky chromophore moiety.

The d_{33} of the reported NLO polymers by other research group were also listed in Table 5-9 for comparison [35, 166]. Results revealed that our polyimides show a somewhat smaller d33 than other groups. Although our polyimides showed smaller nonlinearity, it is large enough for application.

Table 5-9 Second harmonic coefficient and other parameters of NLO Polyimide films and other reported polymers

PI	d_{33}	n_{532}	n_{1064}	Thickness (μm)
PI A-I	9.75	1.7444	1.6087	0.7483
PI B-I	7.54	1.7492	1.6385	0.8882
PI C-I	7.39	1.7287	1.6935	0.9032
PI D-I	6.68	1.7072	1.5329	1.122
PI A-II	10.99	1.7341	1.5955	0.9847
PI B-II	9.12	1.7495	1.5893	0.981
PI C-II	8.57	1.729	1.5538	1.278
PI D-II	7.09	1.708	1.5412	1.55
PI A-III	11.73	1.748	1.5413	1.055
PI B-III	10.91	1.7471	1.5467	3.181
PI C-III	10.52	1.7242	1.5507	1.884
PI D-III	8.34	1.7055	1.5307	1.613
P-19[35]	26.4	-	-	-
P-2[166]	25.6	-	-	-

5.7.3 Long-term Stability of d_{33}

Long-term stability is important for the practical use of NLO polymers. Temporal stabilities of d_{33} values of the polyimides were studied at different temperatures. At room temperature, all NLO polyimides were stable and there was no decay in d_{33} values for 720 hours. The stabilities of the d_{33} values for PI films at 100 °C under air atmosphere are shown in Figure 5-22. At 100 °C in air, the d_{33} values decayed rapidly during the first 200 hr and then basically remained stable after 200 hr. It can be seen that the d_{33} values does not significantly change over 720 hr, since 88~94% of the nonlinearity remained.

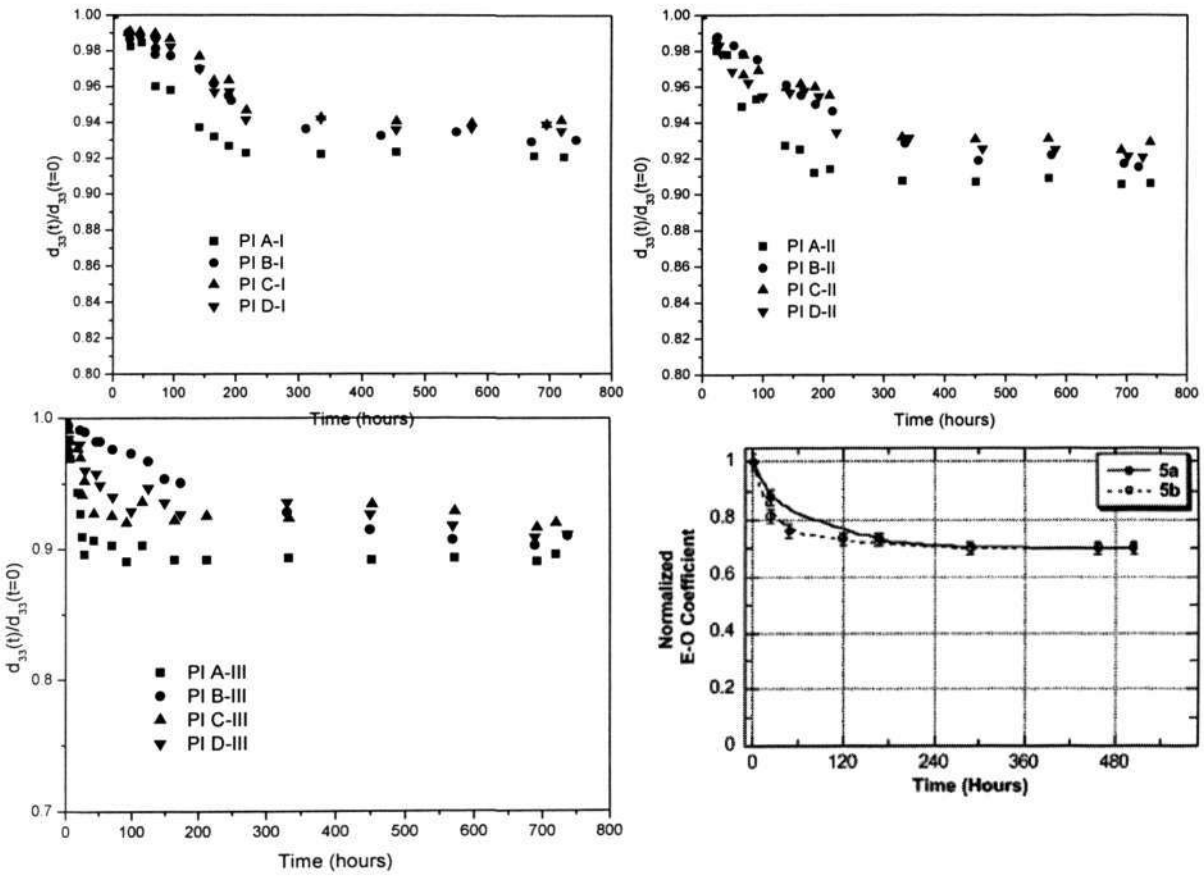

Figure 5-22 Temporal stability of SHG signals of PI at 100 °C in air and other reported polymers at 85 °C [62]

Series PI I exhibits higher stability than series PI II and III because series PI I possess

more rigid structures, more dense packing and lower free volume. Series PI III has lower stabilities due to more flexible structures and larger free volume. Series PI B exhibits higher stability than series PI A due to higher T_g of PI B. According to the above optimized structure, the nitro group at the meta position can lead to larger torsion angles of series PI B so that series PI B can possess more bulky chromophore moieties, which can effectively hinder the relaxation of polymer chain. Results indicates that series PI C and PI D display higher stability of the d_{33} values over 720 hrs than series PI B because of their higher T_g than series PI B. The incorporation of fluorine into the chromophore moiety can lead to more polar chromophore pendant moiety, which can increase the interaction between the polymer chains so that the polymer relaxation is more effectively hindered. Series PI C exhibits higher d_{33} stability than series PI D. This can be attributed to the different fluorine position in chromophore pendant moiety. Series PI C has larger torsion angle and more bulky 3D chromophore moiety so that the relaxation of polymer chain can be effectively hindered.

In comparison with other research work, the temporal stability of nonlinearity of the reported NLO polymers at 85 °C was also shown in Figure 5-22 [62]. Results show that our NLO polyimides showed higher temporal stability of nonlinearity because of their higher T_g.

5.8 Summary

FTIR, ^{1}H NMR and elemental analysis results confirmed that the three series of NLO polyimide based on the diaminoazobenzene chromophores were successfully synthesized.

Viscosity and GPC results show that these polyimides have large molecular weight. Through FTIR, UV, DSC and d_{33} measurement, the optimized imidization temperature

and poling voltage are selected as 230 °C and 6 kV, respectively. The PI unit structures were modeled by AM1/VAMP/Materials studio using series PI I as representative. Results show that the conformation structures of PI main chain are basically the same. However, the conformation structures of chromophores side chain are different because of the different fluorine position.

Results show that all the NLO polyimides displayed high T_g (200~280 °C) and T_{d5} (350~470 °C), and decrease in the sequence: series of PI I > PI II > PI III or series PI C > PI D > PI B > PI A. Results reveal that the NLO PI exhibits good transparency (λ_{max}: 298.5~353.5 nm) and their λ_{max} increase in the order of series PI I > PI II > PI III or series PI A > PI D > PI B > PI C. Results clearly reveals that the fluorine in chromophore side chain can significantly influence their UV-Vis absorption.

Incorporation of fluorine into the chromophore side chain or main chain can lead to better hydrophobic properties. Results also show that the fluorine position in the chromophore side chain can influence the hydrophobic properties.

All these NLO PI possess relatively large d_{33} (7~11 pm/V) and decrease in the sequence of PI I < PI II < PI III or PI D < PI C < PI B < PI A. Results show that the fluorine position in the chromophore side chain also affects the nonlinear optical property. At room temperature, there was no decay of d_{33} for 720 hours. At 100 °C in air, the PI exhibited excellent stability of d_{33} because 88%~94% of the original d_{33} remained over 720 hrs. The stability of d_{33} decreases in the sequence of PI I > PI II > PI III or PI C >PI D > PI B > PI A. Although the new polyimides showed smaller nonlinearities, they exhibited better comprehensive properties and showed large potential application in nonlinear optics.

Chapter 6 Preparation and Characterization of NLO Polyimide/Silicon Composite

6.1 Introduction

Another disadvantage of side-chain NLO polyimide through monomer containing chromophore is the harsh imidization condition, which could increase the possibility of the chromophore decomposition and decrease nonlinearity. However, the lower imidization temperature generally leads to lower thermal stability due to the incomplete imidization. Therefore, lowering the fabrication temperature without sacrificing stability is still a challenge for the development of the NLO polyimide prepared from monomer containing chromophore.

NLO silicon materials are promising materials because they have excellent optical quality, refractive index control of films and ease of device fabrication [208]. Furthermore, NLO silicon materials also possess lower surface energy, lower water absorption and higher contact angle so that the effects of moisture on their properties are low and the stability and reliability of material and device are high. The moisture effect is important for optoelectronic materials and devices because the moisture can result in the change of dielectric constant of the materials and the failure of optoelectronic devices. However, one of the major drawbacks of silicon materials is low temporal stability of nonlinearity at high temperature. Recently, organic-inorganic silicon composite materials have received much attention because of the significant

improvement of stability. By incorporating silicon crosslinked network into a high performance organic polymer such as polyimide, the resulting composite materials may display the advantages of both components. It has been reported that polyimide films containing silicon crosslinked network exhibit higher thermal stability, higher modulus and strength even at a high temperature, and a lower thermal expansion coefficient than PI system [209]. It is interesting to point out that the composites can be prepared at relatively low processing temperature and can exhibit higher temporal stability at elevated temperature. The low processing temperature can decrease the possibility of the chromophore decomposition and increase nonlinearity. At the same time, it can also decrease the light scattering and shrinkage so that it can decrease the optical loss from the curing. Furthermore, it has been found that the internal production of water due to the curing of poly(amic acid) aids the hydrolysis of the alkoxysilane and the carboxylic acid group of the poly(amic acid), being a Bronsted acid, might have a catalytic effect on hydrolysis and condensation of the alkoxysilane [210]. This will not lead to addition of catalyst and water and will decrease phase separation between the silicon and polyimide. Therefore, the incorporation of NLO silicon crosslinked network is a reasonable approach to decrease the cure temperature and enhance long-term NLO stability. In this chapter, polyimide/silicon composite was prepared through the successful synthesis of a NLO alkoxysilane dye in order to decrease the curing temperature and enhance the long-term NLO stability of the polyimides. The effects of silicon crosslinked network on the contact angle, surface energy, water absorption, second order harmonic coefficient d_{33} and its stability were also investigated.

6.2 Synthesis of NLO Polyimide/Silicon Composites

6.2.1 Materials

The materials used in the experiments were summarized in Table 6-1. Disperse red 1 (DR1) was purified by recrystallization from ethanol. Tetrahydrofuran (THF) and Hexane were purified by distillation over sodium chips and benzophenone ketal. The other materials were purchased from Aldrich, Merk and Clariant and used without further purification.

Table 6-1 Materials used in experiment

Name	Molecular Formula	Supplier
Disperse red 1 95%	$C_{16}H_{18}O_3N_4$	Aldrich
3-Isocyanatopropyl triethoxysilane 95%	$C_{10}H_{21}O_4SiN$	Aldrich
Dibutyltin dilaurate 95%	$CH_3CH_2CH_2CH_2)_2Sn[OCO(CH_2)_{10}CH_3]_2$	Clariant
Hexane (HPLC grade)	C_6H_{14}	Merk
1-Methyl-2-pyrrolidone 99.5%	C_5H_9NO	Clariant
Tetrahydrofuran (HPLC grade)	$CH_3CH_2CH_2CHO$	Merk

6.2.2 Synthesis of NLO Silicon Chromophore (SGDR1)

The synthetic route of NLO-active triethoxysilane (SGDR1) was depicted in Figure 6-

1 [210]. The synthesis was carried out via the nucleophilic addition reaction of DR1 and 3-isocyanatopropyl triethoxysilane (ICTES). The reaction must take place in an anhydrous environment because ICTES is very sensitive to moisture. Therefore, strictly anhydrous procedures were used. All equipments were heated in vacuum and purged into dry nitrogen gas in order to get rid of moisture, and solvent were freshly distilled over sodium. As water can react with the ICTES which lead to the failure of ICTES, the mole ratio of ICTES to DR1 was selected to be about 2: 1 to ensure that DR1 can react completely. At a two-necked round-bottomed Schlenk flask equipped with a magnetic stirrer, a nitrogen inlet and a reflux condenser, the ICTES (2.2 ml 8.08 mmol) and DR1 (1.27 g 4.04 mmol) were dissolved in freshly dried THF (30 ml). The mixture was then stirred at room temperature for 10 min. After that, it was refluxed for 4 hours with a catalytic amount (25 μL) of dibutyltin dilaurate (DBTDL). The solution was poured in distilled hexane and the resulting red precipitated powder was collected by suction filtration, washed again with hexane/THF until no DR1 was detected. The product (SGDR1) was finally dried under vacuum at 60°C for 24 hour in 80% yield and then stored in a vacuum desiccator.

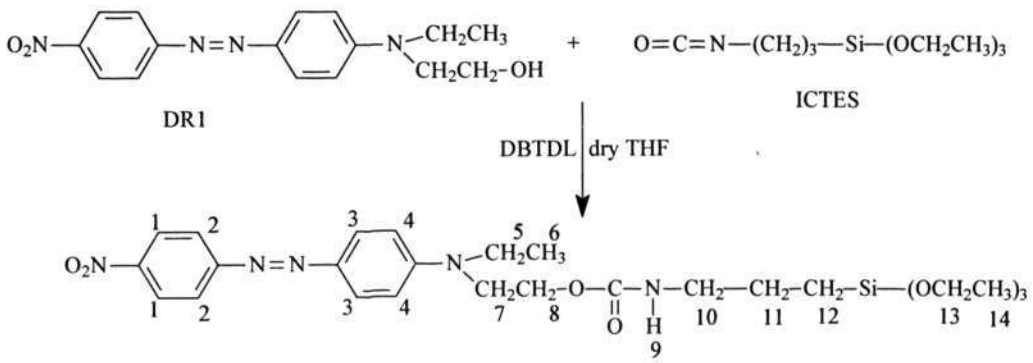

Figure 6-1 Synthetic route of SGDR1

6.2.3 Preparation of NLO Polyimide/SGDR1 Composites

Four kinds of poly(amic acid) containing azobenzene chromophore solutions (series PA III) described in Chapter 5 were used for preparation of PI III/ SGDR1composites. In preparation, the solution of SGDR1 (0.15g) in THF (1 ml) and NMP (1ml) was added into 4 ml of poly(amic acid) solution. The mixed solution was then stirred at room temperature for more than 4 hours to be homogeneous. The resulting solution was filtered through a 0.45 μm Teflon membrane filter and was then spin-coated on a substrate (glass slide or indium-tin oxide glass) at various speeds ranging from 500 rpm to 4000 rpm for different durations from 5 to 30 seconds under clean-room conditions. After it was dried in a vacuum oven at 65 °C for 12hr to remove residual solvent, the films were subjected to concurrent poling and imidization. A corona method described in Chapter 5 was selected to pole the films. In the poling process, the sample was heated to 200 °C, at a heating rate of 5 °C/min and successively held at this temperature for 1 hr, while a high voltage (6 kV) was applied to a corona wire simultaneously. Finally, the sample was cooled to room temperature in the presence of the poling field.

6.3 Characterization of SGDR1

6.3.1 Structure of SGDR1

The ^{1}H NMR spectrum and the spectra peak assignment of SGDR1 are shown in Figure 6-2. It can be seen that the peaks at 8.37, 7.94, 7.84 and 6.92 ppm were attributed to the H atoms of phenylene: H_1, H_2, H_3 and H_4, respectively. The peak at

7.20 ppm was assigned to the proton in carbamate, H_9. The peaks at 4.15, 3.73, 3.67, 3.53, 2.96, 1.45 and 0.53 ppm were assigned to the H atom in methylene H_8, H_{13}, H_7, H_5, H_{10}, H_{11} and H_{12}, respectively. The H atoms in methyl H_6 and H_{14} overlapped at the peak 1.15 ppm.

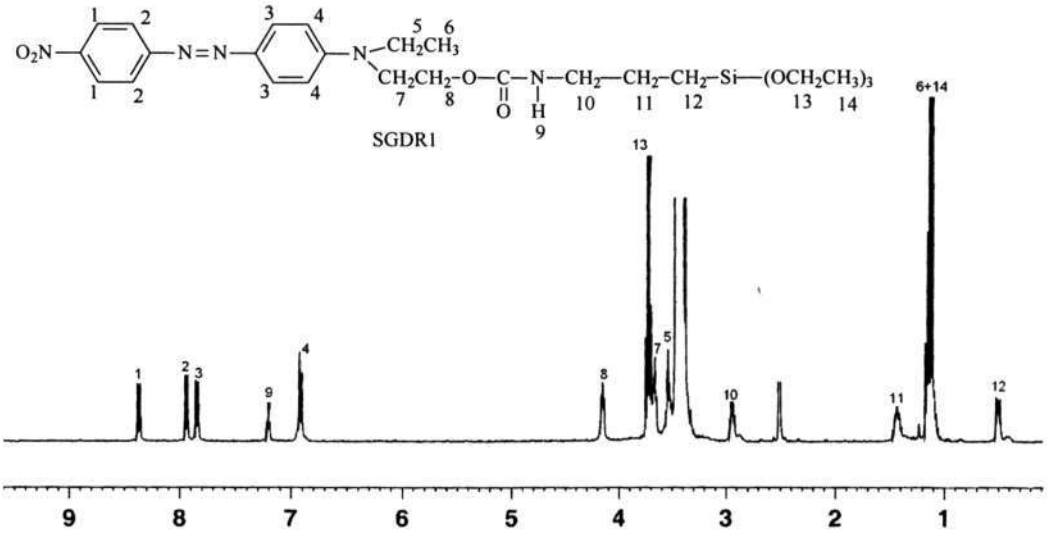

Figure 6-2 ^{1}H NMR spectrum of SGDR1

The infrared spectra of DR1, ICTES and SGDR1 are shown in Figure 6-3. The stretching vibration of the hydroxyl group in DR1 was observed at around 3273 cm^{-1}. For ICTES, the C-H stretching vibration of CH_3 and CH_2 were observed at 2888, 2928 and 2976 cm^{-1}. The Si-O-C_2H_5 stretching peaks of alkoxysilane were located in 1080 and 1166 cm^{-1}. The strong absorption peak corresponding to N=C=O stretching was observed at 2272 cm^{-1}. In spectrum of SGDR1, the absorption peaks of N=C=O and OH vanish and the new absorption peaks at 3327, 1690 and 1542 cm^{-1} emerge, contributed by the NH stretching, carbonyl (C=O) stretching and NH bending, respectively. In addition, the C-C stretching of phenylene and asymmetric stretching and symmetric stretching of NO_2 were observed at 1604, 1509 and 1343 cm^{-1}, respectively.

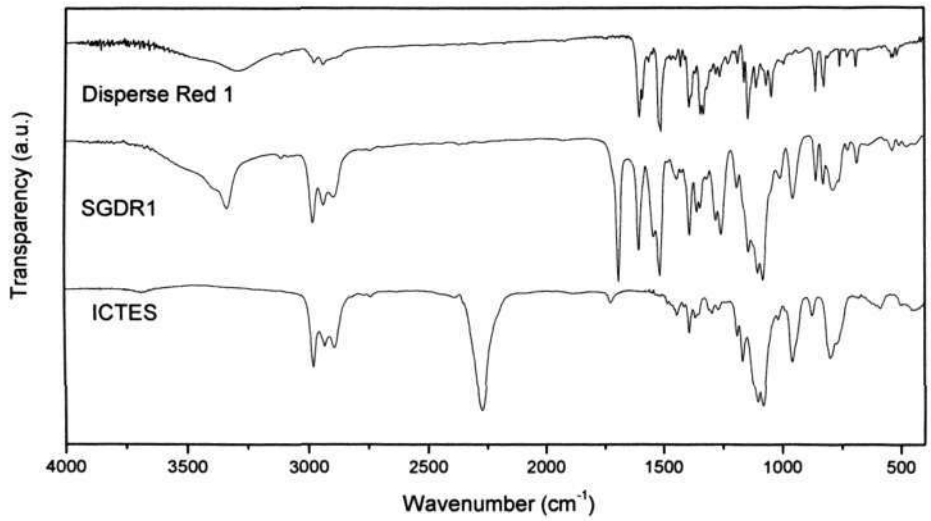

Figure 6-3 FTIR spectra of Disperse Red 1, SGDR1 and ICTES

Elemental analysis results are listed in Table 6-2. Based on ^{1}H NMR, FTIR and element analysis results, the structure of SGDR1 was confirmed to be as hypothesized.

Table 6-2 Elemental analysis results of SGDR1

	C	H	N	O
Calculated	55.57%	7.00%	12.47%	19.95%
Experimental	55.77%	7.01%	12.38%	19.88%

6.3.2 Properties of SGDR1

6.3.2.1 Thermal Properties

The thermal properties of the SGDR1 were characterized through DSC and TGA. The

DSC and TGA results are presented in Figure 6-4 and Figure 6-5, respectively. Results show that the melting point of the SGDR1 is 97 °C and the onset decomposition temperature of the SGDR1 is 225 °C. Therefore, the chromophore has high enough thermal stability so that it can endure the curing temperature.

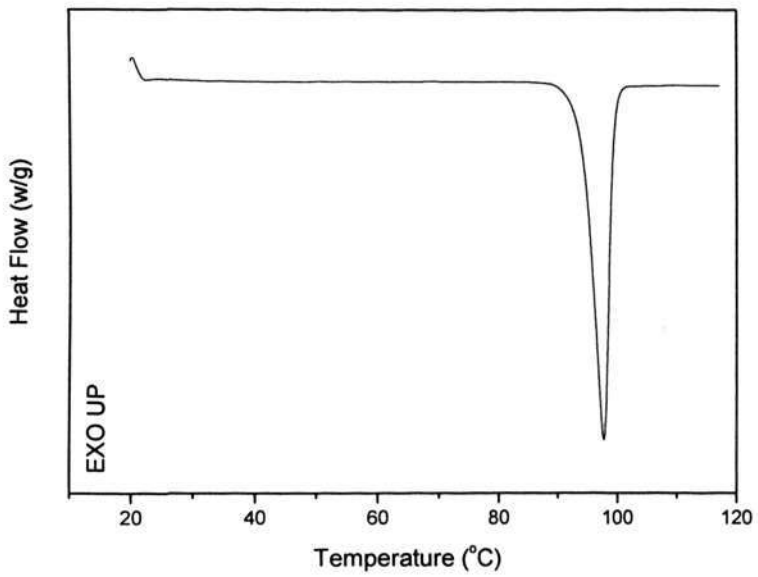

Figure 6-4 DSC of SGDR1

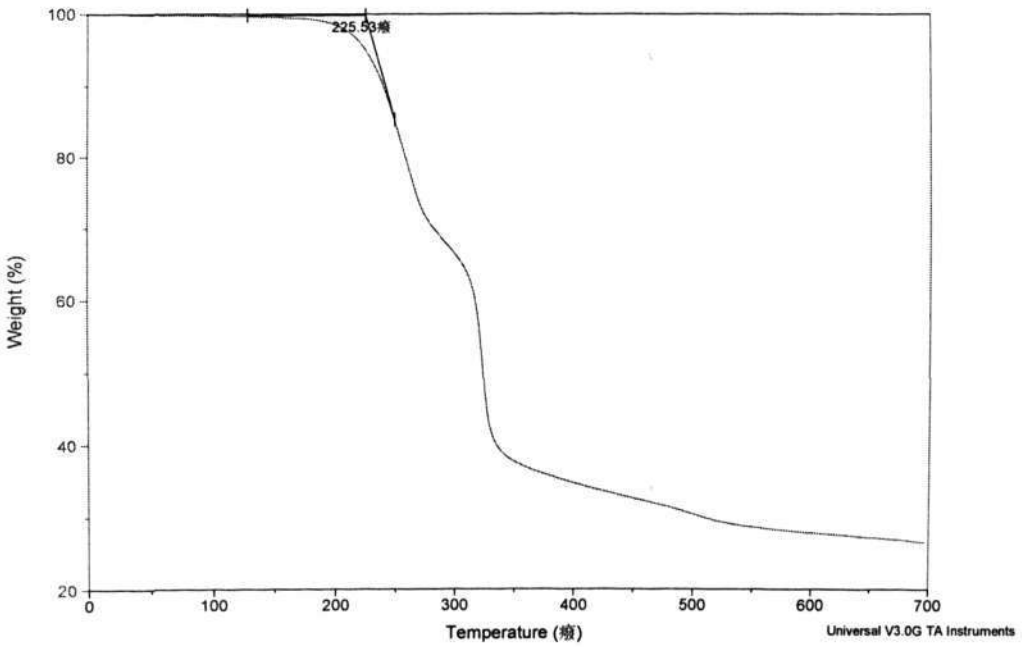

Figure 6-5 TGA of SGDR1

6.3.2.2 UV-Vis Absorption

The UV-Vis spectra of SGDR1 in NMP and THF are depicted in Figure 6-6. It can be seen that the λ_{max} of SGDR1 in NMP and THF are 498 and 474 nm, respectively. Results reveal that the red-shift of λ_{max} in NMP was due to the larger polarity of NMP. Compared with λ_{max} of DR1 in THF (489 nm listed in Table 4-2), SGDR1 exhibited blue-shift of λ_{max} because DR1 has a donor group [-N(CH_2CH_3)(CH_2CH_2OH)] and SGDR1 has a different donor group containing silicon group, which decreased the electron-release behavior.

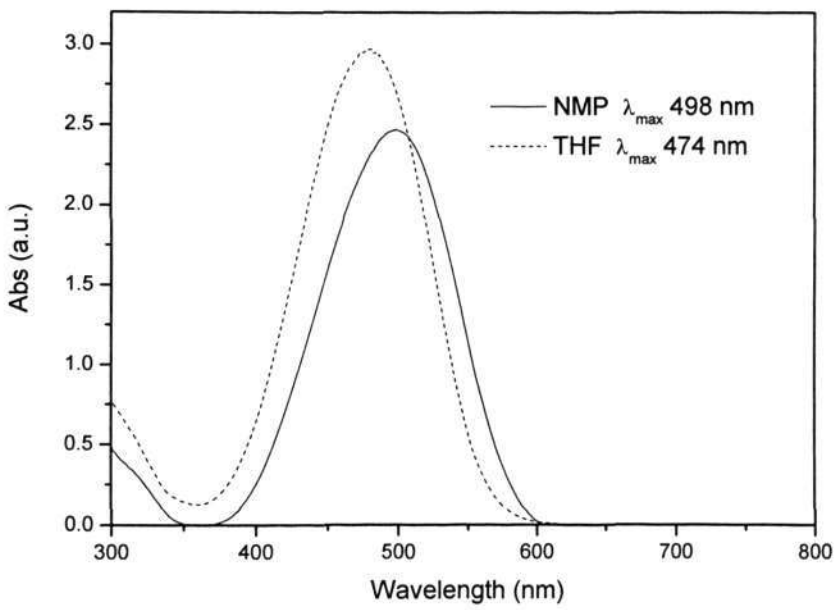

Figure 6-6 UV-Vis spectra of SGDR1 in NMP and THF

6.4 Characterization of NLO Polyimide/SGDR1 Composites

6.4.1 Structures of Polyimide/SGDR1 Composites

FTIR spectra of polyimide/SGDR1 composites cured at 65 and 200 °C are shown in Figure 6-7. After curing of poly(amic acid)/SGDR1 at 200 °C for 1 hour, the

characteristic absorption peak of imide group at 1780 cm^{-1} was emerged. It is noted that the characteristic absorption peak of Si-O-C_2H_5 around 1070 cm^{-1} disappeared and the absorption peak around 1100 cm^{-1} became broader after curing. This elucidated that Si-O-Si bond was formed. The FTIR data also indicate that the NLO moieties did not decompose during the curing process. This is illustrated by the symmetric nitro absorption at 1340 cm^{-1} and the C-N stretching of the aromatic nitro compound at 860 cm^{-1} which showed negligible change after curing. FTIR results suggest that PI III/SGDR1composites were well prepared through curing at 200 °C.

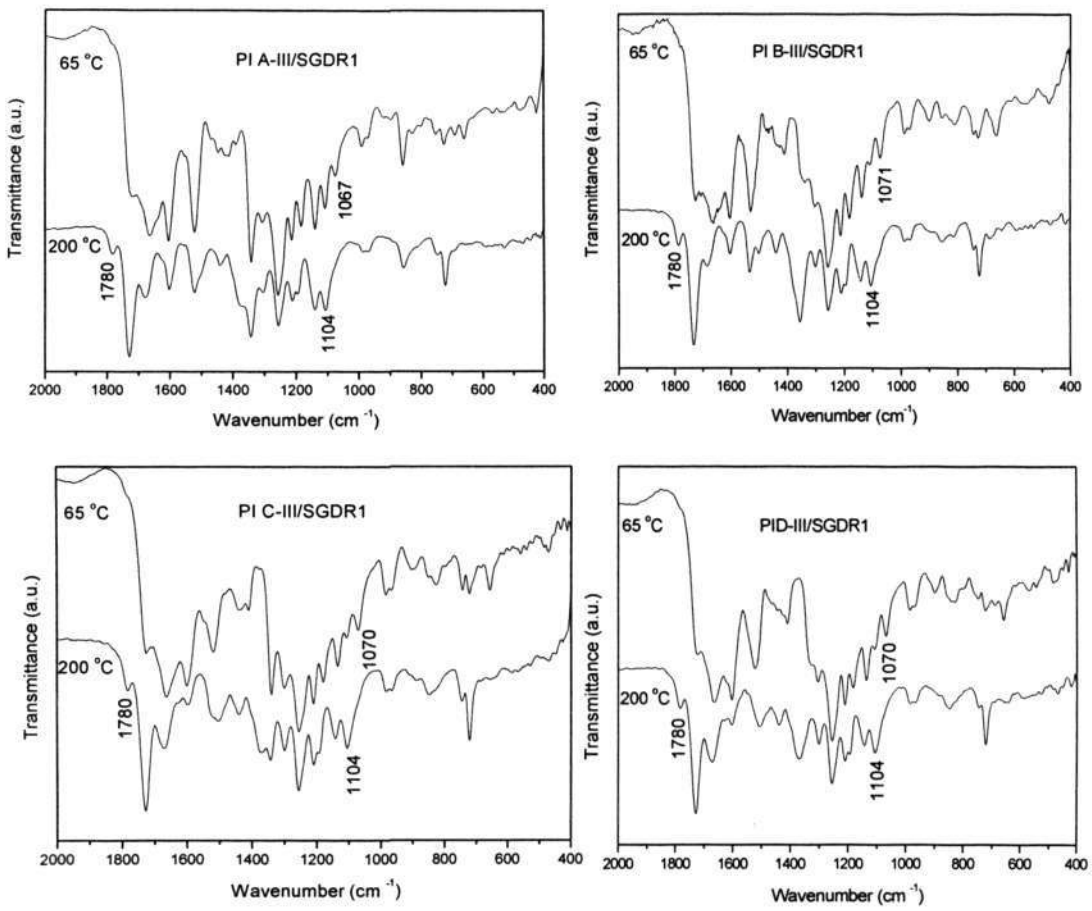

Figure 6-7 FTIR spectra of PI III/SGDR1 composites （PI A-III/SGDR1，PI B-III/SGDR1， PI C-III/SGDR1 and PI D-III/SGDR1）cured at 65 and 200 °C

6.4.2 Properties of NLO Polyimide/SGDR1 Composite Films

6.4.2.1 Thermal Properties

Thermal stabilities of polyimide/SGDR1 composites were characterized through DSC and TGA. DSC and TGA results of the composites are shown in Figure 6-8 and Figure 6-9, respectively. The parameters of their thermal properties are listed in Table 6-3. Results reveal that all composites display high T_g (235.9~266.2 °C) and T_{d5} (383.6~430.9 °C). The thermal stabilities of the NLO polyimide/silicon composites were higher than that of SGDR1 because the polyimide with high thermal stability was incorporated into the composite, whereas the SGDR1 was crosslinked when the composite was cured. In comparison with corresponding PI III cured at 200 °C (Table 5-3), all PI III/SGDR1 exhibited higher T_g due to the formation of silicon cross-linked network, which can effectively hinder the movement of the polymer chain. It was also found that the T_g of the series PI III/SGDR1 increased with the same sequence of the series PI III (PI C-III > PI D-III > PI B-III > PI A-III). Similar with NLO PI systems, the fluorine in the chromophore side chain of PI in composite can increase the polarity of the chromophore pendant group so that the movement of the polymer chain can be effectively hindered. The fluorine in different position can lead to different 3D conformation structure of chromophore side chain in PI so that the fluorine position can affect T_g of the composites differently. TGA results revealed that the decomposition temperature (T_{d5}) of series PI III/SGDR1 is higher than that of corresponding series PI III. This is also due to the formation of silicon cross-linked network. Furthermore, the decomposition temperature of composite also decreases with the same sequence of the series PI III possibly because the thermal stability of

composite is mainly determined by the chromophore moiety. The higher the thermal stability of chromophore, the higher the thermal stability of composite. The above results indicate that the fluorine and the fluorine position in the chromophore side chain of PI also affect the thermal stabilities of PI III/SGDR1 composites.

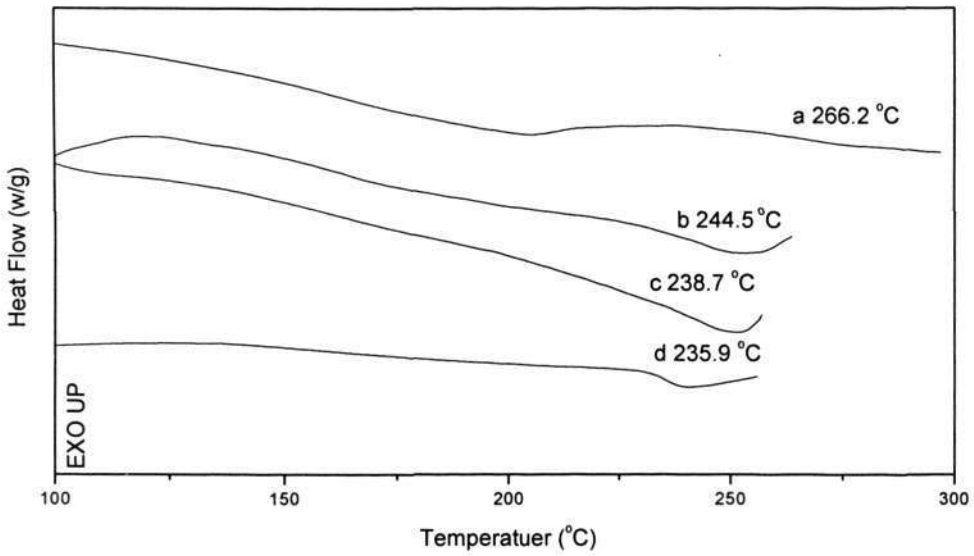

Figure 6-8 DSC of PI III/ SGDR1composites (a: PI C-III/SGDR1, b: PI D-III/SGDR1, c: PI B-III/SGDR1 and d: PI A-III/SGDR1)

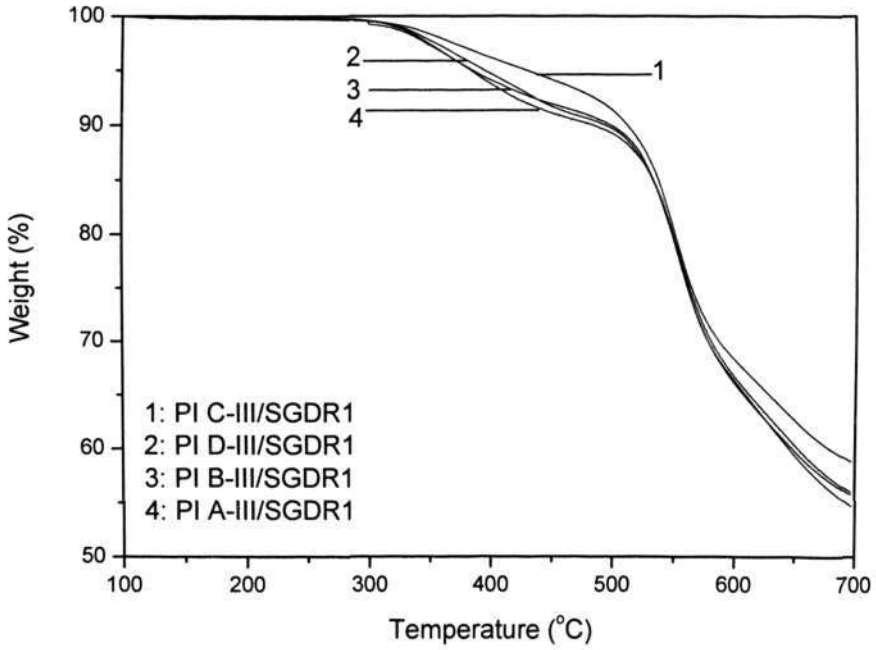

Figure 6-9 TGA of PI III/SGDR1 composites (1: PI C-III/SGDR1, 2: PI D-III/SGDR1, 3: PI B-III/SGDR1 and 4: PI A-III/SGDR1)

Table 6-3 Thermal properties of NLO PI III/SGDR1

	T_g (°C)	T_{d5} [a] (°C)	T_{d1} [b] (°C)	T_{d2} [c] (°C)	R_w (%) [d]
PI A-III/SGDR1	235.9	383.6	274.5	472.3	55.09
PI B-III/SGDR1	238.7	385.5	278.3	459	53.72
PI C-III/SGDR1	266.2	430.9	279.8	430.9	57.49
PI D-III/SGDR1	244.5	395	278.9	474.1	55.18

[a]: T_{d5} the decomposition temperature at 5% weight loss

[b]: T_{d1} the first decomposition temperature

[c]: T_{d2} the second decomposition temperature

[d]: R_w, Residual weight retention at 700 °C

6.4.2.2 UV-Vis Absorption

UV spectra of the PI III/SGDR1 composites films cured at 200 °C were shown in Figure 6-10. The λ_{max} of composite films was found to be as following: 350 and 457 nm for PI A-III/SGDR1; 331.5 and 472 nm for PI B-III/SGDR1; 293.5 nm for PI C-III/SGDR1 and 348.5 nm for PI D-III/SGDR1. The peaks at 350, 331.5, 293.5 and 348.5 nm were attributed to the absorption peaks of PI A-III, PI B-III, PI C-III and PI D-III, respectively and exhibited the same order with that of series PI III (PI C-III < PI B-III < PI D-III < PI A-III). However, the absorption around 400~500 nm was significantly increased. Compared with the UV absorption of SGDR1 (Figure 6-2), the increased absorption around 400~500 nm was attributed to SGDR1. PI A-III/SGDR1 and PI B-III/SGDR1 display a second maximum absorption peak around

400~500 nm and the second λ_{max} are 457 and 472 nm, respectively. However, PI C-III/SGDR1 and PI D-III/SGDR1 displayed a shoulder peak around 400~500 nm. This could be due to the fluorine in the chromophore side chain of PI III in composite, which can lead to different conformation structure of SGDR1 during the cure. Results reveal that the fluorine and the fluorine position in the chromophore side chain of PI also affected the UV absorption of the PI III/SGDR1composites films.

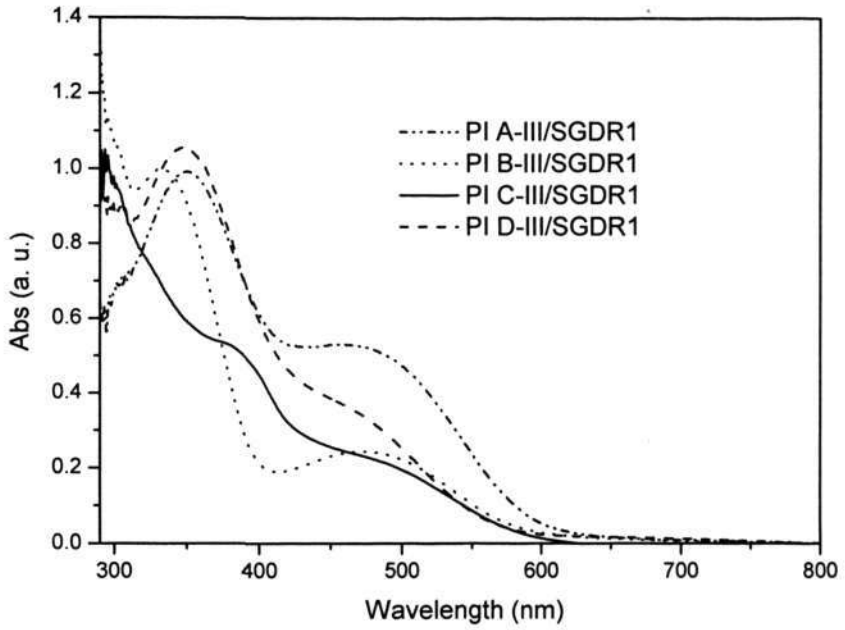

Figure 6-10 UV spectra of PI III/SGDR1composite films cured at 200 °C

6.4.2.3 Hydrophobic Properties

As is well known, water absorption and moisture content are very important to the electro-optical devices. It was reported that the incorporation of silicon is an effective method to decrease the water absorption [211]. The relationships between contact angles and time of the PI III/SGDR1 composites are shown in Figure 6-11. The average contact angles, surface energies and water absorptions of the composite films

are listed in Table 6-4. All these composite films exhibited excellent hydrophobic properties because their contact angles were larger than 80 degree. In comparison with that of PI III series as listed in Table 5-7, the series PI III/SGDR1 composite films all exhibited higher contact angle, lower surface energy and water absorption because of the incorporation of hydrophobic silicon segments. PI C-III/SGDR1 and PI D-III/SGDR1 exhibited better hydrophobic properties than PI B-III/SGDR1 and PI A-III/SGDR1 due to the incorporation of hydrophobic fluorine in the chromophore side-chain of PI. It was also found that PI A-III/SGDR1 exhibited different hydrophobic properties with PI B-III/SGDR1, which is possibly related to the nitro group in different position. PI C-III/SGDR1 also displayed the different hydrophobic properties with PI D-III/SGDR1 because of the different fluorine position in chromophore side chain of PI. The results reveal that the fluorine and the fluorine position in the chromophore side chain of PI also affected the hydrophobic properties of PI III/SGDR1 composites films.

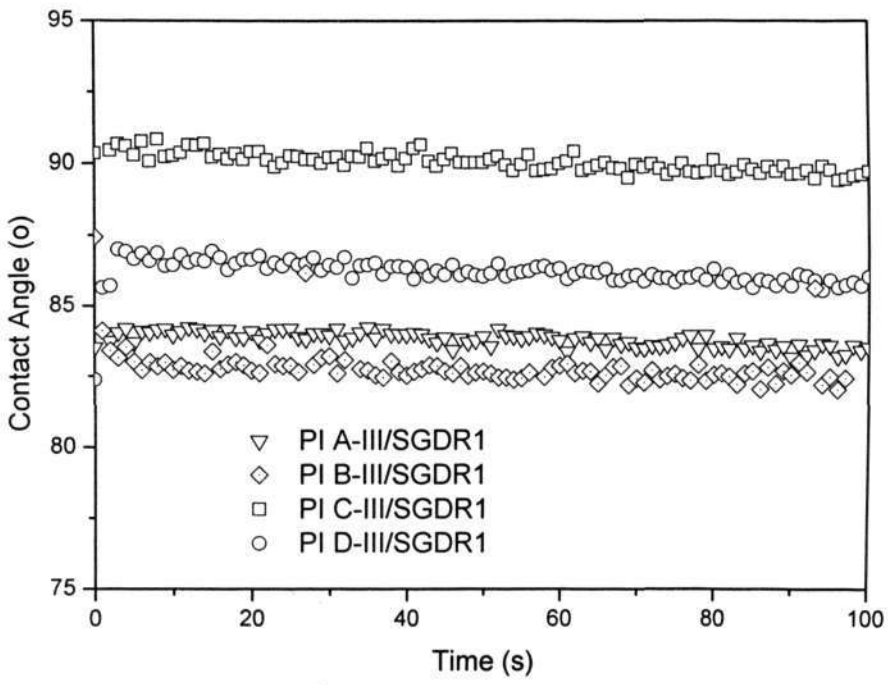

Figure 6-11 Contact angles of PI III/SGDR1 composites films

Table 6-4 Average contact angles, surface energy and water absorptions of PI III/SGDR1 composites

Sample	Average contact angle (°)	Water absorption (%)	Surface Energy (mN/m)
PI A-III/SGDR1	83.80	0.12	22.34
PI B-III/SGDR1	82.82	0.26	23.02
PI C-III/SGDR1	90.04	0.08	18.17
PI D-III/SGDR1	86.81	0.11	20.28

6.4.2.4 SHG Coefficient and Temporal Stability

The refractive index at 532 and 1064 nm, the thickness and d_{33} values of the composite films were determined and are listed in Table 6-5. Results show that all these PI III/SGDR1 composite films display high nonlinearity (d_{33}: 17.73~19.68 pm/V). PI C-III/SGDR1 and PI D-III/SGDR1 possess smaller d_{33} value than PI A-III/SGDR1 and PI B-III/SGDR1 because the fluorine in chromophore side-chain of PI is a weak π-donor and a strong δ-acceptor. The d_{33} value of PI B-III/SGDR1 was smaller than that of PI A-III/SGDR1 because the nitro group in chromophore side-chain of PI B-III is located in meta position. The PI C-III/SGDR1 had larger d_{33} than PI D-III/SGDR1. This is related to the conformation structure of chromophore moiety in PI. The chromophore moiety of PI D-III has a smaller torsion and aggregates easier so that the d_{33} is smaller. Results reveal that series PI III/SGDR1 have higher d_{33}

values than corresponding series PI III because NLO-active SGDR1 was incorporated into the composites.

Temporal stabilities of d_{33} value of the PI III/SGDR1 composite were studied at room temperature and 100 °C, respectively. Results show that there is no decay of d_{33} at room temperature after 720 hrs. Figure 6-12 show temporal stabilities of d_{33} value of the PI III/SGDR1 composites at 100 °C. Results show that PI A-III/SGDR1, PI B-III/SGDR1, PI C-III/SGDR1 and PI D-III/SGDR1 remained 90%, 91%, 94% and 92% of the original d_{33} values, respectively. The series PI III/SGDR1 composites attained higher temporal stabilities than corresponding PI III because the silicon crosslinked network can hinder the poling relaxation of the chromophore. PI III/SGDR1composite exhibited the same sequence in the d_{33} value and the temporal stability of d_{33} with PI III series. This implies that the fluorine and the fluorine position in the chromophore side chain of PI also influence the nonlinearities and the temporal stabilities of nonlinearity of series PI III/SGDR1.

Table 6-5 Second harmonic coefficient (d_{33}) and other parameters of NLO PI III/SGDR1 composite films

Samples	d_{33}	n_{532}	n_{1064}	Thickness (μm)
PI A-III/SGDR1	19.68	1.7373	1.5267	1.781
PI B-III/SGDR1	18.91	1.7288	1.5245	1.924
PI C-III/SGDR1	18.39	1.6947	1.5271	2.316
PI D-III/SGDR1	17.73	1.6898	1.5266	2.155

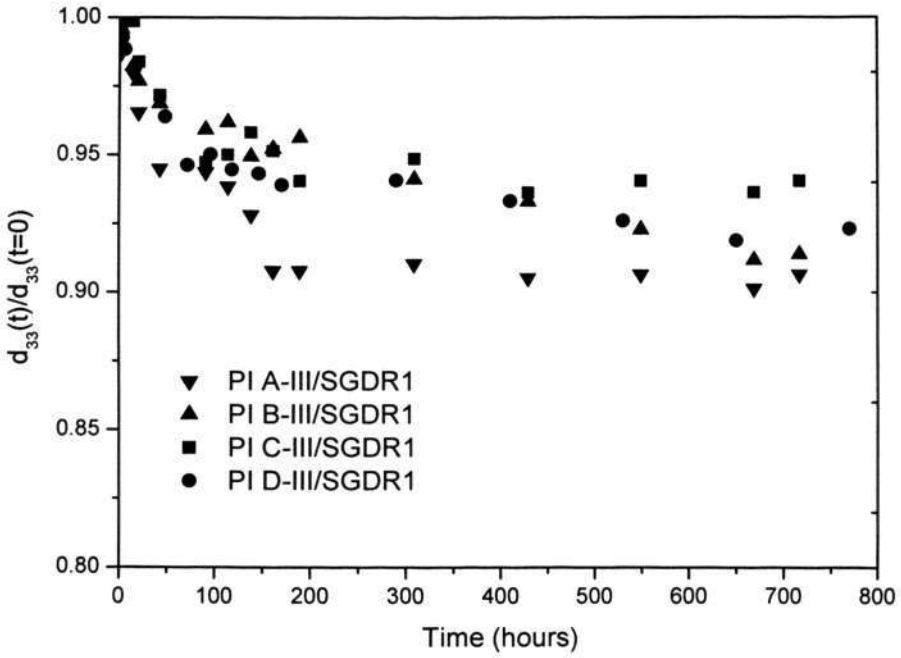

Figure 6-12 Temporal stability of d_{33} of NLO PI III/SGDR1 composites at 100 °C

6.5 Summary

^{1}H NMR, FTIR and elemental analysis results showed that a NLO-active silane chromophore SGDR1 was successfully synthesized. UV results show that the λ_{max} of SGDR1 in THF and NMP are 474 and 498 nm, respectively. DSC and TGA results show that its melting point was about 97 °C and onset decomposition temperature was about 225 °C.

Novel NLO PI III/SGDR1 composite films were successfully prepared. FTIR results confirm that the imidization and the crosslink reaction of silicon were completed after curing at 200 °C. DSC results show that these composites exhibit high T_g (235.9~266.2 °C) and T_{d5} (383.6~430.9 °C). All composites had higher T_g and T_{d5} than

the corresponding NLO series PI III although the composites were cured at lower temperature (200 °C). UV results show that the λ_{max} of PI A-III/SGDR1, PI B-III/SGDR1, PI C-III/SGDR1 and PI D-III/SGDR1 were 350 and 457 nm, 331.5 and 472 nm, 293.5 nm, and 348.5 nm, respectively. PI III/SGDR1 exhibits high contact angle (82.82~90.04°), low surface energy (18.17~23.02 mN/m) and low water absorption (0.08~0.26%). Results indicate that these composite films show better hydrophobic properties than the corresponding series PI III. All the NLO composite films exhibited higher d_{33} value (17.73~19.68 pm/V) than the corresponding NLO polyimides, no decay of d_{33} at room temperature over 720 hrs, and at least 90% of initial d_{33} remained at 100 °C over 720 hrs. The composites also exhibited higher temporal stability than corresponding NLO polyimide. Results show that the silicon crosslinked network can significantly improve the properties of the composites. Furthermore, results show that the fluorine and fluorine position in the chromophore side chain of PI can significantly affect properties of composites.

Chapter 7 Conclusions and Recommendations

7.1 Conclusions

The purpose of this research is to develop the novel second-order NLO polyimides and polyimide/silicon composite based on the new fluoronitroaryl diaminoazobenzene chromophores, to study the effects of the fluorine and fluorine position in the chromophore on the structures and properties of the NLO fluorinated chromophores, polyimide and polyimide/silicon composite, and to investigate the effects of the silicon network on the properties of the composites films. The main findings are summarized below:

7.1.1 Synthesis of Novel Fluorinated Diaminoazobenzene Chromophores

^{1}H NMR, ESI-MS, element analysis and FTIR results shows that two novel fluorinated diaminoazobenzene chromophore monomers and their non-fluorinated analogues, which can be used for NLO side-chain polyimide, were successfully synthesized as designed. DSC and TGA results reveal that these diaminoazobenzene chromophore monomers have good thermal stability (T_d: 240~270 °C). The incorporation of fluorine into diaminoazobenzene chromophores can increase thermal stability. The results of UV absorption show that 2R-4N-DIAMINE exhibits largest λ_{max} and lowest transparency; 2R-4F-3N-DIAMINE has smallest λ_{max} and highest transparency. 2R-4F-3N-DIAMINE displays a significant blue-shift of λ_{max} compared

with 2R-3N-DIAMINE. However, 2R-2F-5N-DIAMINE displays a bathochromic shift of λ_{max}. The fluorine position can significantly influence thermal stability and the UV absorbance.

The solvatochromic method was used to characterize the hyperpolarizability of the chromophore. Results show that the β values of these nitroaryl azo diaminobenzenes were in the same order with that of DR 1, which was large enough to generate second harmonic coefficient for application. The effects of the fluorine and fluorine position on the dipole moments and hyperpolarizability were studied through comparison with fluorinated chromophores and corresponding analogues. Results reveal that incorporation of fluorine into chromophores can decrease the hyperpolarizability, and the fluorine group in different position will lead to different electronic distribution in the charge-transfer states of the chromophores.

7.1.2 Synthesis of Novel NLO Polyimides

Three novel series of NLO polyimide based on the newly developed fluoronitroaryl diaminoazobenzene chromophores and their analogues were successfully synthesized and confirmed through FTIR, ^{1}H NMR and element analysis. Viscosity and GPC results reveal that they have large molecular weights. The optimized conformation structures of the representative series PI I were modeled through AM1/VAMP/Materials studio. Results indicates that the conformation structures of the polyimide main chain are basically the same. However, the different position of fluorine in the chromophore side chain can lead to significantly different conformation structures of the chromophore side chain. The fluorine in ortho position

can result in larger torsion of the chromophore side chain, and the fluorine in para position can lead to smaller torsion. The best imidization and poling conditions were determined to be 6 kV and 230 °C through FTIR, UV-Vis absorption, DSC and d_{33}.

DSC and TGA results show that all the NLO polyimide displayed high T_g (200~280°C) and T_{d5} (350~470 °C). UV-Vis absorption results reveal that NLO polyimides exhibited small λ_{max} (298.5~353.5 nm) and high transparency. The contact angle, surface energy and water absorption results show that the incorporation of fluorine into the chromophore side chain can improve the hydrophobic properties. All NLO PIs possess relatively large d_{33} (7~11 pm/V) and excellent stability of d_{33}. For all polyimides, there was no decay of d_{33} over 720 hrs at room temperature and 88~94% of d_{33} remained over 720 hrs at 100 °C.

The effects of fluorine and fluorine position in the chromophore side chain on the structures and properties of NLO polyimide were studied in detail. The fluorine in ortho position was found to result in larger torsion of chromophore side chain, which can increase the non-planarity and the steric hinder effect. Hence, the fluorine in ortho position can increase thermal stability, transparency and d_{33} through improvement of the aggregation. However, the fluorine in para position can lead to the small torsion of the chromophore side-chain and exhibit reverse effect. Furthermore, the effects of main chain structure on the structures and properties were also studied. The rigid main chain can increase stability but decrease transparency and poling efficiency, whereas the flexible main chain can increase transparency and d_{33}.

7.1.3 Preparation of NLO Polyimide/Silicon Composites

^{1}H NMR, FTIR and element analysis results confirms that a NLO-active silane chromophore SGDR1 was successfully synthesized. UV results show that λ_{max} of SGDR1 in NMP and THF are 498 and 474 nm, respectively. DSC and TGA results show that the melting point and onset decomposition temperature of SGDR1 are 97 and 225.4 °C, respectively.

Novel NLO PI/silicon composite films were successfully prepared. All the composites have higher T_g (235.9~244.5 °C) and T_{d5} (383.6~430.9 °C) than corresponding NLO series PI III although they were cured at lower temperature (200 °C). UV results show that the composites exhibited high transparency. The composite films exhibited better hydrophobic properties and larger d_{33} value than the corresponding NLO polyimides. All the NLO composite films exhibited no decay of d_{33} after 720 hrs at room temperature and still remained at least 90 % of d_{33} after 720 hrs at 100 °C. The composites exhibited higher temporal stability of d_{33} than corresponding NLO polyimide. The effects of silicon cross-linked network on the properties were studied. Results indicate that the silicon cross-linked network can improve the properties comprehensively. The effects of fluorine and the fluorine position in the chromophore side-chain of the polyimide on the properties of composites films is the same with that on the properties of PIs.

7.2 Recommendations for Further Studies

Following work might be recommended for further studies:

In order to confirm the different conformation structures, it is recommended that the structures of the polyimide should be characterized through small angle X-ray scattering and near-field scanning optical microscopy.

To study the effect of the silicon on the properties systemically, different amount of the silicon dye on the structures and properties can be taken. The different amount of silicon dye will lead to different composite structures and will affect their properties.

Although the optical loss of the material is mainly affected by their UV absorption, the effects of fluorine, fluorine position and silicon on the optical loss should be studied, which is very important for waveguide or other devices fabrication.

Quantum mechanical and kinetic Monte Carlo modeling of NLO material structures is powerful tools to predict the structure before attempting synthesis. Based on the results, most attempts do lead to significant improvement in achievable NLO activity.

References

[1] S. F. Hubbard, K. D. Singer, F. Li, S. Z. D. Cheng, and F. W. Harris, Nonlinear optical studies of a fluorinated poled polyimide guest-host system, *Applied Physics Lett.*, 65, pp265-267,1994

[2] T. C. Kowalczyk, K. D. Singer, A. J. Beuhler, D. A. Wargowski, P. A. Cahill, C. H. Seager, M. B. Meinhardt, and S. Ermer., Crosslinked polyimide electro-optical materials, *J. Appl. Phys.*, 78, pp5876-5883, 1995

[3] D. R. Kanis, M. A. Ratner and T. J. Marks, Design and construction of molecular assemblies with large second-order optical nonlinearities. Quantum chemical aspects, *Chem. Rev.* 94, pp195-242, 1994

[4] L. A. Hornak, *Polymers for lightwave and integrated optics: technology and applications*, pp102-104, Marcel Dekker, New York, 1992

[5] D. F. Eaton, Nonlinear optical materials, *Science*, 253, pp281-287, 1991

[6] L. R. Dalton, W. H. Steier, B. H. Robinson, C. Zhang, A. Ren, S. Garner, A. Chen, T. Londergan, L. Irwin, B. Carlson, L. Fifield, G. Phelan, C. Kincaid, J. Amend, Alex Jen, From molecules to opto-chips: organic electro-optic materials, *J. Mater. Chem.*, 9, pp1905-1920, 1999

[7] P. N. Prasad and D. J. Williams, *Introduction to Nonlinear Optical Effects in Molecules and Polymers*, pp53-260, John Wiley & Sons, New York, 1991

[8] G. R. Meredith, D. J. VanDusen, and D. J. Williams, Optical and nonlinear optical characterization of molecularly doped thermotropic liquid crystalline polymers, *Macromolecules*, 15, pp1385-1389, 1982

[9] T. Verbiest, D. M. Burlan, M. C. Jurich, V. Y. Lee, R. D. Miller and W. Volksen, Exceptionally thermally stable polyimides for second-order

nonlinear optical application, *Science*, 268, pp1604-1606, 1995

[10] Y. Q. Shi, C. Zhang, H. Zhang, J. H. Bechtel, L. R. Dalton, B. H. Robinson and W. H. Steier, Low (sub-1-volt) halfwave voltage polymeric electro-optic modulators achieved by controlling chromophore shape, *Science*, 288, pp119-120, 2000

[11] J. L. Oudar and D.S. Chemla, Hyperpolarizabilities of the nitroanilines and their relations to the excited state dipole moment, *J. Chem. Phys.*, 66, pp2664-2668, 1977

[12] L. T. Cheng, W. Tam, S. H. Stevenson, G. R. Meredith, G. Rikken and S. R. Marder, Experimental investigations of organic molecular nonlinear optical polarizabilities. 1. Methods and results on benzene and stilbene derivatives, *J. Phys. Chem.*, 95, pp10631-10643,1991

[13] L. T. Cheng, W. Tam, S. R. Marder, A. E. Stiegman, G. Rikken and C. W. Spangler, Experimental investigations of organic molecular nonlinear optical polarizabilities. 2. A study of conjugation dependences, *J. Phys. Chem.*, 95, pp10643-10652,1991

[14] S. R. Marder, D. N. Beratan and L.-T. Cheng, Approaches for optimizing the first electronic hyperpolarizability of conjugated organic molecules, *Science*, 252, pp103-106, 1991

[15] S. R. Marder, C. B. Gorman, B. G. Tiemann and L.-T. Cheng, Stronger acceptors can diminish nonlinear optical response in simple donor-acceptor polyenes, *J. Am. Chem. Soc.*, 115, pp3006-3007, 1993

[16] S. R. Marder, J. L. Perry, B. G. Tiemann, C. B. Gorman, S. Gilmour, S. L. Biddle and G. Bourhill, Direct observation of reduced bond-length alternation in donor/acceptor polyenes, *J. Am. Chem. Soc.*, 115, pp2524-

2526, 1993

[17] V. P. Rao, A. K. Y. Jen and Y. Cai, Achieving excellent tradeoffs among optical, chemical and thermal properties in second-order nonlinear optical chromophores, *Chem. Commun.*, pp1237-1238, 1996

[18] M. A. Pauley, C. H. Wang and A. K. Y. Jen, Hyper-Rayleigh scattering studies of first order hyperpolarizability of tricyanovinylthiophene derivatives in solution, *J. Chem. Phys.*, 102, pp6400-6405, 1995

[19] P. Boldt, G. Bourhill, C. Bräuchle, Y. Jim, R. Kammler, C. Müller, J. Rase and J. Wichern, Tricyanoquinodimethane derivatives with extremely large second-order optical nonlinearities, *Chem. Commun.*, pp793-795, 1996

[20] C. R. Moylan, R. J. Twieg, V. Y. Lee, S. A. Swanson, K. M. Betterton and R. D. Miller, Nonlinear optical chromophores with large hyperpolarizabilities and enhanced thermal stabilities, *J. Am. Chem. Soc.*, 115, pp12599-12600, 1993

[21] W. Tam, L. T. Cheng, J. D.Bierlein, L. K. Cheng, Y. Wang, A. E. Feiring, G. R. Meredith, D. F. Eaton, J. C. Calabrease, G. .L. A.Rikken, in Materials for Nonlinear Optics Chemical Perspectives, S. R. Marder, J. E. Sohn, G. D. Stucky, Eds., *ACS Symposium* Series 455, American Chemical Society, Washington, DC, pp158, 1991

[22] C. R. Moylan, R. D. Miller, R. J. Twieg, V. Y. Lee, in Polymers for second-order Nonlinear optics, G.. A. Lindsay, K. D. Singer, Eds, *ACS Symposium* Series 601, American Chemical Society, Washington, DC, pp66, 1995

[23] N. Matsuzawa, and D. J. Dixon, Semiempirical calculations of hyperpolarizabilities for donor-acceptor molecules: comparison to experiment, *J. Phys. Chem.*, 96, pp6232-6241, 1992

[24] R. D. Miller, V. Y. Lee, C. R. Moylan, Substituted azole derivatives as nonlinear optical chromophores, *Chem. Mater.*, 6, pp1023-1032, 1994

[25] C. R. Moylan, R. D. Miller, R. J. Twieg, K. M. Betterton, V. Y. Lee, T. J. Matray, C. Nguyen, Synthesis and nonlinear optical properties of donor-acceptor substituted triaryl azole derivatives, *Chem. Mater.*, 5, pp1499-1508, 1993

[26] R. S. H. Liu, R. S. Muthyala, X.-S. Wang, A. E. Asato, P. Wang and C. Ye, Correlation of substituent effects and energy levels of the two lowest excited states of the azulenic chromophore, *Org. Lett.*, 2, pp269-271, 2000

[27] M. Matsui, Functionality of fluorine-containing dyes, *J. Fluor. Chem.*, 96, pp65-69, 1999

[28] X. Wu, J. Wu, Y. Liu and A. K-Y Jen, Highly Efficient, Thermally and chemically stable nonlinear optical chromophores based on the a-perfluoroaryl-dicyanovinyl electron acceptors., *Chem. Commun.*, pp2391-2393, 1999

[29] J. L. Hua, W. Zhang, Z. Li, J. G. Qin, Y. C. Shen, Y. Zhang and Z. H. Lu, Arylaldehydes-pentafluorophenyl hydrazones as second-order nonlinear optical chromophores: A novel approach for remarkably defeating the nonlinearity-transparency trade-off, *Chem. Lett.*, 31, pp232-233, 2002

[30] J. D. Luo, H. Ma, M. Haller, Alex K.-Y. Jen and Richard R. Barto, Large electro-optic activity and low optical loss derived from a highly fluorinated dendritic nonlinear optical chromophore, *Chem. Commun.*, pp888-889, 2002

[31] P. Gunter, *Nonlinear Optical Effects and Materials*, pp163-286, Springer-Verlag, New York, 2000

[32] K. D.Singer, M. G. Kuzyk, W. R. Holland, J. E. Sohn, S. J. Lalama, R. B. Comizzoli, H. E. Katz and M. L. Schilling, Electro-optic phase modulation and optical second-harmonic generation in corona-poled polymer films, *Appl. Phys. Lett.*, 53, pp1800-1802, 1988

[33] H. Katz, K.D. Singer, J. Sohn, C. Dirk, L. King and H. Gordon, Greatly enhanced second-order nonlinear optical susceptibilities in donor-acceptor organic molecules, *J. Am. Chem. Soc.*, 109, pp6561-6563, 1987

[34] Y. Shuto, M. Amano and T. Kaino, Electrooptic light modulation in poled azo-dye-substituted polymer waveguides, *Jpn. J. Appl. Phys.*, 30, pp320-326, 1991

[35] D. Briers, G. Koechelberghs, I. Picard, T. Verbiest, A. Persoons and C. Samyn, Novel chromophore-functinalized poly[2-(trifluoromethyl) adamantly acrylate-methyl vinyl urethane]s with high poling stabilities of the nonlinear optical effect, *Macromol. Rapid Commun.*, pp841-846, 2003

[36] Y. Shi, W. Steier, L. Yu, M. Chen and L. Dalton, Large stable photoinduced refractive index change in a nonlinear optical polyester polymer with disperse red side groups, *Appl. Phys. Lett.*, 58, pp1131-1133, 1991

[37] C. Ye, N. Minami, T. Marks, J. Yaw and G. Wow, Persistent, efficient frequency doubling by poled annealed films of a chromophore-functionalized poly(p-hydroxystyrene), *Macromolecules*, 21, pp2899-2901, 1988

[38] D. Dai, T. J. Marks, J. Yang, P. M. Lundquist and G. K. Wong, Polyphenylene ether based thin-film nonlinear optical materials having high chromophore densities and alignment stability, *Macromolecules*, 23,

pp1891-1894, 1990

[39] N. Nemoto, F. Miyata, Y. Nagase, J. Abe, M. Hasegawa and Y. Shirai, Polyamides for nonlinear optics containing second-order NLO-chromophores with high density, *Chem. Mater.*, 8, pp1527-1534, 1996

[40] Y. W. Kim, J. I. Jin, M. Y. Jin, K. Y. Choi, J. J. Kim and T. Zyung, Synthesis and characterization of novel polyamides carrying NLO moieties, *Polymer*, 38, pp2269-2275, 1997

[41] K. J. Moon, H, K. Shim, K. S. Lee, J. Zieba and P. N. Prasad, Synthesis, Characterization, and second-order optical nonlinearity of a polyurethane structure functionalized with a hemicyanine dye, *Macromolecules*, 29, pp861-867, 1996

[42] N. Tsutsumi, O. Matsumoto, W. Sakai and T. Kiyotsukuri, Nonlinear optical polymers. 2. Novel NLO linear polyurethane with dipole moments aligned transverse to the main backbone, *Macromolecules*, 29, pp592-597, 1996

[43] Z. Li, Ch. Huang, J. L. Hua, J. G. Qin, Z. Yang and C. Ye, A new postfunctinal approach to prepare second-order nonlinear optical polyphophazenes containing sulfonyl-based chromophore, *Macromolecules*, 37, pp371-376, 2004

[44] Z. Li, J. Li, J. G. Qin, A. J. Qin and C. Ye, Synthesis and characterization of polysiloxanes containing carbazolyl and sulfonyl-indole based chromophore as side chains, Polymer, 46, pp363-368, 2005

[45] G. Green, H. Jr. Hall, J. Mulvaney, J. Noonan and D. Williams, Donor-acceptor-containing quinodimethanes. Synthesis and copolyesterification of highly dipolar quinodimethanes, *Macromolecules*, 20, pp716-722, 1987

[46] M. Mitchell, J. Mulvaney, H. Jr. Hall, C. Willand, H. Hampsch, D.

Williams, New mainchain nonlinear optical polymers with high glass transition temperature, *Polym. Bull.*, 28, pp381-388, 1992

[47] G. Green, I. J. Weinschenk, J. Mulvaney, H. Jr. Hall, The synthesis of polyesters containing a nonrandomly placed highly polar repeating unit, *Macromolecules*, 20, pp722-726, 1987

[48] H. Katz and M. Schilling, Head-to-tail assemblies of dipolar, piperazine-linked chromophores: synthesis, x-ray structure, and dielectric characterization, *J. Am. Chem. Soc.*, 111, pp7554-7557, 1989

[49] F. Fuso, A. Padias and H. Jr. Hall, Poly[(ω-hydroxyalkyl)thio-α-cyanocinnamates] linear polyesters with NLO-chromophores in the main chain, *Macromolecules*, 24, pp1710-1713, 1991

[50] I. Teraoka, D. Jungbaier, B. Reck, D. Yoon, R. Twieg, and C. Willson, Stability of nonlinear optical characteristics and dielectric relaxations of poled amorphous polymers with main-chain chromophores, *J. Appl. Phys.*, 69, pp2568-2576, 1991

[51] D. Jungbauer, I. Teraoka, D. Yoon, B. Reck, J. Swalen, R. Twieg, and C. Willson, Second-order nonlinear optical properties and relaxation characteristics of poled linear epoxy polymers with tolane chromophores, *J. Appl. Phys.*, 69, pp8011-8017, 1991

[52] R. Meyrueix, J. Lecomte and G. Tapolsky, Decay of the nonlinear susceptibility components in main-chain functionalized poled polymers, *Proc. SPIE*, 1560, pp454, 1991

[53] K. Y. Sandhya, C. K. S. Pillai, Masataka Sato and Naoto Tsutsumi, Highly stable rigid main-chain nonlinear optical polymers with nematic phase: Effect of liquid-crystalline phase on nonlinear optical response, *J. Polym.*

Sci. Part A: Polym. Chemistry, 41, pp1527-1535, 2003

[54] M. A. Hubbard, T. J. Marks, J. Yang and G. K. Wong, Poled polymeric nonlinear optical materials. Enhanced second harmonic generation stability of crosslinkable matrix/chromophore ensembles, *Chem. Mater.*, 1, pp167-169, 1989

[55] J. Park, T. J. Marks, J. Yang and G. K.Wong, Chromophore-functionalized polymer thin film nonlinear optical materials. Effects of in situ crosslinking on second harmonic generation temporal characteristics, *Chem. Mater.*, 2, pp229-231, 1990

[56] Y. Jin, S. H. Carr, T. J. Marks, W. Lin and G. K. Wong, Poled chromophore-functionalized polymeric nonlinear optical materials. Probing second harmonic generation temporal characteristics via site-selective crosslinking/hydrogen bonding, *Chem. Mater.*, 4, pp963-965, 1992

[57] M. Eich, G. C. Bjorklund, D. Y. Yoon, Poled amorphous polymers for second-order nonlinear optics, *Polym. Adv. Technol.*, 1, pp189-196, 1990

[58] D. Jungbauer, B. Reck, R. Twiea, D. Yoon and W. C. Swalen, Highly efficient and stable nonlinear optical polymers via chemical crosslinking under electric field, *Appl. Phys. Lett.*, 56, pp2610-2612, 1990

[59] M. A. Hubbard, T. J. Marks, W. Lin and G. K. Wong, Poled polymeric nonlinear optical materials. Enhanced second harmonic generation temporal stability of epoxy-based matrixes containing a difunctional chromophoric comonomer, *Chem. Mater.*, 4, pp965-968, 1992

[60] C. Zhang, C. G. Wang, J. L. Yang, L. R. Dalton, G. L. Sun, H. Zhang and W. H. Steier, Electric poling and relaxation of thermoset polyurethane second-

order nonlinear optical materials: Role of cross-linking and monomer rigidity, *Macromolecules*, 34, pp235-243, 2001

[61] J. A. Dharmadhikari, R. C Aiyer, K. Vijayamohanan, P. Sushama; A. A. Athawale, Evidence for second-order optical nonlinearity in γ-ray induced partially cross-linked polyacrylonitrile, *J. Phys. Chem. B*, 105, pp5110-5113, 2001

[62] M. Haller, J. D. Luo, H. X. Li, T.-D. Kim, Y. Liao, B. H. Robinson, L. R. Dalton and A. K.-Y. Jen, A novel lattice-hardening process to achieve highly efficient and thermally stable nonlinear optical polymers, *Macromolecules*, 37, pp688-690, 2004

[63] B. K. Mandel, J. Kumar, J. Huang and S. K. Tripathy, Novel photo-crosslinked nonlinear optical polymers, *Macromol. Chem. Rapid Commun.*, 12, pp63-68, 1991

[64] B. K. Mandel, R. J. Jeng, J. Kumar, J. Huang and S. K. Tripathy, New photocrosslinkable polymers for second-order nonlinear optical processes, *Macromol. Chem. Rapid Commun.*, pp607-612, 1991

[65] M. Chen, L. P. Yu, L. R. Dalton, Y. Q Shi and William H. Steier, New polymers with large and stable second-order nonlinear optical effects, *Macromolecules*, 24, pp5421-5428, 1991

[66] J. X. Lu and J. Yin, Synthesis and characterization of photocrosslinkable, side-chain, second-order nonlinear optical poly(ester imide)s with great film-forming ability and long-term dipole orientation stability, *Journal of Polym. Sci., Part A: Polym. Chem.*, 41, pp303-312, 2003

[67] A. J. Ikushima, T. Fujiwara and K. Saito, Silica glass: A material for photonics, *J. Appl. Phys.*, 88, pp1201-1213, 2000

[68] R. J. Jeng, Y. M. Chen, J. I. Chen, J. Kumar and S. K. Tripathy, Phenoxysilicon polymer with stable second-order optical nonlinearity *Macromolecules*, 26, pp2530-2534, 1993

[69] F. Chaumel, H. W. Jiang and A. Kakkar, Sol-gel materials for second-order nonlinear optics, *Chem. Mater.*, 13, pp3389-3395, 2001

[70] Y. Nosaka, N. Tohriwa, T. Kobayashi, and N. Fuji, Two-dimensionally poled sol-gel processing of titania film doped with organic compounds for nonlinear optical activity, *Chem. Mater.*, 5, pp930-932, 1993

[71] Y. Zhang, P. N. Prasad and R. Burzynski, Second-order nonlinear optical properties of N-(4-nitrophenyl)-(s)-prolinol-doped sol-gel-processed materials, *Chem. Mater.*, *4*, pp851-855, 1992

[72] Zhanjia J. Hou, Liying Y. Liu., L. Xu, Zhiling L. X., Wencheng C. Wang, F. M. Li and X. Mingxin Y., Improved second harmonic generation from organic-dye-doped polymer/silica Hybrid Materials, *Chem. Mater.*, 11, pp3177-3180, 1999.

[73] R.-H. Lee, G.-H. Hsiue, and R.-J. Jeng, Organically modified inorganic sol-gel materials for second-order nonlinear optics, *J. Appl. Polym. Sci.*, 79, pp1852-1859, 2001

[74] J. Kim, J. L. Plawsky, E. Van Wagenen and G. M. Korennowski, Effect of processing parameters and polymerization behavior on the nonlinear optical response of sol-gel materials, *Chem. Mater.*, 5, pp1118-1125, 1993.

[75] D. Riehl, F. Chaput, Y. Levy, J.-P. Boilot, F. Kajzar and P.-A. Chollet, Second-order optical nonlinearities of azo chromophores covalently attached to a sol-gel matrix, *Chem. Phys. Lett.*, 245, pp36-40, 1995

[76] D. H. Choi, J. H. Park, T. H. Rhee, N. Kim, and S.-D. Lee, Improved

Temporal stability of the second-order nonlinear optical effect in a sol-gel matrix bearing an active chromophore, *Chem. Mater.*, 10, pp705-709, 1998

[77] D. H. Choi, S. J. Lim, W. S. Jahng and N. Kim, Organically modified sol-gel materials for second-order nonlinear optics, *Thin Solid Film,* 287, pp220-224, 1996

[78] P.-H. Sung, S.-L. Wu and C.-Y. Lin, Sol-gel process of nonlinear optical silica films with organic chromophore as side chain, *J. Mater. Sci.* 31, pp2443-2446, 1996

[79] G.-H. Hsiue, R.–H. Lee and R. J. Jeng, All sol-gel organic-inorganic nonlinear optical materials based on melanines and an alkoxysilane dye, *Polymer,* 40, pp6417-6428, 1999

[80] P.-H. Sung and T.-F. Hsu, Thermal stability of NLO sol-gel networks with reactive chromophores, *Polymer*, 39, pp1453-1459, 1998

[81] H. K. Kim, S.-J. Kang, S.-K. Choi, Y.-H. Min and C.-S. Yoon, Highly efficient organic/inorganic hybrid nonlinear optic materials via sol-gel process: Synthesis, optical properties and photobleaching for channel waveguides, *Chem. Mater.,* 11, pp779-788, 1999

[82] H. W. Jiang and A. K. Kakkar, From simple acid-base hydrolytic chemistry to soluble high T_g inorganic-organic hybrid materials with large and stable second-order nonlinear optical susceptibilities, *Adv. Mater.,* 10, pp1093-1097, 1998

[83] H. W. Jiang and A. K. Kakkar, An alternative route based on acid-base hydrolytic chemistry to NLO active organic-inorganic hybrid materials for second-order nonlinear optics, *J. Am. Chem. Soc.,* 121,pp 3657-3665, 1999

[84] K. D. Singer, J. E. Sohn and S. J. Lalama, Second harmonic generation in

poled polymer films, *Appl. Phys. Lett.*, 49, pp248-250, 1986

[85] Z. Sekkat and M. Dumont, Photoassisted poling of azo dye doped polymeric films at room temperature, *Appl. Phys. B,* 54, pp486-489, 1992

[86] W. Chalupczak, C. Fiorine, F. Charra, J. M. Nunzi and P. Rainond, Efficient all-optical poling of an azo-dye copolymer using a low power laser, *Optics Comm.,* 126, pp103-107, 1996

[87] J. Wu, J. Valley, S. Ermer, E. Binkley, J. Kenney, G. Lipscomb and R. Lytel, Thermal stability of electro-optic response in poled polyimide systems, *Appl. Phys. Lett.,* 58, pp225-227, 1991

[88] S. Yitzchaik, G. Berkovic and V. Krongauz, Charge injection asymmetry: A new route to strong optical nonlinearity in poled polymers, *J. Appl. Phys.,* 70, pp3949-3951, 1991

[89] M. Stiihelin, C. Walsh, D. Burland, R. Miller, R. Twieg and W.Volksen, Orientational decay in poled second-order nonlinear optical guest-host polymers: Temperature dependence and effects of poling geometry, *J. Appl. Phys.,* 73, pp8471-8479, 1993.

[90] A. Suzuki, Y. Matauoka, A. Ikushima, Substrate effect on poling process of nonlinear optical polymer films, *Jpn. J. Appl. Phys.*, 30, ppL1493-1495, 1991

[91] H. Ling, W. Holland, H. Gordon, Dc electrical behavior of polymers used in electro-optic devices, *J. Appl. Phys.*, 70, pp6669-6673, 1991

[92] M. Mortazavi, A. Knoesen, S. Kowel, B. Higgins and A. Dienes, Second-harmonic generation and absorption studies of polymer-dye films oriented by corona-onset poling at elevated temperatures, *J. Opt. Soc. Am. B*, 6, pp733-741, 1989

[93] H. Hampsch, J. Torkelson, S. Bethke and S. Grubb, Second harmonic generation in corona poled, doped polymer films as a function of corona processing, *J. Appl. Phys.*, 67, pp1037-1041,1990

[94] A. Knoesen, N. Molau, D. Yankelevich, M. Mortazavi and A. Dienes, Corona-poled nonlinear polymeric films: In situ electric field measurement, characterization and ultrashort-pluse applications, *Int. J. Nonlinear Opt. Phys.*, 1, pp73-102, 1991

[95] F. Charra, F. Kajzar, J.-M. Nunzi, P. Raimond and E. Idiart, Light-induced second-harmonic generation in azo-dye polymers, *Opt. Lett.*, 18, pp941-943, 1993

[96] B. F. Levine and C. G. Bethea, Second and third order hyperpolarizabilities of organic molecules, *J. Chem. Phys.*, 63, pp2666-2682, 1975

[97] J. L. Oudar, Optical nonlinearities of conjugated molecules. Stilbene derivatives and highly polar aromatic compounds, *J. Chem. Phys.*, 67, pp446-457, 1977

[98] K. D. Singer and A. F. Garito, Measurements of molecular second order optical susceptibilities using dc induced second harmonic generation, *J. Chem. Phys.*, 75, pp3572-3580, 1981

[99] M. S. Paley, J. M. Harris, H. Looser, J. C. Baumert, G. C. Bjorklund, D. Jundt and R. J. Twieg, A solvatochromic method for determining second-order polarizabilities of organic molecules, *J. Org. Chem.*, 54, pp3774-3778, 1989

[100] A. Miniewicz, K. Palewska, J. Lipinski, R. Kowal and B. Swedek, On the spectroscopic and nonlinear optical properties of 3-(1,1-dicyanoethenyl)-1-phenyl-4,5-dihydro-1h-pyrazole (DCNP), *Molecualr Crystals and Liquid*

Crystals Science & Technology Section A- Molecular Crystals & Liquid Crystals, 252, pp333-340, 1994

[101] Y. G. Liu, A. G. Jiang, L. Xiang, J. Gao and D. Y. Huang, Nonlinear optical chromophores with good transparency and high thermal stability, *Dyes and Pigments,* 45, pp189-193, 2002

[102] K. Matczyszyn, W. Bartkowiak, and J. Leszczynski, Influence of the environment on kinetics and electronic structure of asymmetric azobenzene derivatives experiment and quantum-chemical calculations, *J. Mol. Str.*, 53, pp565-566, 2001

[103] B. Philip and K. Sreeumar, Second-harmonic response of a series of chiral polyesters: a joint experimental and theoretical study, *J. Polym. Sci. Part A: Polym. Chem.*, 40, pp2868-2877, 2002

[104] S. Bruni, E. Cariati, F. Cariati, F. A. Porta, S. Quici and D. Roberto, Determination of the quadratic hyperpolarizability of trans-4-[4-(dimethylamino)styryl] pyridine and 5-dimethylamino-1, 10-phyenanthroline from solvatochromism of absorption and fluorescence spectra: a comparison with the electric-field-induced second-harmonic generation technique, *Spectrochimica Acta Part A*, 57, pp1417-1426, 2001

[105] K. Clays, A. Persoons, Hyper-rayleigh scattering in solution, *Phys. Rev., Lett.*, 66, pp2980-2983, 1991

[106] J. Zyss, T. C. Van, Ch. Dhenaut and I. Ledoux, Harmonic rayleigh scattering from nonlinear octupolar molecular media: the case of crystal violet, *Chem. Phys.,* 177, pp281-296,1993

[107] J. Zyss and I. Ledoux, Nonlinear optics in multipolar media: theory and experiments, *Chem. Rev.,* 94, pp77-105, 1994

[108] C. Bosshard, G. Knopfle, P. Pretre and P. Gunter, Second-order polarizabilities of nitropyridine derivatives determined with electric-field-induced second-harmonic generation and a solvatochromic method: A comparative study, *J. Appl. Phys.*, 71, pp1594-1605, 1992

[109] J. Sworakowski, J. Lipinski, L. Ziolek, K. Palewska, and S. Nespurek, Solvatochromism of a zwitterionic benzimidazole-based pyridinium betaine dye: UV-Vis spectroscopic measurement and quantum-chemical calculations, *J. Phys. Chem.*, 100, pp12288-12294, 1996

[110] S. Kucharski, R. Janik and P. Kaatz, First hyperpolarizability of the heterocyclic sulfonamides for Langmuir-blodgett films by calculation, solvatochromism, and hyper-rayleigh scattering, *J. Phys. Chem. B*, 101, pp8967-8974, 1997

[111] Sh.-Sh. P. Chou, G.-T. Hsu and H.-C. Lin, Synthesis and second-order nonlinearities of sulfonyl-substituted pyrrole Imino dyes, *Tetrahedron Lett.*, 40, pp2157-2160, 1999

[112] P. G. Lacroix, I. Malfant, G. Iftime, A. C. Razus, K. Nakatani, and J. A. Delaire, Azo-azulene derivatives as second-order nonlinear optical chromophores, *Chem. Eur. J.*, pp2599-2608, 2000

[113] R. C. Eckardt, H. Masuda, Y. X. Fan and R. L. Byer, Absolute and relative nonlinear optical coefficients of KDP, KD*P, BaB_2O_4, $LiIO_3$, MgO:$LiNbO_3$, and KTP measured by phase-matched second-harmonic generation, *IEEE J. Quant. Electron*, 26, pp922-933, 1990

[114] M. M. Choy and R. L.Byer, Accurate second-order susceptibility measurements of visible and infrared nonlinear crystals, *Phys. Rev. B.*, 14, pp1693-1706, 1976

[115] A. Kitamoto, T. Kondo, I. Shoji and R. Ito, Absolute measurement of second-order nonlinear optical coefficient of $LiNbO_3$ by parametric processes, *Opt. Rev.*, 2, pp280-284, 1995

[116] W. L. Faust, and C. H. Henry, Mixing of visible and near-resonance infrared light in GaP, *Phys. Rev. Lett.*, 17, pp1265-1268, 1966

[117] G. D. Boyd, H. Kaspar and J. H. McFee, Linear and nonlinear optical properties of $AgGaS_2$, $CuGaS_2$, and $CuInS_2$, and theory of the wedge technique for the measurement of nonlinear coefficients, *IEEE, J. Quantum Electron.*, 7, pp563-573, 1971

[118] J. Jerphagnon and S. K. Kurtz, Maker Fringes: A detailed comparison of theory and experiment for isotropic and uniaxial crystals, *J. Appl. Phys.*, 41, pp1667-1681, 1970

[119] J. Jerphagnon and S. Kurtz, Optical nonlinear susceptibilities: Accurate relative values for quartz, ammonium dihydrogen phosphate, and potassium dihydrogen phosphate, *Phys. Rev. B.*, 1, pp1739-1744, 1970

[120] D. Chen, H. R. Fetterman, A. Chen, W. H. Steier, L. R. Dalton, W. Wang and Y. Shi, Demonstration of 110 GHz electro-optic polymer modulators, *Appl. Phys. Lett.*, 70, pp3335-3337, 1997

[121] H. Ohya, V. V. Kudryavtsev and S. I. Semenova, *Polyimide Membranes: Applications, Fabrications and Properties,* pp20 Gordon and Breach Publishers, Tokyo, 1996

[122] K. L. Mittal, ed., *Polyimide*, pp5, Plenum Press, New York, 1984

[123] J. W. Wu, J. F. Valley, S. Ermer, E. S. Binkley, J. T. Kenney, G. F. Lipscomb and R. Lytel, Thermal stability of electro-optic response in poled polyimide systems, *Appl. Phy. Lett.*, 58, pp225-227, 1991

[124] J. F. Valley, J. W. Wu, S. Ermer, M. Stiller, E. S. Binkley, J. T. Kenney, G. F. Lipscomb and R. Lytel, Thermoplasticity and Parallel-plate poling of electro-optic polyimide host thin films, *Appl. Phy. Lett.*, 60, pp160-162, 1992

[125] V. P. Rao, Alex K.-Y. Jen and Y. M. Cai, Achieving excellent tradeoffs among optical, chemical and thermal properties in second-order nonlinear optical chromophores, *Chem. Commun.*, pp1237-1238,1996

[126] F. M. Li, K.-H. Kim, J. J. Kulig, P. S. Edward, J. B. William, F. W. Harris, S. Z. D. Cheng, S. F. Hubbard and K. D. Singer, A high-temperature aromatic polyimide film displaying non-linear optical second-harmonic generation based on the approach of the poled guest–host system, *J. Mater. Chem.*, 5, pp253-259, 1995

[127] S. Ermer, J. F. Valley, R. Lytel, G. F. Lipscomb, T. E. Van Eck and D. G. Girton., DCM-polyimide system for triple-stack poled polymer electro-optics devices, *Appl. Phys. Lett.*, 61, pp2272-2274, 1992

[128] H.-S. Wu, J.-H. Jou and Y.-Ch. Li, Real-time poling vapor co-deposition of dye-doped second-order nonlinear optical polymer thin films, *Macromolecules,* 30, pp4410-4414, 1997

[129] A. K. Tripathi, A. R. T. C. Goel, P. K. C. Pillai and K. Singh, Preparation and characterization of polyimide and optically nonlinear transparent polyimide : ceramic films, *IEEE*, 836-841, 1994

[130] J. Lin, M. Hubbard and T. C. Marks, Poled polymeric nonlinear optical materials. Exceptional second harmonic generation temporal stability of a chromophore-functionalized polyimide, *Chem. Mater.*, 4, pp1148-1150, 1992

[131] W. Sotoyama, S. Tasuura and T. Yoshimura, Electro-optic side-chain polyimide system with large optical nonlinearity and high thermal stability, *Appl. Phys. Lett.*, 64, pp2197-2199, 1994

[132] Ch. Jung, M. Jikei and M. Kakimoto, Synthesis of polyamic acid possessing second-order nonlinear optical properties and its application to Langmuir-Blodgett films, *J Opt. Soc. Am. B,* 15, pp471-476, 1998

[133] H. Y. Woo, H.-K. Shim, K.-S. Lee, M.-Y. Jeong and T.-K. Lim, An alternate synthetic approach for soluble nonlinear optical polyimides, *Chem. Mater.,* 11, pp218-226, 1999

[134] J. X. Lu and J. Yin, Synthesis and characterization of photocrosslinkable, side-chain, second-order nonlinear optical poly(ester imide)s with great film-forming ability and long term dipole orientation stability, *J. Polym. Sci, Part A: Polym. Chem.*, 41, pp303-312, 2003

[135] J. X. Lu and J. Yin, X. X. Deng, Q. S. Shen and Z. Q. Cao, Device-quality second-order nonlinear optical poly(ester imide) for electro-optic applications, *Optical Mater.*, 25, pp17-23, 2004

[136] D. Yu and L. P. Yu, Design and synthesis of functionalized polyimides for second-order nonlinear optics, *Macromolecules*, 27, pp6718-6721, 1994

[137] D. Yu, A. Gharavi and L. P. Yu, A generic approach to functionalizing aromatic polyimides for second-order nonlinear optics, *Macromolecules,* 28, pp784-786, 1995

[138] D. Yu, A. Gharavi and L. P. Yu, Novel aromatic polyimides for nonlinear optics, *J. Am. Chem. Soc.,* 117, pp11680-11686, 1995

[139] D. Yu, A. Gharavi and L. P. Yu, Highly stable copolyimides for second-order nonlinear optics, *Macromolecules,* 29, pp6139-6142, 1996

[140] D. Yu, A. Gharavi and L. P. Yu, Novel second-order nonlinear optical, aromatic, and aliphatic polyimides exhibiting high-temperature stability, *Appl. Phys. Lett.*, 66, pp1050-1052, 1995

[141] R. D. Miller, D. M. Burland, M. Jurich, V. Y. Lee, C. R. Moylan, J. I. Thackara, R. J. Twieg, T. Verbiest, and W. Volksen, Donor-embedded nonlinear optical side chain polyimides containing no flexible tether: Materials of exceptional thermal stability for electrooptic applications, *Macromolecules,* 28, pp4970-4974, 1995

[142] Paul J. A. Kenis, Oscar F. J. Noodman, Niek F. van Hulst, Johan F. J. Engbersen and David N. Reinhoudt., Second-order nonlinear optical active calix[4]arene polyimides suitable for frequency doubling in the UV region, *Chem. Mater.,* 9, pp596-601, 1997

[143] M. Ueda, Y. Sakai, T. Nakayama, O. Haba, Y. Ishitaka and Yorihiko Sasaki, Postive-working Alkaline developable photosensitive and second-order nonlinear optical polyimide, *Chem. Lett.*, 26, pp287-288, 1997.

[144] Y. Sui, H.-X, Lu, J. Yin, Y.-G. Liu, Z.-K. Zhu, Z.-G. Wang., Study on side-chain second-order nonlinear optical polyimides based on novel chromophore-containing diamines. II. Copolyimides possessing direct photolithographic features, *J. Polym. Sci. Polym. Chem.*, 39, pp1419-1425, 2001

[145] C. Jung, T. Aoyama, T. Wada, H. Sasabe, M. Jikei, and M. Kakimoto, The photorefractive effect in monolithic structural polyimides, *High Perform Polym.,* 12, pp205-212, 2000

[146] M. H. Davey, V. Y. Lee, L.-M. Wu, C. R. Moylan, W. Volksen, A. Knoesen, R. D. Miller and T. J. Marks, Ultrahigh temperature polymers for

second-order nonlinear optics. Synthesis and properties of robust, processable, chromophore-embedded polyimide, *Chem. Mater.*, 12, pp1679-1693, 2000.

[147] P. Kaatz, P. Pretre, U. Meier, U. Stalder, C. Bosshard, P. Gunter, B. Zysset, M. Stahelin, M. Ahlheim and F. Lehr, Relaxation processes in nonlinear optical polyimide side-chain polymers, *Macromolecules*, 29, pp1666-1678, 1996.

[148] C. Jung, B. Park, M. Jikei, H. Takezoe and M. Kakimoto, Orientational changes of side chain nonlinear optical chromophore in polyimide Langmuir-Blodgett films, *Jpn. J. Appl. Phys.*, 37, pp6636-6640,1998

[149] C. Marestin, R. Mercier, B. Sillion, B. Chauvin, K. Nakatamin and J. A. Delaire, High glass transition temperature electro-optic side-chain polymers, *Synthetic Met.*, 81, pp143-146, 1996

[150] L. Best, A. Rousseau, B. Boutevin, R. Mercier, B. Sillion and E. Toussaere, Synthesis and characterization of aromatic polyimides bearing nonlinear optical chromophores, *High Perform Polym.*, 12, pp169-176, 2000

[151] K. V. Broeck, T. Verbiest, J. Degryse, M. V. Beylen, A. Persoons and C. Samyn., High glass transition chromophore functionalised polyimides for second-order nonlinear optical applications, *Polymer,* 42, pp3315-3322, 2001

[152] J. Y. Do., S. K. Park, J.-J. Ju, S. Park, M.-H. Lee, Nonlinear optical polyimide with various substituents on chromophores: synthesis and glass transition temperature, *Optical Mater.*, 26, pp223-229, 2004

[153] J. D. Luo, M. Haller, H. X. Li, H.-Z. Tang and Alex K.-Y. Jen, A side-

chain dendronized nonlinear optical polyimide with large and thermally stable electrooptic activity, *Macromolecules*, 37, pp248-250, 2004.

[154] Z. Li, Y. X. Zhao, J. Y. Zhou and Y. Q. Shen., Synthesis and characterization of two series of polyimides as nonlinear optical materials, *Eur. Polym. J.*, 36, pp2417-2421, 2000

[155] T.-D. Kim, K.-S. Lee, Y. H. Jeong, J. H. Jo and S. Chang., Nonlinear optical properties of a processable polyimide having azo-dye functionalized with cyanosulfonyl group, *Synthetic Met.*, 117, pp307-309, 2001

[156] K.-S. Lee, K.-J. Moon, H. Y. Woo and H.-K. Shim., An alternative synthetic route to soluble polyetherimide derivatives with high second-order optical nonlinearity, *Adv. Mater.*, 9, pp978-981, 1997

[157] C.-T. Chen, T.-S. Hsu, R.-J. Jeng and H.-C. Yeh., Enhancing the glass-transition temperature of polyimide copolymers containing 2,2 '-bipyridine units by the coordination of nickel malenonitriledithiolate, *J. Polym. Sci. Polym. Chem.*, 38, pp498-503, 2000

[158] T. L. Bouder, O. Maury, H. L. Bozec, I. Ledoux, and J. Zyss, Synthesis of a highly thermally stable octupolar polyimide for nonlinear optics, *Chem. Commun.*, pp2430-2431, 2001.

[159] T. L. Bouder, O. Maury, A. Bondon, K. Costuas, E. Amouyal, I. Ledoux, J. Zyss, and H. L. Bozec, Synthesis, photophysical and nonlinear optical properties of macromolecular architectures featuring octupolar tris(bipyridine) ruthenium(II) moieties: Evidence for a supramolecular self-ordering in a dentritic structure, *J. Am. Chem. Soc.*, 125, pp12284-12299, 2003

[160] C.-B. Yoon and H.-K. Shim, Facile synthesis of new NLO-functionalized polyimides via Mitsunobu reaction, *J. Mater. Chem.*, 9, pp2339-2344, 1999

[161] E. Gubbelmans, T. Verbiest, M. V. Beylen, A. Persoons, and C. Samyn, Chromophore-functionalised polyimides with high-poling stabilities of the nonlinear optical effect at elevated temperature, *Polymer*, 43, pp1581-1585, 2002

[162] H. Saadeh, L. M. Wang and L. P. Yu, A new synthetic approach to novel polymers exhibiting large electrooptic coefficient and high thermal stability, *Macromolecules*, 33, pp1570-1576, 2000

[163] Y. Sui, J. Yin, Z. J. Hou, M. Zhu, J. X. Lu, Y. G..Liu and Z. K. Zhu, A facile approach to prepare soluble side-chain polyimides for second-order nonlinear optics, *J. Polym. Sci. Polym. Chem.*, 39, pp2189-2195, 2001

[164] Y. Sui, J. X. Lu, J. Yin, D. Wang, Z. K. Zhu, Z.-G. Wang, High T_g second-order nonlinear optical poly(urethane-imide)s prepared from Disperse red 19, pyromellitic dianhydride, and tolylene diisocyanate, *J. Appl. Polym. Sci.*, 85, pp944-949, 2002.

[165] G. H. Hsiue, J. K. Kuo, R. J. Jeng, J. I. Chen, X. L. Jiang, S. Marturunkakul, J. Kumar and J. K. Tripathy., Stable second-order nonlinear optical polymer network based on an organosouble polyimide, *Chem. Mater.*, 6, pp884-887, 1994.

[166] C. Wang, C. Zhang, P. Wang, P. Zhu, C. Ye, L. R. Dalton, High T_g donor-embedded polyimides for second-order nonlinear optical applications, *Polymer*, 41, pp2583-2590, 2000

[167] H. Kang, Sh.-J. Li, P. Wang, W. Wu, C. Ye, Second-order nonlinearities of poled films containing the multi-intromolecular charge-transfer

chromophore, *Synthetic Met.*, 121, pp1469-1470, 2001

[168] A. J. Qin, Y. Zhou, F. L. Bai, and C. Ye, Design and synthesis of a thermally stable second-order nonlinear optical chromophore and its poled polymer, *J. Polym. Sci. Part A: Polym. Sci.*, 41, pp2846-2853, 2003

[169] C. Samyn, T. Verbiest, E. Kesters, K. V. Broeck, M. V. Beyle, and A. Persoons, High glass transition chromophore functionalized poly(maleimide-styrene)s for second-order nonlinear optical applications, *Polymer*, 41, pp6049-6054, 2000

[170] R.-J. Jeng, Ch.-C. Chang, Ch.-P. Chen, Ch.-T. Chen, W.-Ch. Su, Thermally stable crosslinked NLO materials based on maleimides, *Polymer*, 44, pp143-155, 2003

[171] T. Hiyama, *Organofluorine compounds: chemistry and applicatio*n, pp140, Springer-Verlag Berlin, 2000

[172] K. H. Saunders and R. L. M. Allen, *Aromatic Diazo compounds*, pp1-343, Edward Arnold, London, 1985

[173] N. Tsutsum, M. Morishima and W. Sakai, Nonlinear optical (NLO) polymer 3 NLO polyimide with dipole moments aligned transverse to the imide linkage, *Macromolecules*, 31, pp7764-7769, 1998

[174] Y. M. Zhou, W. N. Leng, X. J. Liu, Q. H. Xu, J. K. Feng, and J. Z. Liu, Synthesis of nonlinear optical polyimides containing azodiamine derivate chromophores and their electro-optical and thermal properties, *J. Polym. Sci., Part A: Polym. Chem.*, 40, pp2478-2486, 2002

[175] R. J. Abraham, *The Analysis of High Resolution NMR spectra,* pp75, Elsevier, Amsterdam, Netherlands, 1971

[176] George Socrates, *Infrared Characteristic Group Frequencies: Tables and*

Charts, pp50, John Wiley & sons, New York, 1994

[177] E. G. McRae, Theory of solvent effects on molecular electronic spectra frequency shifts., *J. Phys. Chem.,* 61, pp562-572, 1957

[178] W. Liptay, Electrochromism and solvatochromism, *Angrew. Chem. Int. Ed.*, 8, pp177-188, 1969

[179] T. Amos, B. L. Burrows, *Advanced in Quantum Chemistry*, pp289-313, Academic Press, New York, 1973

[180] M. S. Paley, J. M. Harris, H. Looser, J. C. Baumert, G. C. Bjorklund, D. Jundt, and R. J. Twieng, A solventochromic method for determining second-order polarizabilities of organic molecules, *J. Org. Chem.*, 54, pp3774-3778, 1989

[181] E. A. Guggenheim, *Trans. Faraday Soc.*, 45, pp714-717, 1949

[182] Ch. Bosshard, G. Knopfle, P. Pretre and P. Gunter, Second-order polarizabilities of nitropyidine derivatives determined with electric-field-induced second-harmonic generation and a solvatochromic method: A comparative study, *J. Appl. Phys.*, 71, pp1594-1605, 1992

[183] F. L. Pilar, *Elementary Quantum Chemistry,* pp75, McGraw Hill, New York, 1968

[184] M. K. Ghosh and K. L. Mittal, *Polyimides: Fundaments and applications*, pp12-18, Marcel Dekker, Inc., New York, 1996

[185] L. A. Shibaev, Y. N. Sazanov, S. A. Dauengauer, N. G. Stepanov, T. M. Bulina, Complexes of acid amides with polar aprotic solvents: III. Complexes of bis (n-phenyl)-pyromellitic acid amide with solvent mixtures, *J. Therm. Anal.*, 26, pp199-203, 1983

[186] L. Ren, F. S. Zeng, P. Ning, Z. Q. Chen, Z. M. Ko, Effect of addition

orders on the properties of fluorine-containing copolyimides, *J. Appl. Polym. Sci.*, 77, pp3252-3258, 2000

[187] G. M. Bower and I. W. Frost, Aromatic imide polymers for electrical insulation, *J. Polym. Sci.: Part A Polym. Chem.*, 1, pp3135-3138, 1963

[188] W. M. K. P. Wijekoon, Y. Zhang, S. P. Karna, P. N. Prasad, A. C. Griffin, A. M. Bhatti, Second-order nonlinear optical effects in novel side-chain liquid crystalline polymers and monomers under bias of an applied dc electric field, *J. Opt. Soc. Am. B* ,9, pp1832-1842, 1992

[189] S. S. Lee, S. M. Garner, V. Chuyanov, H. Zhang, W. H.Steier, F. Wang, L. R. Dalton, A. H. Udupa, and H. R. Fetterman, Optical intensity modulator, based on a novel electrooptic polymer incorporating a high $\mu\beta$ chromophore, *IEEE J. Quantum Electronic*, 36, pp527-532, 2000

[190] Q. W. Pan, Ch. S. Fang, Z. H. Qin, Q. T. Gu, X. W. Wu, W. Shi, J. Z. Qin, Thermally stable guest-host polyetherketone poled polymer for electro-optical applications, *Chin. Phys. Lett.*, 19, pp1125-1127, 2002

[191] P. A. Riberiro, D. T. Balogh and J. A. Giacmetti, Corona poling and electroactivity in a side-chain methylacrylate copolymer, *IEEE Trans. Dielectrics and Electrical Insulation*, 7, pp572-577, 2000

[192] T. Fukuda, H. Matsuda, T. Kimura, T. Shiraga, M. Kato, and H. Nakanishi, Improved method of corona poling for highly developed dipolar orientation, *Polym. Adv. Technol.*, 11, pp583-588, 2000

[193] D. M. Hirst, *A computational approach to chemistry*, Blackwell Scientific Publications, 1990

[194] M. J. S. Dewar, E. G. Zoebisch, E. F. Healy, and J. J. P. Stewart, AM1: A new general purpose quantum mechanical molecular model, *J. Am. Chem.*

Soc., 107, pp3902-3909, 1985

[195] J. R. Fried, *Polymer Science and Technology*, pp156-161, Prentice Hall PTR, New Jersey, 1995

[196] J. G. Liu, M. H. He, Z. X. Li, Z. G. Qian, F. S. Wang, S. Y. Yang, Synthesis and characterization of organosoluble polyimides with trifluoromethyl-substituted benzene in the side chain, *J. Polym. Sci. Part A: Polym. Chem.*, 40, pp1572-1582, 2002

[197] T. D. Kim, J. D. Luo, Y. Q. Tian, J. W. Ka, N. M. Tucker, M. Haller, J. W. Kang, L. R. Dalton, A. K.-Y. Jen, Diels-Alder "click chemistry" for highly efficient electrooptic polymers, *Macromolecules*, 39, pp1676-1680, 2006

[198] R. J. Jeng, Y. M. Chen, A. K. Jain, J. Kumar, S. K. Tripathy, Stable second-order nonlinear optical polyimide/inorganic composite, *Chem. Mater.* 4, pp1141-1144, 1992

[199] L. A. Laius, M. I. Bessonor, Ye. V. Kallistova, N. A. Adrova and F. S. Flovinskii, Infrared spectral absorption study of the formation kinetics of polypyromellitimide (PPMI), *Polymer Sci. USSR*, A: 9, pp2470-2478, 1967

[200] J. W. Jr. Verbicky and L. Williams, Thermolysis of N-alkyl-substituted phthalamic acids. Steric inhibition of imide formation, *J. Org. Chem.*, 46, pp175-177, 1981

[201] J. Melcher, Y. Daben and G. Arlt. Dielectric effects of moisture in polyimide, *IEEE, Transactions on Electrical Insulation*, 24, pp31-38, 1989

[202] D. D. Deton, D. R. Day, Dd. F. Priore, and S. D. Sentrial, Moisture diffusion in polyimide films in integrated circuits, *J. Electron. Mater.*, 14, pp119-123, 1985

[203] T. Matsuura, M. Ishizawa, Y. Hasuda, and Shiro Nishi, Polyimides

derived from 2,2'-bis(trifluoromethyl)-4,4'-diaminobiphenyl. 2. Synthesis and characterization of polyimides prepared from fluorinated benzenetetracarboxylic dianhydrides, *Macromolecules*, 25, pp3540-3545, 1992

[204] S. Y. Yang, Z. Y. Ge, D. X. Yin, J. G. Liu, Y. F. Li and L. Fan, Synthesis and characterization of novel fluorinated polyimides derived from 4,4′-[2,2,2-trifluoro-1-(3-trifluoromethylphenyl)ethylidene]diphthalic anhydride and aromatic diamines, *J. Polym. Sci. Part A: Polym. Chem.*, 42, pp4143-4152, 2004

[205] Li Ren, G. Y. Li, J. R. Shen, and D. M. Jia, Effect of monomer addition sequences on the properties of silicon-containing copolyimides, *Polym. International*, 54, pp1097-1101, 2005

[206] R. C. Eckardt, H. Masuda, Y. X. Fan, R. L. Byer, Absolute and relative nonlinear optical coefficients of KDP, KD*P, BaB_2O_4, $LiIO_3$, MgO:$LiNbO_3$, and KTP measured by phase-matched second-harmonic generation, *IEEE J. Quant. Electron*, 26, pp922-933, 1990

[207] L. Ren, G. Y. Li, X. Hu, X. L. Xia, J. R. Shen and D. M. Jia, Synthesis and characterization of fluoronitroaryl azo diaminobenzene chromophores, *Tetrahedron Lett.*, 46, pp1511-1513, 2005

[208] C. J. Brinker, and G. W. Scherrer, Eds, *Sol-Gel Science*, pp80, Academic Press, Orlando, 1990

[209] M. Palmlof, T. Hjertberg, and B. A. Sultan, Crosslinking reactions of ethylene vinyl silane copolymers at processing temperature, *J. Appl. Polym. Sci.*, 42, pp1193-1203, 1991

[210] Y. J. Cui, M. Q. Wang, L. J. Chen, G. D. Qian, Synthesis and

spectroscopic characterization of an alkoxysilane dye containing C. I. Disperse Red 1, *Dyes and Pigments*, 62, pp43-47, 2004

[211] P. Sysel and D. Oupicky, Polyimide-polysiloxane block copolymers synthesized from α,ω-(3-aminophenoxy) terminated poly[oxy(dimethylsilyl)-1,4-phenylene (dimethylsilylene)]s, *Polym. International*, 40, pp275-279, 1996

Publications

1. Li Ren, G. Y.Li Li etc, Synthesis and Characterization of Side-chain Second-Order Nonlinear optical Polyimides Based on Novel Fluorine-containing Chromophores, ICMAT, 2003
2. G. Y. Li, Li Ren, etc Preparation and Characterization of Second-Order Nonlinear Optical Fluorinated Polyimide/Inorganic Composites ICMAT 2005
3. Li Ren, G. Y. Li, etc Effects of monomer addition sequence on the Properties of Silicon-Containing Copolyimides *Polymer International* 54,1097, 2005,
4. Li Ren, G. Y. Li, etc, Synthesis and characterization of fluoronitroaryl azo diaminobenzene chromophores, *Tetrahedron Letters*, 46 1511, 2005
5. Li Ren, G. Y. Li, etc, Synthesis and characterization of a new fluorinated nonlinear optical chromophore *Dyes and Pigments*, 67 207, 2005
6. G. Y. Li, Li Ren, etc Preparation and Characterization of Second-Order Nonlinear Optical Fluorinated Polyimide/Inorganic Composites, *Transactions of Nonferrous Metals Society of China*, Accepted
7. Li Ren, G. Y. Li etc Effect of nitro position on the structures and properties of diaminoazobenzene chromophores, *Dyes and Pigments,* Submitted
8. Li Ren, G. Y. Li etc Synthesis and characterization of novel second-order nonlinear optical polyimides based on fluorinated chromophore (I), *Journal of Polymer Science Part A: Polymer Chemistry*, Submitted
9. Li Ren, G. Y. Li etc Novel second-order nonlinear optical polyimides based on fluorinated chromophore, *Macromolecular Rapid Communications*, Submitted